BioMed Research International

Neural Engineering for Rehabilitation

Guest Editors: Han-Jeong Hwang, Do-Won Kim, Janne M. Hahne, and Jongsang Son

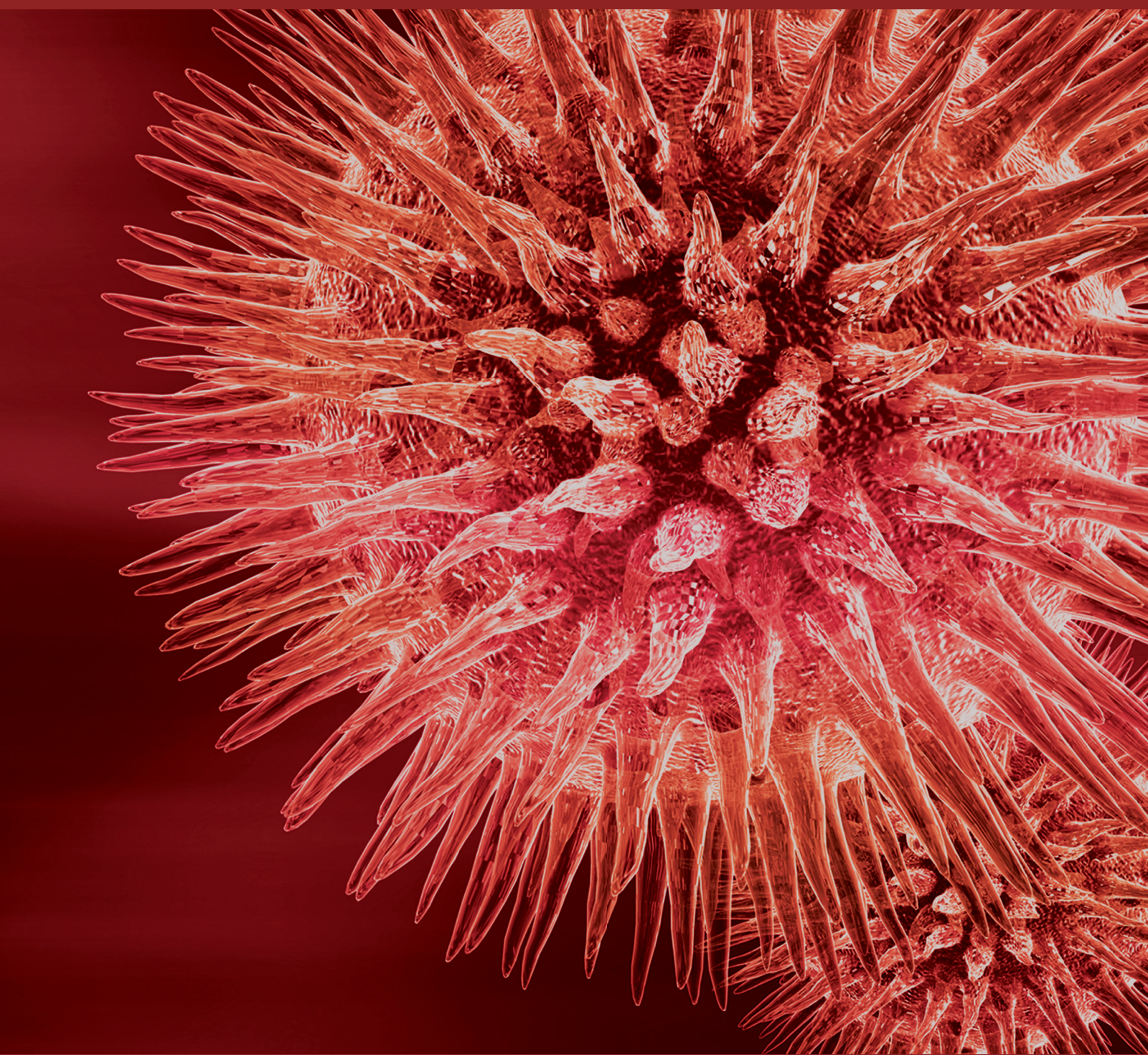

Neural Engineering for Rehabilitation

BioMed Research International

Neural Engineering for Rehabilitation

Guest Editors: Han-Jeong Hwang, Do-Won Kim, Janne M. Hahne, and Jongsang Son

Contents

Hindawi
BioMed Research International
Volume 2017, Article ID 9638098, 2 pages
https://doi.org/10.1155/2017/9638098

Editorial

Neural Engineering for Rehabilitation

Han-Jeong Hwang,[1] Do-Won Kim,[2] Janne M. Hahne,[3] and Jongsang Son[4,5]

[1]*Department of Medical IT Convergence Engineering, Kumoh National Institute of Technology, Gumi 730-701, Republic of Korea*
[2]*Department of Biomedical Engineering, Chonnam National University, Yeosu 59626, Republic of Korea*
[3]*Department of Neurorehabilitation Engineering, University Medical Center Göttingen, Georg-August University Göttingen, 37075 Göttingen, Germany*
[4]*Sensory Motor Performance Program, Rehabilitation Institute of Chicago, Chicago, IL 60611, USA*
[5]*Department of Physical Medicine & Rehabilitation, Northwestern University, Chicago, IL 60611, USA*

Correspondence should be addressed to Han-Jeong Hwang; h2j@kumoh.ac.kr

Received 27 March 2017; Accepted 27 March 2017; Published 30 April 2017

Neural engineering (also called neuroengineering) is an interdisciplinary research area, and its fundamental goal is to understand underlying mechanisms of the nervous system and to provide rehabilitative solutions for the treatment of neurological disorders, such as autism, stroke, multiple sclerosis, epilepsy, and Alzheimer's and Parkinson's disease. So far, neural engineering has played a crucial role in advancing neurorehabilitation technologies by developing novel assistive and rehabilitation tools/methods/systems, thereby providing more effective and efficient rehabilitation. This special issue aims at sharing the current state-of-the-art trends and future directions in the field of neural engineering for rehabilitation, and it includes eight up-to-date articles related to neurorehabilitation. The selected articles cover a wide range of neurorehabilitation research topics: neurofeedback, brain-computer interface (BCI), hybrid BCI, transcranial direct current stimulation (tDCS), thermotherapy, robot-aided neurorehabilitation, relation between the features of olfactory stimuli and electroencephalography (EEG), and diagnosis of autism spectrum disorder based on EEG.

In the article entitled "Data-Driven User Feedback: An Improved Neurofeedback Strategy considering the Interindividual Variability of EEG Features" by C.-H. Han et al., the authors proposed data-driven user feedback to improve a neurofeedback strategy considering the interindividual variability of EEG features. In the experiment, subjects performed a meditation paradigm, where a babbling brook sound, a picture of a beautiful valley, and a quiet pure-tone beep sound with a period of three seconds were simultaneously provided to each subject. By dividing the entire range of an EEG feature into a lot of bins using nonuniform bin sizes, the authors could optimize bin sizes and permit users to experience a wider range of feedback without a customization process. Each individual experienced significantly increased feedback levels, which were 139% and 144% of the original levels with uniform bin sizes in the offline and online experiments, respectively. It is expected that the proposed method could effectively increase the overall range of feedback levels, thereby providing an improved neurofeedback strategy.

The article entitled "Vowel Imagery Decoding Toward Silent Speech BCI Using Extreme Learning Machine with Electroencephalogram" by B. Min et al. investigated four different classifiers to decode imagined speech based on EEG signals, where five vowels, /a/, /e/, /i/, /o/, and /u/, were tested. The authors employed four EEG features (mean, variance, standard deviation, and skewness) and reduced the dimensionality of the feature vector using a sparse regression model. For classification, they tested two variants of support vector machine (SVM) and of an extreme learning machine. As a result, the extreme learning machine showed a mean accuracy of about 70% for all pairwise classification, which was better than the SVM's variants. The results could be utilized to enhance the performance of imagined-speech-based BCIs and fundamentally contribute to increasing the quality of life for patients with neurological disorders.

The article entitled "Evaluation of a Compact Hybrid Brain-Computer Interface System" by J. Shin and colleagues suggested a way of realizing a compact hybrid EEG and near-infrared spectroscopy (NIRS) acquisition system using a portable NIRS device with an economic EEG system. To prove its feasibility, the authors conducted a typical BCI experiment in which subjects performed a mental arithmetic (MA) task. They classified MA tasks from baseline and compared the classification accuracies obtained using each of the modalities (EEG or NIRS) and the hybrid system. The hybrid EEG and NIRS system showed an increase of performance compared to the unimodal EEG and NIRS systems by 6.2% and 2.5%, respectively, demonstrating the feasibility of the implemented hybrid system. As the proposed hybrid system is based on portable platforms, its potential use is not confined to a laboratory environment and can be extended to real-life situations, such as neurorehabilitation.

The article entitled "Effect of Anodal-tDCS on Event-Related Potentials: A Controlled Study" by A. Izzidien et al. investigated the impact of anodal tDCS on three different EEG phenomena that are event-related potential (ERP), synchronization (ERS), and desynchronization (ERD). The authors showed that absolute ERP power significantly increased after tDCS stimulation, but not for ERD and ERS, concluding that tDCS may help enhance the accuracy of ERP-based BCI spellers for patients with neurological disorders. Since the ERP power was significantly improved at Pz, tDCS stimulation may help the development of neurorehabilitation methods, especially targeting the parietal lobe.

In the article entitled "Integrative Evaluation of Automated Massage Combined with Thermotherapy: Physical, Physiological, and Psychological Viewpoints" by D.-W. Kim et al., the effect of massage therapy was investigated alone and in combination with infrared heating on physical, physiological, and psychological aspects. Various physical, physiological, and psychological changes were observed, mostly showing significantly positive effect on physical functioning, increased parasympathetic response, and decreased psychological stress and anxiety, especially when massage therapy was combined with infrared heating. The results indicate that thermotherapy could lead to enhanced physical functions during rehabilitation.

The article entitled "Patient-Centered Robot-Aided Passive Neurorehabilitation Exercise Based on Safety-Motion Decision-Making Mechanism" by L. Pan et al. presented a novel motion control approach for patient-centered robot-aided passive neurorehabilitation exercise from the safety point of view. The proposed approach included observing and assessing the physical state of training impaired-limb and motion performances and regulating training parameters (e.g., motion speed and training range) in real time. The authors demonstrated the efficacy of the suggested control strategy in two experiments performed with healthy subjects and stroke patients. The research results could be used to design a rehabilitation program, ensuring the safety of patients for emergency events.

The article entitled "Analysis of the Influence of Complexity and Entropy of Odorant on Fractal Dynamics and Entropy of EEG Signal" by H. Namazi et al. analyzed the relationship between olfactory characteristics and EEG features. The authors used five pleasant odorants and investigated how their molecular complexity and entropy were related to EEG features. The authors found that the complexity of the EEG is positively coupled with the molecular complexity of the odorant, but the entropy of EEG showed an opposite trend. Understanding the relation between external stimuli (olfactory in this study) and brain reaction could help the development of rehabilitation therapy for different brain diseases.

The article entitled "EEG-Based Computer-Aided Diagnosis of Autism Spectrum Disorder Using Wavelet, Entropy, and ANN" by R. Djemal et al. proposed a diagnosis method of autism spectrum disorder based on machine-learning approach. The authors used discrete wavelet transform (DWT) and entropy as features and artificial neural network as a classifier. The highest diagnosis accuracy was obtained (96%) when using standard deviations of extracted DWT coefficients. The results could be used to diagnose autism patients more accurately, providing an appropriate rehabilitation method for autism spectrum disorder.

In this special issue, we provide the eight research articles showing recent advances in neural engineering for rehabilitation. We hope that this special issue will further contribute to promoting the development of neurorehabilitation and fundamentally providing clinically feasible neurorehabilitative methods. To this end, more clinical studies with real patients are especially required to accurately evaluate the clinical effect of new rehabilitative methods even though experiments performed with healthy subjects generally show similar clinical effects.

Han-Jeong Hwang
Do-Won Kim
Janne M. Hahne
Jongsang Son

Hindawi
BioMed Research International
Volume 2017, Article ID 9816591, 9 pages
https://doi.org/10.1155/2017/9816591

Research Article

EEG-Based Computer Aided Diagnosis of Autism Spectrum Disorder Using Wavelet, Entropy, and ANN

Ridha Djemal, Khalil AlSharabi, Sutrisno Ibrahim, and Abdullah Alsuwailem

Electrical Engineering Department, College of Engineering, King Saud University, Box 800, Riyadh 11421, Saudi Arabia

Correspondence should be addressed to Ridha Djemal; rdjemal@ksu.edu.sa

Received 21 August 2016; Revised 2 December 2016; Accepted 13 February 2017; Published 18 April 2017

Academic Editor: Do-Won Kim

Autism spectrum disorder (ASD) is a type of neurodevelopmental disorder with core impairments in the social relationships, communication, imagination, or flexibility of thought and restricted repertoire of activity and interest. In this work, a new computer aided diagnosis (CAD) of autism based on electroencephalography (EEG) signal analysis is investigated. The proposed method is based on discrete wavelet transform (DWT), entropy (En), and artificial neural network (ANN). DWT is used to decompose EEG signals into approximation and details coefficients to obtain EEG subbands. The feature vector is constructed by computing Shannon entropy values from each EEG subband. ANN classifies the corresponding EEG signal into normal or autistic based on the extracted features. The experimental results show the effectiveness of the proposed method for assisting autism diagnosis. A receiver operating characteristic (ROC) curve metric is used to quantify the performance of the proposed method. The proposed method obtained promising results tested using real dataset provided by King Abdulaziz Hospital, Jeddah, Saudi Arabia.

1. Introduction

Autism spectrum disorder (ASD) is a neurodevelopment disorder that includes (*classic*) *autism*, *Asperger's syndrome*, and *pervasive developmental disorder not otherwise specified* (PDD-NOS) [1]. ASD diagnosis is mainly based on behavioral and interview test such as using diagnostic and statistical manual of mental disorders, 5th edition (DSM-5) [2]. Different types of autism were previously classified as different disorders, but now in DSM-5 all fall under one umbrella that is ASD. Computer aided diagnosis (CAD) system is a computer system (or program) built to aid clinician or medical doctor to diagnose certain disease or disorder. CAD gives second opinion for the clinician to diagnose the disorder. CAD system is not intended to diagnose by itself but as an assisting tool for clinician for diagnosing therefore saving the time and increasing the accuracy.

Recently, researchers tried to develop computer aided autism spectrum disorders diagnosis based on *electroencephalogram* (EEG) signals [3]. EEG has high temporal resolution and is relatively cheap and widely available for clinicians. Applying Fourier transform directly to such signal is not practically suitable because the nature of EEG signals is rather complex, nonlinear, and nonstationary. Wavelet transform is able to represent the EEG signal in multiscale time-frequency domain and captures subtle changes in the signal. This research work aims to investigate a new autism diagnosis procedure based on *discrete wavelet transform* (DWT) combined with Shannon entropy and *artificial neural network* (ANN).

DWT decomposes the EEG segment into several frequency subbands. Several statistical features (mean, variance, and standard deviation) and several entropy functions (log energy entropy, threshold entropy, Renyi entropy, and Shannon entropy) are used to extract the feature from each EEG subband. Then ANN classifies the corresponding EEG segment based on these extracted features. The best classification accuracy is obtained using Shannon entropy as features extraction. The rest of this paper is organized as follows: Section 2 provides brief literature review to the topic. Section 3 highlights the EEG dataset used in this work and the feature extraction and the classification methods. Experimental results are presented and discussed in Section 4. Section 5 concludes the paper and highlights the future research direction.

2. Literature Review

The development of automatic mechanism to analyze brain signals would improve the speed and the accuracy of the clinician to diagnose certain disease or disorder. Several computer aided diagnosis (CAD) methods for autism diagnosis have been investigated by several previous studies. In the work presented by Sheikhani et al. [4], the datasets were recorded by 21 electrodes with both earlobes chosen as common referential electrodes and extracted from two groups: 10 (9 boys and 1 girl) ASD and 7 (4 boys and 3 girls) non-ASD children. A short time Fourier transform (STFT) technique was used to extract EEG signal features and then applied as an input to nearest neighbors (KNN) classifier to get classification accuracy up to 82.4%. In their later paper [5], the authors improved the method and used larger data for testing (17 ASD and 11 normal subjects) which obtained up to 96.4% distinction level.

Ahmadlou et al. [6] investigated fractal dimension (FD) to measure complexity and dynamical changes in ASD brain. The method was tested on a database of eyes-closed EEG data obtained from two groups: 9 ASD and 8 non-ASD children. The dataset was recorded according to 10–20 international system, each consisting of 19 channels, and digitized with sampling rate of 256 Hz. An accuracy of 90% was achieved with a radial basis function classifier. Later, the same group also presented ASD diagnosis using visibility graph (VG) [7] and fuzzy synchronization likelihood (fuzzy SL) and enhanced probabilistic neural network (EPNN) classifier [8]; the two proposed methods obtain around 95.5% accuracy.

Fan et al. 2015 [11] presented spectral features of EEG signals from a 14-channel EEG neuroheadset, together with therapist ratings of behavioral engagement, enjoyment, frustration, boredom, and difficulty to train a group of classification models. They used seven classification techniques and compared the results: Bayes network, naive Bayes, support vector machine (SVM), multilayer perceptron, K-nearest neighbors (KNN), random forest, and decision tree classifier (J48), to obtain the classification accuracy ranging 75–85%.

It was reported by Bosl et al. [9] that an EEG dataset was collected from 79 subjects: 46 ASD and 33 non-ASD subjects. The EEG dataset was recorded by 64-channel Sensor Net System and Net Station software, amplified, band-pass filtered at 0.1 to 100.0 Hz, and sampled at a frequency of 250 Hz. They used minimum mean square error (MMSE) as a feature vector and then the multiclass k-nearest neighbors (KNN), the support vector machine (SVM), and naive Bayesian (NB) classification algorithms have been applied to classify typical signal and autistic signal. The classification accuracy is over 80% at age of 9 months. Classification accuracy for boys was close to 100% at age of 9 months and ranged between 70% and 90% at 12 and 18 months. For girls, classification accuracy was highest at age of 6 months but declines thereafter.

In Alhaddad et al. [10] the dataset was collected from 12 children: 8 (5 boys and 3 girls) with ASD and 4 (all of them are boys) with non-ASD. The dataset was recorded by g.tec EEG acquisition system which has 16 channels with AFz electrode as GND and right ear lobe as reference and then filtered using band-pass filter with a frequency band (0.1–60 Hz) and digitized at 256 Hz. The notch filter was also used at 60 Hz. Optimum preprocessing techniques were used in this study. They used two feature extraction techniques: time and frequency domains (raw data and FFT). Fisher linear discriminant (FLD) is used as classifier. They obtained a classification accuracy up to 90%. Later Alsaggaf and Kamel [12] used the same dataset and processing techniques used by Alhaddad for autism disorders diagnosis and obtained 80.27% accuracy.

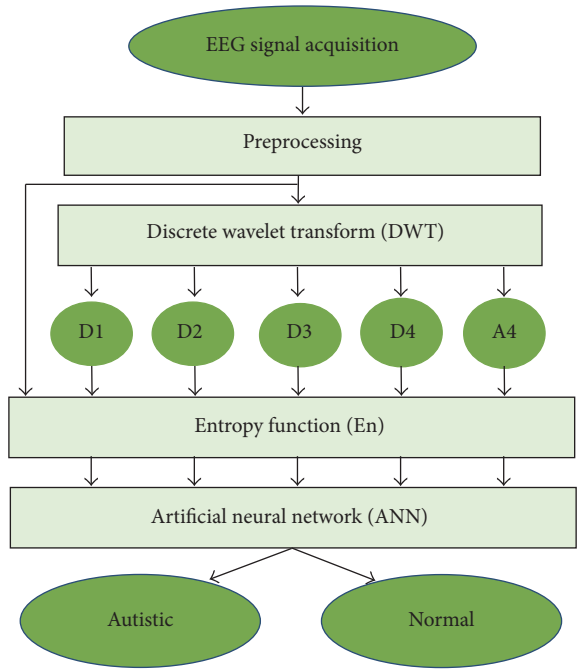

Figure 1: Block diagram of the proposed method.

3. Methods and Materials

3.1. Methods Overview. Figure 1 shows the overview of the proposed method. In the beginning, some preprocessing is done in the input EEG. This preprocessing step includes segmentation process, filtering, and overlapping the EEG segment.

After preprocessing, EEG segment as an input is fed to discrete wavelet transform (DWT). DWT dismantles the EEG segment into detail coefficients (D1–D4) and the corresponding approximate coefficient (A4) for EEG subbands such as delta, theta, alpha, beta, and gamma. Entropy values are then extracted from the original EEG segment and these coefficients to estimate the time series distribution and to reduce the dimension of the extracted features. Several statistical features (mean, standard deviation, etc.) are used also for feature extraction. Artificial neural network (ANN) is used as classifier.

3.2. Dataset. Autism dataset used in this work is provided by King Abdulaziz University (KAU) Brain Computer Interface (BCI) Group, Jeddah, Saudi Arabia (see http://malhaddad.kau.edu.sa/Pages-BCI-Datasets.aspx). The data recording

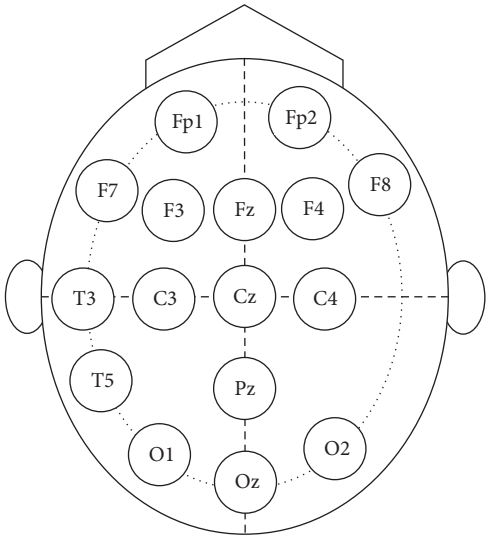

Figure 2: Electrodes placement of autism data acquisition system.

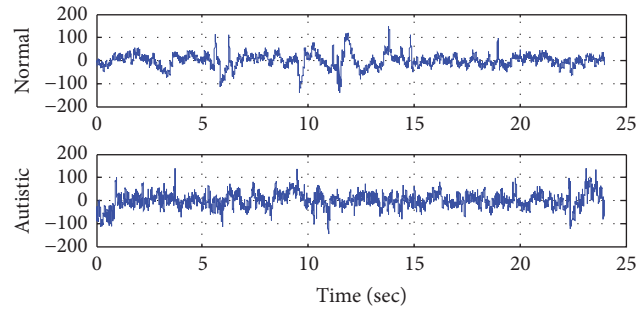

Figure 3: Example of raw normal and autistic EEG signal.

was done in the laboratory of KAU Hospital. We obtained permission to use the data from our college in KAU. To ensure the anonymity of the subjects, all personal information is not published (name, address, etc.). The data is described in more detail in [10]. Dataset was recorded in relaxing state and divided into two groups: the first one is called normal group and contains ten healthy volunteer subjects (all of them are males, age 9–16 years) with normal intelligence and without any mental disorder. The second one is called autistic group and contains nine subjects (six males and three females, age 10–16 years) with autism spectrum disorders. The EEG signals were recorded from subjects scalp in relaxing state by EEG data acquisition system that contains the following components: a g.tec EEG cap with high accuracy Ag/AgCl sensors (electrodes), g.tec USB amplifiers, and BCI2000 software. The data acquisition system has 16 channels, which are labeled based on 10–20 international acquisition system as shown in Figure 2. All electrodes, 16 channels, are used to record the EEG data.

The dataset was filtered by band-pass filter with pass band frequency (0.1–60 Hz) and notch filter with stop band frequency (60 Hz) and all EEG signals were digitized at frequency sampling 256 Hz. The EEG recording varies from around 12 to 40 minutes for autistic subjects with a total up to 173 minutes, while, for normal subjects, recording varies from 5 to 27 minutes with a total up to 148 minutes. Figure 3 shows the typical EEG signals for normal and autistic subjects. For more detailed information about the dataset, please refer to Alhaddad et al. [10].

3.3. Preprocessing. In the preprocessing stage, the acquired EEG signal will be treated through a signal processing block to remove the artifacts and noises in the signal. EEG signals are usually burred with noises derived from many factors such as bad electrode location and dirty hairy leather [13]. Furthermore, the presence of these artifacts is also due to the interference with signals coming from other parts of the body such as heart and muscle activities. It is mandatory to remove all artifacts and enhance the signal to noise ratio by filtering the acquired data. The filtering block aims to remove artifacts, improve the stationary, and increase accuracy. Many alternatives have been explored in [14] as follows:

(i) The first one is using frequency domain transforms such as fast Fourier transform (FFT) or using time-frequency domain such as discrete wavelet transform (DWT).

(ii) Subtracting artifacts from the acquired signal: this technique requires an average artifacts template estimation to be subtracted from the original EEG signal.

(iii) Using the same static filtering for all subjects like finite impulse response (FIR) and infinite impulse response (IIR) filters: FIR filters like Equiripple and Kaiserwin are based on Parks-McClellan algorithm using the Remez exchange algorithm and Chebyshev approximation theory to design filters with an optimal_t between the desired and the actual frequency responses [15].

(iv) Using adaptive filtering techniques: one of the most important interferences in EEG signals is ocular (or eye) artifact. He et al. [16] used adaptive filtering to cancel ocular artifacts by using electrooculogram (EOG) recording, however, providing EOG recording inconvenient and uncomfortable for the patient. The removal of eye-artifact from EEG signal is also presented in [17] by applying the independent component analysis (ICA) to extract information from electrodes close to eyes. Chan et al. in [18] presented an ocular-artifact removal technique based on adaptive filtering using reference signal from the ocular sources components (SCs), which avoids the need for parallel EOG recordings.

In most of the previous works (such as the work of Sheikhani et al. [4, 5] and also Ahmadlou et al. [6–8]), they used artifact-free data. The EEG data is manually prepared or selected by expert. This scheme is good for research and initial analysis, but not for clinical use. The system should be robust and able to automatically tackle noises and artifacts in the EEG signal by necessary preprocessing and artifacts removal. However, if the preprocessing and artifacts removal are not designed properly, they might remove also the useful

information in the EEG leading to inconsistent accuracy values.

Based on the above-mentioned preprocessing design exploration, we used independent component analysis (ICA) for eye-artifact removal and elliptic band-pass filter for filtering. We follow [17] that employed ICA and adaptive filtering to remove ocular-artifacts. Electrodes closed to eye (FP1, FP2, F7, and F8) are used as reference signals for ocular-artifacts removal. After ocular-artifact removal, the signals are then filtered using elliptic band-pass filter. Elliptic band-pass provides better experimental accuracy compared with other filters like Chebyshev type I and type II and Butterworth which are IIR filters [19]. Furthermore, the implementation of the elliptic filter requires less memory and calculation and provides reduced time delays compared with all other FIR and IIR filtering techniques. The proposed computer aided classification system is required to segment each EEG signal into fixed length windows. In our experimental analysis, each EEG signal was segmented into overlapping and nonoverlapping windows.

3.4. Wavelet Decomposition. Wavelet transform techniques are widely used in EEG signal processing for time-frequency decomposition. There are two types of wavelet analysis: continuous wavelet transforms (CWT) and discrete wavelet transforms (DWT). The CWT one is applied for extracting event related potential time-frequency features of the nonstationary EEG signal and combined with the T-student algorithm to choose features that are more effective, resulting in significant classification improvement [20]. However, one obvious drawback of the CWT technique is that it requires excessive calculations. Therefore, we used the DWT in the proposed work to decompose a given EEG signal into approximation and detail coefficients to obtain a first level of decomposition.

The approximation coefficients in every level are further decomposed into next level of approximation and detail coefficients as shown in Figure 4. Selection of decomposition levels and type of mother wavelet are very important in analysis of certain signal using DWT. In this work we used 4-level DWT decomposition with *Daubechies-four* (db4) mother wavelet in order to extract five EEG subbands and to achieve better results in features extraction stage. The features are extracted from the detailed coefficients at various levels (D1–D4) and from the approximation coefficients at the last level (A4). Statistical features, such as mean or standard deviation and entropy value, will be calculated from these five wavelet coefficients (D1, D2, D3, D4, and A4) to construct the feature vector.

The frequency bands of EEG signal corresponding to 4-level DWT decomposition with sampling frequency of 256 Hz on the EEG signal are shown in Table 1. As shown in Table 1, the wavelet coefficients are corresponding to several EEG subbands: *delta* (1–4 Hz), *theta* (4–8 Hz), *alpha* (8–15 Hz), *beta* (15–30 Hz), and *gamma* (30–60 Hz). Different frequency subbands can reveal the characteristics of the time series of EEG signal. Figure 5 shows an example of approximation and details coefficients extracted from an EEG segment of autistic subject.

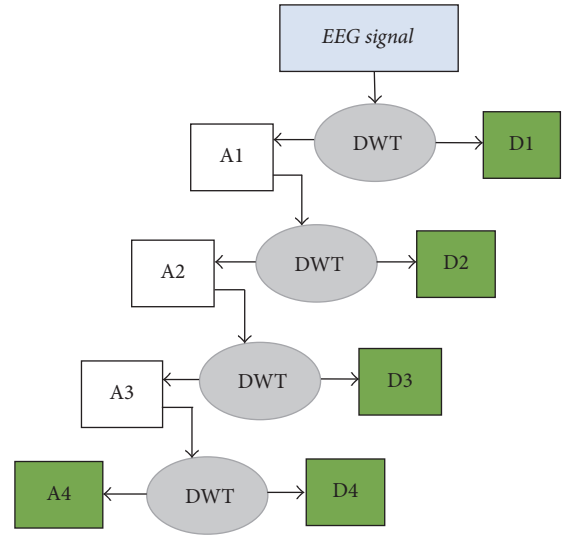

Figure 4: EEG signal decomposition through 4-level DWT.

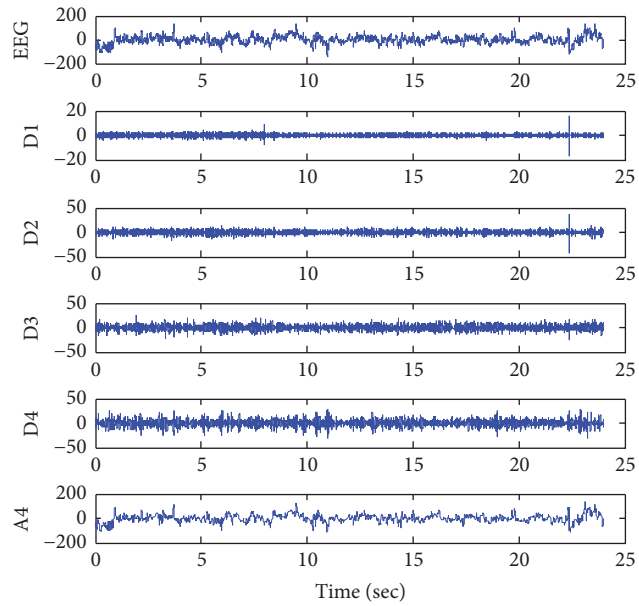

Figure 5: Approximate and details coefficients extracted from an EEG segment of autistic subject.

Table 1: Frequency bands for each wavelet coefficient.

Wavelet coefficients	EEG subbands	Frequency (Hz)
D1	—	128–256
D2	—	64–128
D3	Gamma	32–64
D4	Beta	16–32
A4	Alpha, theta, delta	0–16

3.5. Feature Extraction. Many features can be extracted from the time series of EEG signal such as using statistical features or nonlinear features (entropy). Several previous studies show the effectiveness of using entropy to analyze EEG signal, such

as for epilepsy diagnosis [21, 22] and autism diagnosis [9]. Entropy can be used to measure the complexity, regularity, and the statistic quantification of time series data such as EEG. Bosl et al. [9] have investigated the possibility of using EEG complexity as a biomarker for ASD risk. The abnormal nonlinearity and complexity in the brain signal may reveal brain disorder or cognitive impairments. These motivate us to do further investigation about using entropy as a tool to diagnose ASD.

In this study we investigate five statistical features (mean, standard deviation, variance, skewness, and kurtosis) to be extracted from each DWT output coefficient. There are many types of entropy function. We investigate several entropy functions in this study: log energy and threshold entropies, Renyi entropy, and Shannon entropy. The description for each this entropy is given as follows.

3.5.1. Log Energy Entropy. Log energy entropy is a type of wavelet entropy. We suppose a signal $x = [x_1\ x_2\ x_3\ \cdots\ x_n]$ probability distribution function denoted by $p(x_i)$, where i is the index of signal elements, and the log energy then entropy is defined as

$$H = \sum_{i=1}^{n} \log\left(p_i^{\,2}\right). \tag{1}$$

3.5.2. Threshold Entropy. Threshold entropy is a statistical function used to measure the number of times that the discrete wavelet coefficients are larger than the threshold. The threshold selected in this paper is to equal 0.2. This threshold value is selected based on try-and-error to obtain the best accuracy.

3.5.3. Renyi Entropy. Renyi entropy is a statistical function to measure the diversity and randomness of the discrete signal distribution and to estimate uncertainty of the discrete signal. It can be calculated by the following equation:

$$H = \frac{1}{1-\alpha} \log\left(\sum_{i=1}^{n} p_i^{\alpha}\right), \tag{2}$$

where α is the order of Renyi function, $\alpha \geq 0$ and $\alpha \neq 1$, and p is the probability of the discrete signal variables.

3.5.4. Shannon Entropy. Shannon entropy is a technique used to expect the average value of the information contained in the signal and to measure the average uncertainty of the discrete signal. We used basic Shannon entropy developed by Shannon [23]. For given time series data $X = [x_1\ x_2\ \cdots\ x_N]$, Shannon entropy value can be calculated by the following formula:

$$H = -\sum_{i=1}^{k} (p_i) \log_2 (p_i), \tag{3}$$

where k is the number of unique values in the data (X) and p_i is the probability (or normalized frequency) for these unique values.

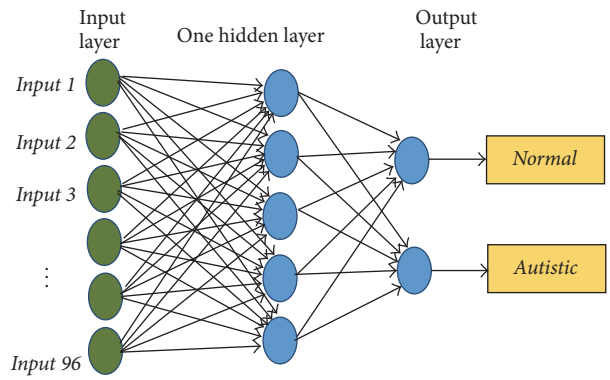

Figure 6: ANN structure.

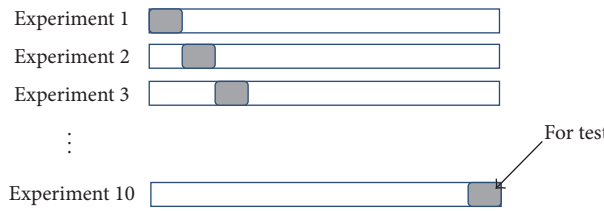

Figure 7: 10-fold cross-validation procedures.

3.6. Artificial Neural Network (ANN) Classifier. ANN is widely used in biomedical engineering field such as modeling, data analysis, diagnostic, and detection. ANN is an information-processing system that is based on simulation of the human cognition process. ANN consisted of several computational neural units connected to each other. In this work, we design an ANN system with one input layer, one hidden layer, and one output layer. Figure 6 shows our neural network structure. The hidden layer is designed with 5 nodes and log-sigmoid transfer function and output layer is designed with 2 nodes and soft-max (normalized exponential) transfer function.

The artificial neural network has to be trained to adjust the connection weights and biases in order to produce the desired mapping. At the training phase, the feature vectors are applied to the network which in turn adjusts its variable parameters, the weights, and biases, to capture the relationship between input patterns and outputs. The performance of ANN depends on the "epochs" process where epochs are the number of iterations of the training vectors used to update the weights of neurons.

3.7. Performance Evaluation. A well-known 10-fold cross-validation is used in all experiments. In the 10-fold cross-validation, the dataset is randomly divided into 10 equal parts (10 subsets). All the subsets are used for the training except one for the test (validation). This process is repeated 10 times (fold). Each subset is exactly used one time for testing data as shown in Figure 7. Thus, we ensure that all the examples in the features matrix are eventually used for both training and testing. The results of 10 times are averaged to produce a single classification performance.

In this current study we use the whole EEG recording for evaluation. The number of samples (or EEG segments) extracted from each subject depends on the segment length. Using one-minute (60 seconds) EEG segment length, we extracted 173 segments from autistic dataset and 148 segments from normal dataset. From these 321 segments, we select randomly 32 segments for testing and the remaining for training. As 10-fold cross-validation, this process is repeated 10 times and the results are averaged.

The performance is compared by considering *receiver operating characteristic* (ROC) parameters such as *true positive* (TP), *true negative* (TN), *false positive* (FP), and *false negative* (FN). True positive (TP) means that EEG segment from autistic subject is correctly diagnosed as autistic class. ROC graph shows the reliability of the classifier. The classification performance is evaluated in terms of sensitivity, specificity, and overall accuracy as in the following formulas:

$$\begin{aligned} \text{Sensitivity} &= \frac{\text{TN}}{\text{FP} + \text{TN}} * 100, \\ \text{Specificity} &= \frac{\text{TP}}{\text{TP} + \text{FN}} * 100, \\ \text{Accuracy} &= \frac{\text{TP} + \text{TN}}{\text{TP} + \text{FP} + \text{TN} + \text{FN}} * 100. \end{aligned} \tag{4}$$

The area under the ROC curve (AUC) is a common metric that can be used to compare different tests. An AUC is a measure of test accuracy. ROC curve describes two-dimensional visualization of ROC curve set for classifiers performance. The easiest possibility is to calculate the area under the ROC curve which is part of the area of the unit square. Consequently the value of AUC will always satisfy the following inequalities:

$$0 \leq \text{AUC} \leq 1. \tag{5}$$

It is clear that if the AUC is close to 1 (area of unit square) AUC indicates very good test.

4. Results and Discussion

The experiments performed have two different scenarios. In the first one, the DWT output with statistical features (mean, standard deviation, etc.) directly as the input for the ANN classifier was used, while, in the second one, different entropy function in the DWT output, where the entropy values are then used as input for ANN classifier, was applied. After selecting the best feature extraction method, we performed some optimization techniques for further increasing of the accuracy. The experiments are carried out by using MATLAB 2013a software on windows 8 PC with Intel core i5 processor 2.30 MHz.

4.1. DWT with Statistical Features (without Entropy). In the first scenario, the discrete wavelet transform (DWT) technique and artificial neural network (ANN) classifier are used to detect the autistic signal without entropy function. Table 2 summarizes the results and shows the classification accuracy rates for our approach, based on many statistical features such as mean, standard deviation, variance, skewness, and kurtosis. Figure 8 shows the ROC curves for ANN classifier based on the previous statistical features. From Table 2 and Figure 8, it is clear that the classification accuracy is low. In the next step, we tried to apply several entropy functions to increase the accuracy.

Table 2: The classification accuracy rates with the statistical features.

Statistical features	Accuracy (%)
Mean	78
Standard deviation	96
Variance	70
Skewness	70
Kurtosis	79

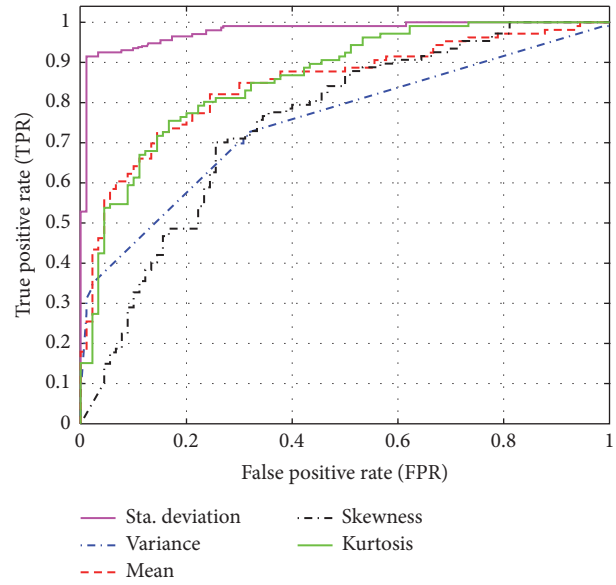

Figure 8: ROC curve with the statistical features.

4.2. DWT with Entropy Functions. In this scenario, DWT with different entropy functions to extract EEG feature were combined. We investigate four different entropy functions as described in the previous section: log energy and threshold entropies, Renyi entropy, and Shannon entropy. Table 3 summarized the average classification accuracy according to the different types of entropies functions used. From Table 3 and Figure 9, it is clear that the best function to extract the features of an EEG signal is Shannon entropy.

4.3. Optimization Process. After selecting DWT + Shannon entropy as the best feature extraction method, we performed some optimization to further increase the accuracy. Optimization process is carried out by the following steps: (a) selecting the best segment length, (b) selecting best frequency band, and (c) testing between nonoverlapping and overlapping segments.

Table 3: Classification accuracy with different entropy functions.

Entropy functions	Accuracy (%)
Log energy	83
Threshold	88.6
Renyi entropy	83.2
Shannon entropy	98.4

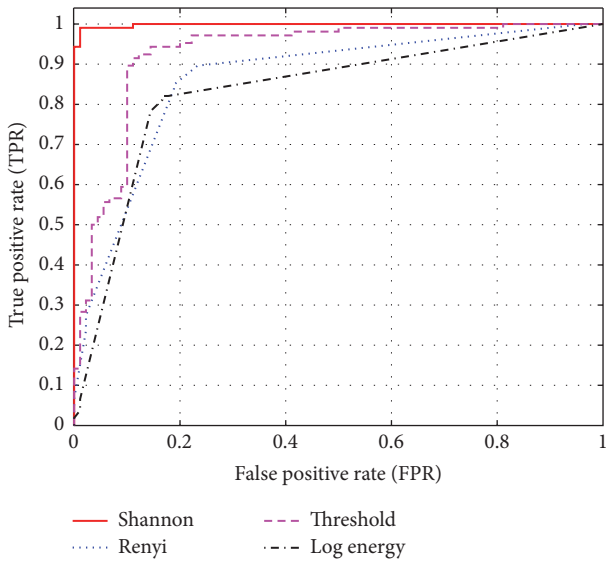

Figure 9: ROC curve with different entropy function.

Table 4: The average classification accuracy for different segments lengths.

Segment length (S)	Accuracy (%)
10	96.8
20	97.2
30	97.5
40	98.0
50	*98.6*
60	98.1
90	97.6
120	95.1
150	93.7
180	91.6

4.3.1. Selecting the Best Segment Length. In the previous sections, the segment length is fixed to be ten seconds. In this section, we implemented our proposed approach with different window sizes (segment length). Table 4 shows the classification accuracy obtained by our proposed approach on the 10-fold cross-validation method. The best result was achieved at segment length of 50 seconds with average accuracy up to 98.6%. We obtained lower accuracy using EEG segment shorter or longer than 50 seconds.

4.3.2. Selecting Best Frequency Band (Wavelet Coefficients). In this section, we investigated the effect of wavelet coefficients on the classification accuracy. In the previous sections, all five wavelet coefficients (D1–D4 and A4) and the original EEG segment are used for classification. In this section, we investigate the accuracy using different combination of wavelet coefficients. Table 5 shows the summary of the results. It is clear that the best result was obtained using combination of all detail coefficients (D1 + D2 + D3 + D4).

Table 5: The effect of combination of wavelet coefficient on the classification performance.

Combination of wavelet coefficients (freq. band)	Accuracy (%)
D2 (64–128 Hz)	94.8
D3 (32–64 Hz)	94.8
D4 (16–32 Hz)	94.6
A4 (0–16 Hz)	88
Original EEG + D1 + D2 + D3 + D4 + A4	98.6
D1 + D2 + D3 + D4 + A4	98.4
D2 + D3 + D4 + A4	97.3
D1 + D2 + D3 + D4	*98.9*
D1 + D2 + D3	97.8
D2 + D3 + D4	96.7
D2 + D3	95.8
D1 + D2	92.7

Table 6: The classification accuracy with overlapping (half-segment).

Segment length (S)	Accuracy (%)
10	98.4
20	98.6
30	98.7
40	99.4
50	99.7
60	99.6
90	99.5
120	99.3
150	99.3
180	99.1

4.3.3. Testing the Effect of Nonoverlapping and Overlapping Segments. In this section, we studied the effect of overlapping segment on the classification accuracy. In (a), the all segments were nonoverlapping but in this section all the segments will be overlapped with half-segment, and window size at one minute and all detail bands (D1 + D2 + D3 + D4) were selected. By comparing Table 4 (nonoverlapping) and Table 6 (with overlapping), it is obvious that better results are obtained using overlapping EEG segment. The highest accuracy (99.8%) is obtained when the length of EEG segment is equal to 60 seconds with half-segment overlapping.

Figure 10 shows the ROC curves for ANN classifier when we used an entropy (En) function to improve the accuracy based on overlapping and nonoverlapping segments and one-minute (50 seconds) segment length. Therefore, Figure 10

Table 7: Summary of final results of the proposed method.

Segments	Frequency bands	Length of segment	Feature extraction	Classifier	Cross-validation method	Classification accuracy average
Nonoverlapping	D1 + D2 + D3 + D4	50 seconds	DWT-En	ANN	10-fold	98.6%
Overlapping (with half-segment)						99.7%

Table 8: Several EEG-based CAD of autism spectrum disorder.

Author	Feature extraction	Classifier	Dataset	Acc (%)
Sheikhani et al. 2008 [4]	STFT, coherence	KNN	Own dataset	82.4
Ahmadlou et al. 2010 [6]	Wavelet, fractal dimension (FD)	RBNN	Own (Iranian dataset)	90
Bosl et al. 2011 [9]	Modified multiscale entropy (MMSE)	SVM	Own (USA)	70–100
Sheikhani et al. 2012 [5]	STFT, coherence	KNN	Own dataset	96.4
Ahmadlou et al. 2012 [7]	Wavelet, visibility graph (VG)	EPNN	Iranian dataset	95.5
Ahmadlou et al. 2012 [8]	Wavelet, fuzzy SL	EPNN	Iranian dataset	95.5
Alhaddad et al. 2012 [10]	FFT	FLDA	Own (KSA dataset)	90
Our work	DWT, Shannon entropy	ANN	KSA dataset	99.7

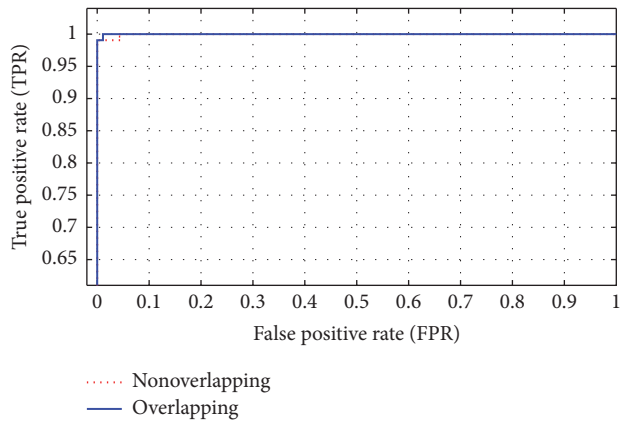

Figure 10: ROC curve for ANN classifier based on overlapping and nonoverlapping segments.

shows that the area under ROC curve is almost one and the accuracy is close to the desired accuracy.

From the experimental results, we found that the good results are obtained from our approach when we used entropy function to get the features of an EEG signal. These results are obtained when the length of segment is one minute and when we choose the detail bands (D1 + D2 + D3 + D4) extracted by DWT and entropy function. All EEG signals are segmented by two ways: nonoverlapping and overlapping segments, but the best results are obtained at overlapping segments with accuracy up to 99.71%. Table 7 summarized the best results. In the all previous results we did not employ ocular-artifact removal algorithm because it is very slow. However, when we employed the ocular-artifact removal algorithm, the accuracy is decreased up to 94%. This means that our artifact removal algorithm should be designed more properly and more investigation is needed.

Table 8 shows the comparison of our proposed method result with the existing methods. Detailed information about the existing methods has been presented in Section 2. It should be noted that most of proposed method is validated by different dataset that makes fair comparison for all methods slightly difficult. Tested using the same dataset, our method achieved higher accuracy (99.71%) than the method proposed by Alhaddad et al. [10] (90%). This shows the effectiveness of the proposed method for autism diagnosis. Another advantage of our proposed method is its simplicity. We use simple Shannon entropy that basically employs only arithmetic and log operations.

5. Conclusion

A computer aided diagnosis (CAD) system has a tremendous potential to assist clinicians during the diagnosis process to save the time and increase the diagnosis accuracy. In this study, a CAD system was proposed in order to classify automatically autistic and nonautistic subject based on EEG signal analysis. Firstly, only discrete wavelet transform (DWT) with statistical features (mean, standard deviation, variance, skewness, and kurtosis) was employed to extract the features of EEG signal. The artificial neural network ANN classifier is used to classify the subject based on the extracted features. However with only DWT and statistical features for feature extraction the classification accuracy is low. We then investigated several entropy functions for feature extraction: log energy and threshold entropies, Renyi entropy, and Shannon entropy.

The highest classification accuracy is obtained with combination of DWT and Shannon entropy for feature extraction. After some optimization process we obtained classification accuracy up to 99.71%. The processing time for feature extraction and classification was also fast enough due to the simplicity of the proposed method. Further research will include testing the proposed method using larger dataset. Adaptive learning to improve the CAD system performance over the time will be investigated as well. We consider also

doing more investigation on preprocessing step, especially in eye-artifact removal, in our future work.

Conflicts of Interest

The authors declare that they have no conflicts of interest.

Acknowledgments

This research work was supported by the research project that is funded by King Abdulaziz City for Science and Technology (KACST), Saudi Arabia, with Grant no. AT-34-147. The authors, also, would like to thank KAU Brain Computer Interface (BCI) Group for providing their own autism dataset.

References

[1] S. Bhat, U. R. Acharya, H. Adeli, G. M. Bairy, and A. Adeli, "Autism: cause factors, early diagnosis and therapies," *Reviews in the Neurosciences*, vol. 25, no. 6, pp. 841–850, 2014.

[2] American Psychiatric Association, *Diagnostic and Statistical Manual of Mental Disorders DMS-5*, American Psychiatric Association, Arlington, Va, USA, 5th edition, 2013.

[3] M. Ahmadlou and H. Adeli, "Electroencephalograms in diagnosis of autism," in *Comprehensive Guide to Autism*, V. B. Patel, V. R. Preedy, and C. R. Martin, Eds., pp. 327–343, Springer, New York, NY, USA, 2014.

[4] A. Sheikhani, H. Behnam, M. R. Mohammade, M. Noroozian, and P. Golabi, "Connectivity analysis of quantitative Electroencephalogram background activity in Autism disorders with short time Fourier transform and Coherence values," in *Proceedings of the 1st International Congress on Image and Signal Processing (CISP '08)*, pp. 207–212, IEEE, Hainan, China, May 2008.

[5] A. Sheikhani, H. Behnam, M. R. Mohammadi, M. Noroozian, and M. Mohamamadi, "Detection of abnormalities for diagnosing of children with autism disorders using of quantitative electroencephalography analysis," *Journal of Medical Systems*, vol. 36, no. 2, pp. 957–963, 2012.

[6] M. Ahmadlou, H. Adeli, and A. Adeli, "Fractality and a wavelet-chaos-neural network methodology for EEG-based diagnosis of autistic spectrum disorder," *Journal of Clinical Neurophysiology*, vol. 27, no. 5, pp. 328–333, 2010.

[7] M. Ahmadlou, H. Adeli, and A. Adeli, "Improved visibility graph fractality with application for the diagnosis of autism spectrum disorder," *Physica A: Statistical Mechanics and its Applications*, vol. 391, no. 20, pp. 4720–4726, 2012.

[8] M. Ahmadlou, H. Adeli, and A. Adeli, "Fuzzy Synchronization Likelihood-wavelet methodology for diagnosis of autism spectrum disorder," *Journal of Neuroscience Methods*, vol. 211, no. 2, pp. 203–209, 2012.

[9] W. Bosl, A. Tierney, H. Tager-Flusberg, and C. Nelson, "EEG complexity as a biomarker for autism spectrum disorder risk," *BMC Medicine*, vol. 9, article 18, 2011.

[10] M. J. Alhaddad, M. I. Kamel, H. M. Malibary et al., "Diagnosis autism by fisher linear discriminant analysis FLDA via EEG," *International Journal of Bio-Science and Bio-Technology*, vol. 4, no. 2, pp. 45–54, 2012.

[11] J. Fan, J. W. Wade, D. Bian et al., "A Step towards EEG-based brain computer interface for autism intervention," in *Proceedings of the 37th Annual International Conference of the IEEE Engineering in Medicine and Biology Society (EMBC '15)*, pp. 3767–3770, IEEE, Milan, Italy, August 2015.

[12] E. A. Alsaggaf and M. I. Kamel, "Using EEGs to diagnose autism disorder by classification algorithm," *Life Science Journal*, vol. 11, no. 6, article no. 40, pp. 305–308, 2014.

[13] K.-K. Shyu, P.-L. Lee, M.-H. Lee, M.-H. Lin, R.-J. Lai, and Y.-J. Chiu, "Development of a low-cost FPGA-based SSVEP BCI multimedia control system," *IEEE Transactions on Biomedical Circuits and Systems*, vol. 4, no. 2, pp. 125–132, 2010.

[14] K. Belwafi, R. Djemal, F. Ghaffari, and O. Romain, "An adaptive EEG filtering approach to maximize the classification accuracy in motor imagery," in *Proceedings of the IEEE Symposium on Computational Intelligence, Cognitive Algorithms, Mind, and Brain, (CCMB '14)*, pp. 121–126, IEEE, December 2014.

[15] M. S. A. Megat Ali, M. N. Taib, N. M. Tahir, A. H. Jahidin, and M. Yassin, "EEG sub-band spectral centroid frequencies extraction based on Hamming and equiripple filters: a comparative study," in *Proceedings of the IEEE 10th International Colloquium on Signal Processing and Its Applications (CSPA '14)*, pp. 199–203, IEEE, Kuala Lumpur, Malaysia, March 2014.

[16] P. He, G. Wilson, and C. Russell, "Removal of ocular artifacts from electro-encephalogram by adaptive filtering," *Medical and Biological Engineering and Computing*, vol. 42, no. 3, pp. 407–412, 2004.

[17] C. Guerrero-Mosquera and A. N. Vazquez, "Automatic removal of ocular artifacts from EEG data using adaptive filtering and independent component analysis," in *Proceedings of the 17th European Signal Processing Conference, EUSIPCO 2009*, pp. 2317–2321, August 2009.

[18] H.-L. Chan, Y.-T. Tsai, L.-F. Meng, and T. Wu, "The removal of ocular artifacts from EEG signals using adaptive filters based on ocular source components," *Annals of Biomedical Engineering*, vol. 38, no. 11, pp. 3489–3499, 2010.

[19] Y. Hashimoto and J. Ushiba, "EEG-based classification of imaginary left and right foot movements using beta rebound," *Clinical Neurophysiology*, vol. 124, no. 11, pp. 2153–2160, 2013.

[20] V. Bostanov, "BCI competition 2003—data sets Ib and IIb: feature extraction from event-related brain potentials with the continuous wavelet transform and the t-value scalogram," *IEEE Transactions on Biomedical Engineering*, vol. 51, no. 6, pp. 1057–1061, 2004.

[21] N. Kannathal, M. L. Choo, U. R. Acharya, and P. K. Sadasivan, "Entropies for detection of epilepsy in EEG," *Computer Methods and Programs in Biomedicine*, vol. 80, no. 3, pp. 187–194, 2005.

[22] K. AlSharabi, S. Ibrahim, R. Djemal, and A. Alsuwailem, "A DWT-entropy-ANN based architecture for epilepsy diagnosis using EEG signals," in *Proceedings of the 2nd International Conference on Advanced Technologies for Signal and Image Processing (ATSIP '16)*, pp. 288–291, Monastir, Tunisia, March 2016.

[23] C. E. Shannon, "A mathematical theory of communication," *The Bell System Technical Journal*, vol. 27, pp. 379–423, 1948.

Hindawi
BioMed Research International
Volume 2017, Article ID 6820482, 11 pages
https://doi.org/10.1155/2017/6820482

Research Article

Evaluation of a Compact Hybrid Brain-Computer Interface System

Jaeyoung Shin,[1] Klaus-Robert Müller,[1,2] Christoph H. Schmitz,[3] Do-Won Kim,[1,4] and Han-Jeong Hwang[5]

[1]*Machine Learning Group, Berlin Institute of Technology, Berlin, Germany*
[2]*Department of Brain and Cognitive Engineering, Korea University, Seoul, Republic of Korea*
[3]*NIRx Medizintechnik GmbH, Berlin, Germany*
[4]*Department of Biomedical Engineering, Chonnam National University, Yeosu, Republic of Korea*
[5]*Department of Medical IT Convergence Engineering, Kumoh National Institute of Technology, Gumi, Republic of Korea*

Correspondence should be addressed to Do-Won Kim; do-won.kim@campus.tu-berlin.de and Han-Jeong Hwang; h2j@kumoh.ac.kr

Received 28 July 2016; Accepted 20 October 2016; Published 8 March 2017

Academic Editor: Maria G. Knyazeva

We realized a compact hybrid brain-computer interface (BCI) system by integrating a portable near-infrared spectroscopy (NIRS) device with an economical electroencephalography (EEG) system. The NIRS array was located on the subjects' forehead, covering the prefrontal area. The EEG electrodes were distributed over the frontal, motor/temporal, and parietal areas. The experimental paradigm involved a Stroop word-picture matching test in combination with mental arithmetic (MA) and baseline (BL) tasks, in which the subjects were asked to perform either MA or BL in response to congruent or incongruent conditions, respectively. We compared the classification accuracies of each of the modalities (NIRS or EEG) with that of the hybrid system. We showed that the hybrid system outperforms the unimodal EEG and NIRS systems by 6.2% and 2.5%, respectively. Since the proposed hybrid system is based on portable platforms, it is not confined to a laboratory environment and has the potential to be used in real-life situations, such as in neurorehabilitation.

1. Introduction

Brain-computer interfaces (BCIs) assist people who cannot use their muscles to communicate with the external environment. One of the early uses of BCIs was to aid communication with people who have severe impairment of muscle movement, for instance, late-stage ("locked-in") patients with amyotrophic lateral sclerosis (ALS, also known as Lou Gehrig's disease) [1]. Thanks to the rapid advance of neuroimaging modalities, BCI technology has broadened its application areas into the game industry, entertainment, and social neuroscience, for example, by providing alternative communication methods [2–6].

BCIs can be established by means of several brain imaging modalities, such as near-infrared spectroscopy (NIRS) [7], electroencephalography (EEG) [8], functional magnetic resonance imaging (fMRI) [9], magnetoencephalography (MEG) [10], and electrocorticogram (ECoG) [11]. Invasive BCI systems, such as ECoG-based BCIs, generally involve risks associated with the surgical operation for implanting microelectrodes in the brain and are thus limited for many potential BCI users. MEG- and fMRI-based systems only allow stationary and time-limited use due to their cost, complexity, size, and restricting environment. More compact and economical neuroimaging technologies, such as EEG or NIRS, hold the promise of providing lightweight, portable BCI systems for continuous use in more unrestrained and natural settings outside the lab, creating the opportunity for many new applications, such as neurorehabilitation.

EEG-based BCI systems have been most commonly used for rehabilitation training and for providing communication and control channels to individuals with limited motor functions [12–15]. A lightweight EEG-based BCI system with acceptable performance has been established but is often

prone to drawbacks such as low signal-to-noise ratio (SNR) and susceptibility to motion artifacts and volume conduction [16–19].

NIRS is an emerging neuroimaging modality that records the cortical hemodynamic response based on changes in local optical transmission as measured by pairs of near-infrared light sources and detectors placed on the scalp surface [20]. This method is less sensitive to motion artifacts compared to EEG [21]. NIRS has by now been recognized as a promising neuroimaging modality that has overcome some of the drawbacks of EEG [22]. Recently, portable and cost-effective NIRS systems have become available [23] and have been actively used in the field of rehabilitation [24–26]. A defining characteristic of NIRS is the inherent delay of the measured hemodynamic response on the order of several seconds (typically > 5 s) [27], which limits its use in time-critical BCI applications and which requires a relatively long interstimulus interval (ISI) to gain task-relevant responses of reasonable quality. The resulting increase of the experimental time not only drops the overall information transfer rate usually quantified by bit rate per minute but can also exhaust the NIRS-based BCI users more easily [28].

To overcome the disadvantages of these individual methods, NIRS-EEG hybrid (HYB) BCI systems have been suggested to take advantage of superior performance provided by combining both modalities [29–36]. However, despite the comparatively low cost and compactness of both EEG and NIRS systems, the experimental setup of a hybrid system still poses practical challenges, even in a laboratory environment. Until now, each system required an individual amplifier, recording platform, and its own leads, which need to be affixed to the scalp with reliable optical and electrical contact. This poses added challenges and leads to generally increased setup times for HYB systems [32, 37, 38].

To date, to the best of our knowledge, no study that aims to reduce the complexity of hybrid NIRS-EEG BCI systems and validate their performance has been reported. In this study, we implement a lightweight and portable NIRS-EEG hybrid instrument and demonstrate its use for a hybrid BCI that has the potential for mobile and continuous use. We recorded NIRS and EEG signals simultaneously while the subject performed a word-picture matching test using simple mental arithmetic (MA), which is similar to the task in Power et al. [39]. The proposed hybrid system was validated by comparing its classification accuracies to those of the unimodal systems (EEG and NIRS).

2. Materials and Methods

2.1. Subjects. Eleven right-handed healthy subjects participated voluntarily in the experiment (1 male and 10 females, average age: 25.7 ± 3.2 years [mean ± standard deviation]). None of them had a history of neurological, psychiatric, or other disorders that might affect the experimental results. A written experiment summary was given to the participants, and each participant signed a written consent form prior to the experiment and obtained a financial reimbursement after the experiment. This study was approved by the Ethics Committee of the Institute of Psychology and Ergonomics, Berlin Institute of Technology (approval number: SH_01_20150330).

2.2. Apparatus. In the experiment, 14 EEG electrodes and eight NIRS probes (5 sources and 3 detectors) were placed on the scalp by means of a stretchy fabric cap (EASYCAP GmbH, Herrsching am Ammersee, Germany). The EEG system used was an EPOC device (Emotiv Inc., San Francisco, USA) and was selected for easy setup, wireless form factor, and, in particular, its economical price. The system had been verified in previous studies to show comparable performance to other commercial EEG devices with much higher prices [40–49].

In its original state, the EPOC uses a rigid headpiece of headphone-like appearance, which would not have allowed easy integration with NIRS. In a recent study, Debener et al. [50] demonstrated performance enhancement of the EPOC system by replacing the original head gear with a traditional fabric cap and ring electrodes. Following Debener et al.'s instructions, we dismantled the original hardware and moved the amplifier electronics into a small custom plastic case attached to the back of the cap. To provide good skin contact, we used passive Ag-AgCl ring electrodes (EASYCAP GmbH) with conductive gel. To measure task-related brain activation, a custom channel layout was chosen according to the international 10-10 system [51]. Fourteen electrodes were placed on frontal (F7, F3, Fz, F4, and F8), motor/temporal (C3 and C4/T7 and T8), and parietal (P7, P3, Pz, P4, and P8) areas. Reference and ground electrodes were attached on the left (TP9) and right (TP10) mastoids, respectively. The EEG signals were sampled at a 128 Hz sampling rate with provided software named "test bench" from the manufacturer. A portable NIRS system (NIRSport, NIRx Medical Technologies, NY, USA) was used to map hemodynamic responses. Five sources and three detectors were located over the prefrontal area around Fpz, Fp1, and Fp2 with an interoptode distance of 30 mm. Adjacent pairs of source and detector optodes comprised nine physical channels. NIRS signals were recorded at a 12.5 Hz sampling rate with NIRStar software, provided by the manufacturer. Figure 1 shows the channel layout of NIRS optodes and EEG electrodes and the headgear setup on a phantom head.

2.3. Experimental Protocol. Subjects sat still in a comfortable armchair in front of a 24-inch LCD monitor. NIRS and EEG signals were acquired simultaneously from each subject while performing MA as a cognitive task and rest condition as a baseline task (BL). During MA, the subjects were instructed to subtract a single-digit number (between 6 and 9) from a random three-digit number and subtract it again from the result over and over as fast as possible until the trial ended (e.g., 544 − 7 = 537, 537 − 7 = 530, and 530 − 7 = 523). During the BL task, they were instructed not to think anything to maintain a low cognitive load state, while moving the body as little as possible. Even though the subject was instructed not to move the head and body, unintended subtle movement and unavoidable ocular movement might occur during the experiment. The quality of the EEG signal is easily affected

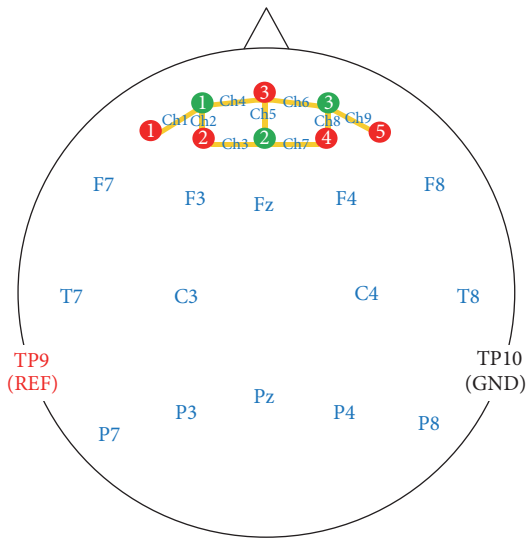

(a)

(b)

FIGURE 1: Channel layout of near-infrared spectroscopy (NIRS; Ch1–Ch9) and electroencephalography (EEG; (a)) and a headgear setup on a phantom head (b). Five sources (red circles, 1–5) and three detectors (green circles, 1–3) are located around Fp1, Fpz, and Fp2. Fourteen electrodes are located at Fz, F3, F4, F7, F8, C3, C4, T7, T8, Pz, P3, P4, P7, and P8. Reference and ground electrodes are located on TP9 and TP10, respectively.

by such artifacts, while the quality of the NIRS signal is less vulnerable to them.

Figure 2 presents a timing sequence of a single trial. The experiment was designed as a Stroop word-picture test. A similar task was used in Power et al. [39]. A single trial was composed of task presentation (congruent or incongruent task, 2 s), followed by initial MA problem presentation (2 s), task period (10 s), and rest period (15–17 s). At the task presentation stage, two pictures (e.g., animals, fruits, and sport activities) were displayed on the screen side by side, and the name of either of the two objects was shown on the top of the screen. First, the left picture was highlighted using a red box. After 2 s, a random MA problem replaced the word. After 2 s, the problem was replaced by a black fixation cross with a short beep (250 ms) and the task period started. After the task period, a rest period with a random length of 15–17 s started with a short beep (250 ms), in which a large black fixation cross was displayed in the middle of screen. After the trial was finished, the same procedure was iterated with the right picture highlighted instead of the left one. If the displayed name matched the picture (congruent), subjects were asked to perform the MA task. On the other hand, if they were not matched (incongruent), subjects were asked to try not to think anything as a baseline task during the task period. During the rest period, subjects were instructed to relax and think nothing (BL). Therefore, congruent and incongruent trials were presented in a row as a pair, either "congruent first-incongruent later" or "incongruent first-congruent later," for the same picture set. They were presented in a random order. A single trial consisted of both MA and BL trials, and a session consisted of 10 trials (i.e., 10 MA + 10 BL). After finishing a single session, a short break was given in which subjects were allowed to move their bodies but not to leave the seat. The session was repeated three times constituting three sessions. Overall, although the number of "congruent first-incongruent later" and "incongruent first-congruent later" trials might not be equal within each session, a total of 30 MA and 30 BL were acquired across the three sessions.

2.4. Data Analysis

2.4.1. Point-Biserial Correlation Coefficient. A point-biserial correlation coefficient (*r-value*) is a measure of correlation between a dichotomous variable and a continuous variable. The *r-value* was estimated to determine the spectral and spatial distribution of separability. The *r-value* at the time of interest is defined as [52]

$$r(t) = \frac{\sqrt{N_1 \cdot N_2}}{N_1 + N_2} \frac{E[x \mid y = 1] - E[x \mid y = 2]}{\sigma[x \mid y \in \{1, 2\}]}, \quad (1)$$

where $t \in [1, 2, \ldots, T]$ and t is the length of the time of interest and N_1 and N_2 denote the total number of trials of class 1 and class 2 (MA and BL in this study), respectively. x denotes the data points that belong to class label $y = 1$ or 2. $E[\cdot]$ and $\sigma[\cdot]$ are mean and standard deviation operators, respectively. The r-value was also utilized to calculate the most discriminative frequency band for the EEG feature extraction and a spatial distribution of separability for the NIRS temporal response.

2.4.2. Preprocessing. Offline EEG and NIRS data analyses were performed using MATLAB 2013b (The MathWorks, Natick, USA), in particular with the EEGLAB toolbox and BBCI toolbox [2, 53]. For NIRS data, raw light intensity signals were band-pass filtered (3rd-order Butterworth zero-phase filter with a passband of 0.01–0.2 Hz). Concentration changes of oxyhemoglobin (Δ[HbO]) and deoxyhemoglobin (Δ[HbR]) were then calculated according to the modified Lambert–Beer law [54, 55]. Baseline correction was performed using 5 s of prestimulus period. For EEG, the data

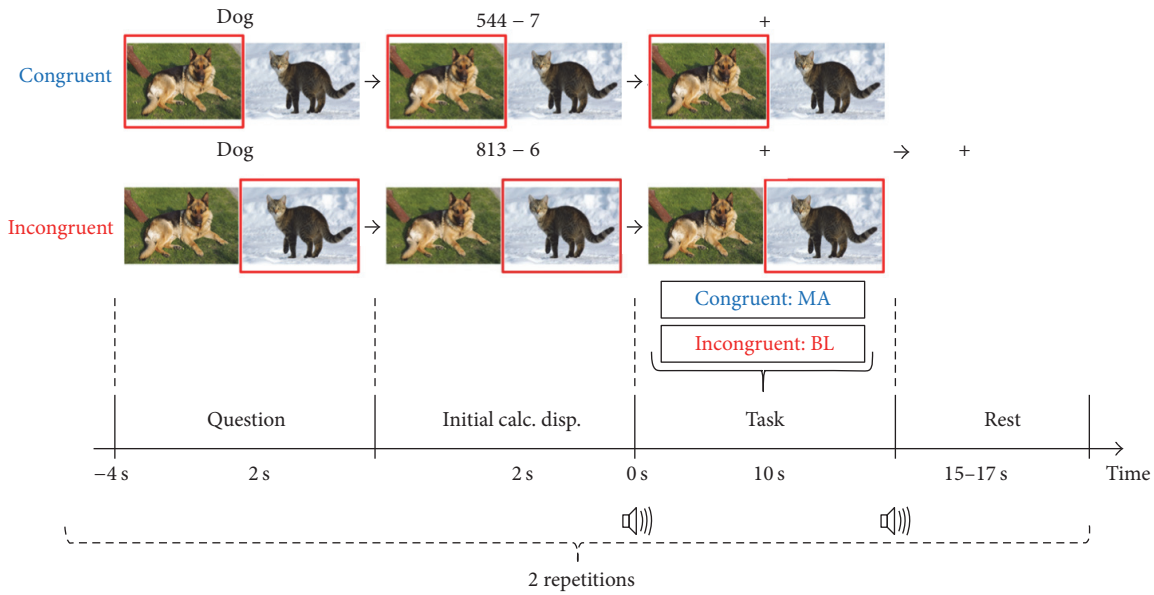

FIGURE 2: Timing sequence diagram of a single trial for the Stroop word-picture matching test. The whole process was done twice consecutively for congruent and incongruent tasks, which comprised a single trial. "Congruent first-incongruent later" and "incongruent first-congruent later" tasks were randomly presented. At the task presentation, the left- or right-side picture was sequentially selected. The name of either picture was displayed for 2 s. At initial mental arithmetic (MA) problem presentation, an example of a three-digit number minus a one-digit number (6 to 9) was shown instead of the name for 2 s. In a task period starting with a short beep (250 ms) and black fixation cross, subjects performed MA or baseline (BL) task if the word and picture were matched (congruent) or mismatched (incongruent), respectively. After 10 s, a rest period started with a short beep (250 ms), and a large black fixation cross was displayed at the center of the screen.

were rereferenced according to the common average reference method. Subject-dependent band-pass filtering (3rd-order Butterworth zero-phase filter) was performed using the point-biserial correlation coefficient. The subject-dependent passbands showing the highest *r-values* were determined by a heuristic method [56]. The passbands were selected in α- (1 of 14 subjects), β- (2 of 14), θ- to α- (4 of 14), α- to β- (3 of 14), and θ- to β-bands (4 of 14).

2.4.3. Classification. We performed a single trial classification of NIRS and EEG data to discriminate MA- and BL-related responses [29, 57]. To examine classification accuracy change with respect to different time windows, a sliding time window was used to extract the features of both modalities (window size: 5 s, step size: 1 s) between −5 and 25 s from stimulus onset to account for the hemodynamic delay with respect to brain activation [58]. The relatively long window size was chosen to consider the relatively slow hemodynamic responses compared to EEG, thereby increasing the performance of each modality as well as the HYB system. Both NIRS and EEG features were calculated for each sliding time window. All NIRS and EEG channels were used for feature extraction and classification (9 and 14 channels). For NIRS, the mean values and average slopes of Δ[HbO] and Δ[HbR] of each channel were calculated as NIRS features, which are widely used for NIRS data classification [7]. For EEG, the common spatial pattern (CSP) algorithm was applied to the preprocessed EEG data. EEG features were calculated as the log-scaled variance of CSP-filtered data (first and last 2 components containing the most discriminative information). The feature vectors of each sliding time window were independently used for the classification. Tenfold cross-validation was performed 10 times for each sliding window.

For classification, shrinkage linear discriminant analysis (sLDA) was used [52]. The shrinkage parameter was estimated as described previously [59, 60]. In order to confirm the advantage of adding EEG data to NIRS data, the correct answer ratio was estimated not only for the EEG or NIRS data individually but also for a combination of both modalities. For the latter case, a metaclassification approach based on sLDA was used. Normalization is not necessary when concatenating EEG and NIRS features for metaclassification. This is because, for metaclassification, both EEG and NIRS individual classifiers yield LDA-projected EEG and NIRS features with the same scale, which are combined for the input of the metaclassifier. The detailed information regarding the metaclassifier is provided in Fazli et al. [32].

3. Results

3.1. Grand Average of EEG and NIRS Data Patterns. Grand average event-related (de)synchronization (ERD/ERS) patterns evoked by MA, BL, and their difference (i.e., MA-BL) at the two midline sites (Fz and Pz) in the frequency band of 4–35 Hz (theta to beta band) are shown in Figure 3. Fz and Pz represent frontal and parietal areas, respectively. Two dotted lines at $t = 0$ and 10 s denote the onset of task and rest time, respectively. During MA (0–10 s), ERDs were broadly observed ranging from θ- to β-band, while clear ERS patterns appeared in a narrow band around 10 Hz. On the other

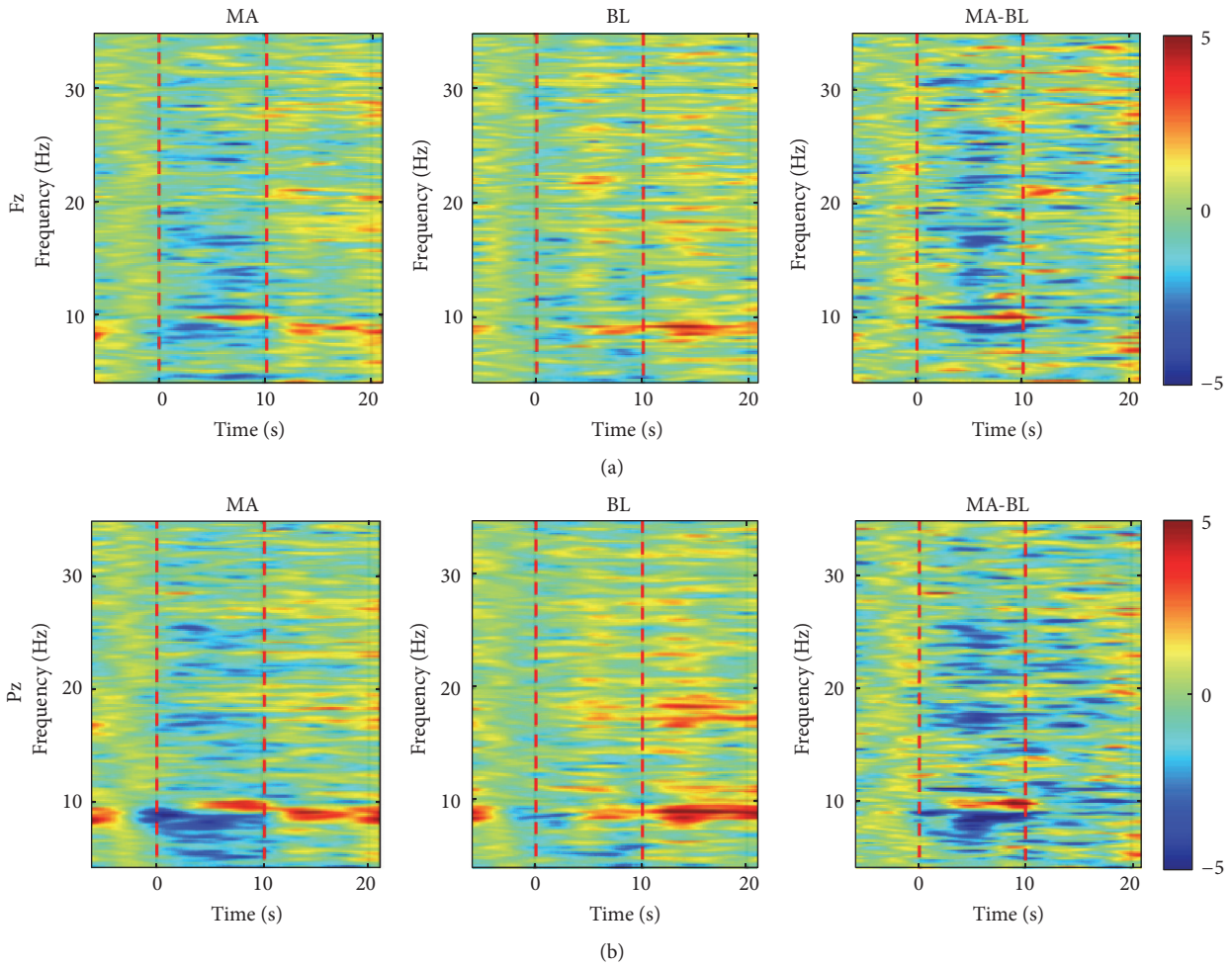

Figure 3: Grand average time-frequency analysis results for event-related (de)synchronization (ERD/ERS) in the frequency band of 4–35 Hz in frontal ((a) MA, BL, and MA-BL at Fz from left to right) and parietal areas ((b) MA, BL, and MA-BL at Pz from left to right).

hand, fewer ERD/ERS patterns were observed during BL task. Thus, the distinct difference of ERD/ERS between MA and BL was widely observed in the corresponding frequency band. In Figure 3, α-band or β-band (8–30 Hz) is included in the passband of 12 (85.7%) or 9 (64.3%) of 14 subjects, respectively. Figures 4(a)–4(d) show the grand average of CSP patterns that correspond to the eigenvectors for the highest and lowest two eigenvalues (λ) for CSP [56]. Note that frontal and parietal areas are mainly associated with task-relevant activation. Figures 5(a) and 5(b) show the grand average time courses of the NIRS responses and the time-dependent scalp plot of $\log(p)$ significance values based on the *r-value*, respectively. The red and blue solid lines in Figure 5(a) correspond to MA-related and BL-related activation, respectively, with $\log(p)$ significance values indicated in the horizontal color bar below the curve plots. Two channels with the highest significance for each chromophore are presented, where Δ[HbO] gradually decreases and Δ[HbR] increases after onset time and they start returning to the baseline after about 15 s during MA. Compared to MA, no distinct responses are observed during BL task. Figure 5(b) represents spatial maps of $\log(p)$ significance values for the NIRS measurements. The color bar on the right side indicates the scale of $\log(p)$. In the color bar, red (positive) and blue (negative) colors indicate the higher values of MA-related data and BL-related data, respectively. In the scalp plot, significant Δ[HbR] patterns on the left hemisphere are mostly due to MA, while Δ[HbO] shows a bilateral pattern. Interestingly, significant Δ[HbO] patterns appear (10–15 s) and disappear (20–25 s) with a slight delay compared with Δ[HbR].

3.2. Classification. Table 1 denotes the maximum accuracies of each subject among the tested time windows. Eight of eleven subjects showed the EEG accuracy exceeding the BCI performance threshold (>70% for binary communication [61]) and scored 82.0 ± 11.2% on average. All subjects exceeded the threshold accuracy when NIRS data was used (HbR + HbO) and scored 85.7 ± 4.9% on average. For all three cases combining EEG data with NIRS data, classification performance was significantly improved (e.g., HbR: 81.4 ± 7.2% versus HbR + EEG: 86.3 ± 8.4%; Wilcoxon rank-sum test, $p < 0.05$). Since HbR + HbO scored the highest mean accuracy among the tested NIRS chromophores (HbR, HbO,

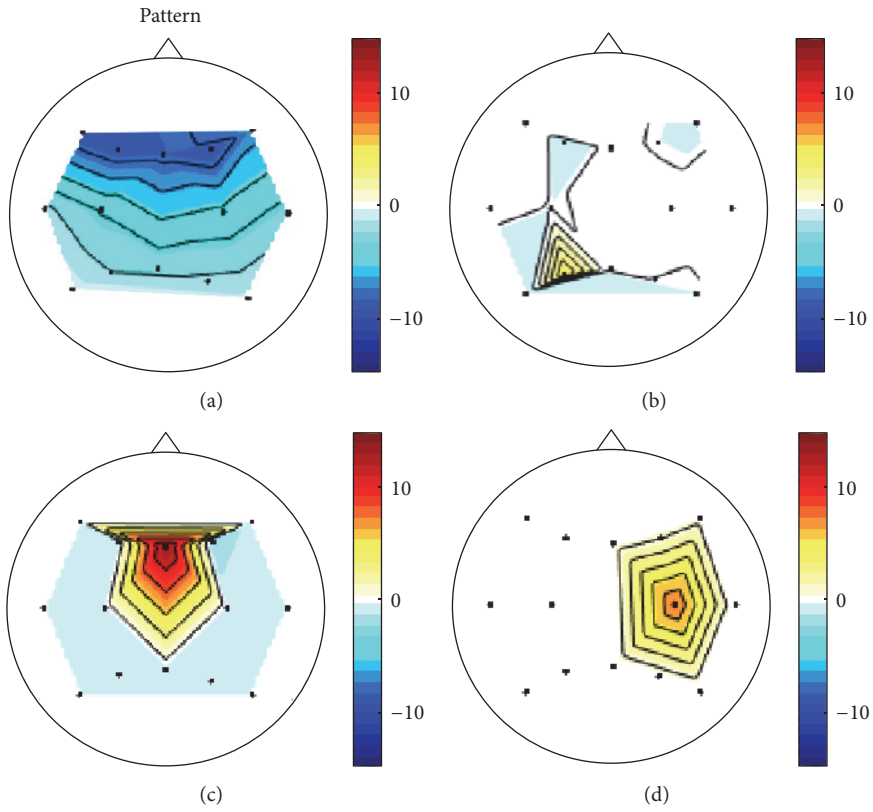

Figure 4: Grand average spatial patterns for all corresponding eigenvalues: λ = (a) 0.36, (b) 0.41, (c) 0.67, and (d) 0.77. Note that the signs of the spatial patterns are irrelevant.

Table 1: Maximum classification accuracies of each subject for near-infrared spectroscopy (NIRS), electroencephalography (EEG), and their possible combination (HYB) after onset of task period.

Subject	EEG	HbR	+EEG	HbO	+EEG	HbR + HbO	+EEG
VP001	66.8	86.3	86.0	86.7	84.7	89.0	87.5
VP002	85.8	78.2	**86.0**	85.2	84.8	84.3	**85.8**
VP003	88.7	87.2	**91.5**	87.5	**90.2**	90.5	**93.3**
VP004	67.5	82.2	82.0	72.2	**77.7**	83.0	82.5
VP005	88.3	80.8	**88.3**	83.0	**90.0**	82.0	**88.3**
VP006	96.7	90.5	**97.3**	85.8	**96.7**	93.5	**98.0**
VP007	93.8	86.8	**93.7**	89.5	**94.2**	90.3	**93.7**
VP008	88.2	81.8	**89.7**	90.5	**92.0**	89.8	**91.8**
VP009	61.5	62.3	**64.5**	74.3	**75.2**	78.3	77.0
VP010	86.8	83.2	**90.3**	76.7	**90.3**	83.3	**91.2**
VP011	78.3	76.5	**79.5**	79.5	**82.0**	78.5	**81.2**
Mean	82.0	81.4	**86.3****	82.8	**87.1***	85.7	**88.2***
Std	11.2	7.2	8.4	5.9	6.5	4.9	5.9

$^{*}p < 0.05$ and $^{**}p < 0.01$ (Wilcoxon signed rank-sum).
*HbR/HbO: deoxyhemoglobin/oxyhemoglobin.
*Std: standard deviation.

and HbR + HbO), HbR + HbO represents the NIRS result hereafter. The classification of HbR + HbO + EEG could enhance the accuracy by 2.5% and 6.2% compared to NIRS and EEG alone, respectively.

The grand average classification accuracies with error bars indicating the standard errors are presented in Figure 6. During the task period (gray shaded period), EEG accuracy reached the highest value at $t = 6$ s. Due to the hemodynamic delay, NIRS showed the highest value 4 s after the end of the task ($t = 14$ s). The classification performance of the hybrid modality was significantly higher than that of EEG or NIRS for most time periods or was at least comparable. In Figure 6,

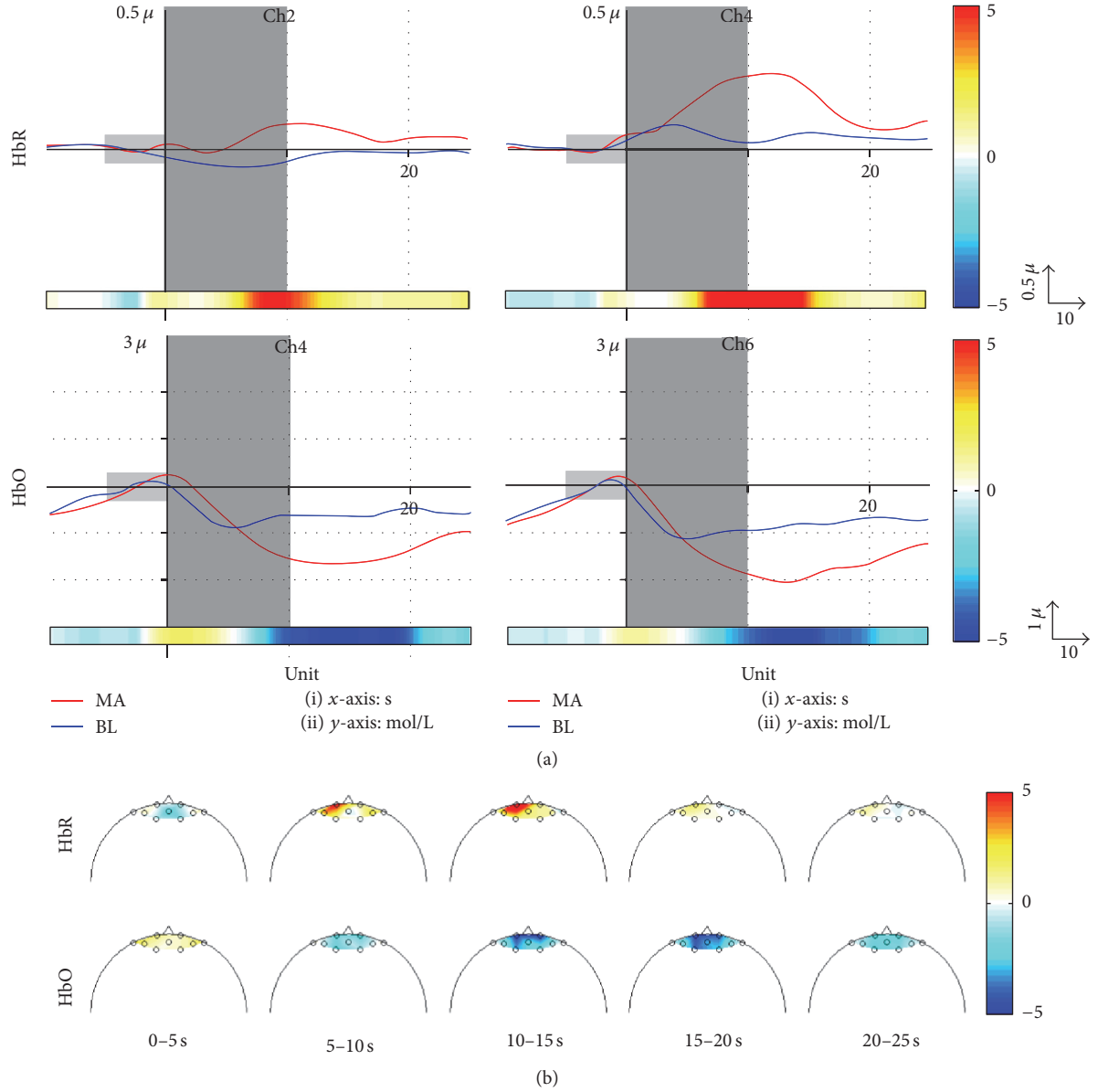

FIGURE 5: (a) Grand average time courses of changes in deoxyhemoglobin (Δ[HbR]) and oxyhemoglobin (Δ[HbO]). The log(p) significance of each channel is shown horizontally at the bottom of each subplot. The red and blue solid lines correspond to MA-related and BL-related activation, respectively. A small gray shade depicts the baseline period of −5 to 0 s, and a large gray patch indicates the task period of 0 to 10 s. A solid vertical line indicates the onset of the task period. The units of the x- and y-axes are seconds and mol/L, respectively. (b) Time-dependent scalp plots of log(p) significance of Δ[HbR] and Δ[HbO] based on the *r-value*. A color bar on the right side denotes a scale of log(p) significance for both (a) and (b). The positive and negative values in the color bar indicate that MA-related activation shows higher and lower values than those of BL-related activation, respectively.

red and blue asterisks represent time windows in which the classification accuracies of the HYB were significantly higher than those of EEG or NIRS alone, respectively.

Figure 7 shows the performance comparison between the NIRS and HYB. The comparisons were made where the EEG, HYB, and NIRS scored the maximum accuracy according to the results shown in Figure 6 (t = 6, 11, and 14 s, resp.). At t = 6, the performance comparison between the EEG and HYB was also provided (see red circles). The number on the upper left side denotes the percentage of the improved results by HYB. All subjects' performances were improved by HYB at t = 6 and 11 s ($p < 0.01$). At t = 14 s, the HYB was not capable of showing significantly better performance than NIRS ($p = 0.482$). This might be caused by less contribution of EEG features to the performance after t = 10 s, when less task-relevant activation was produced after the task period.

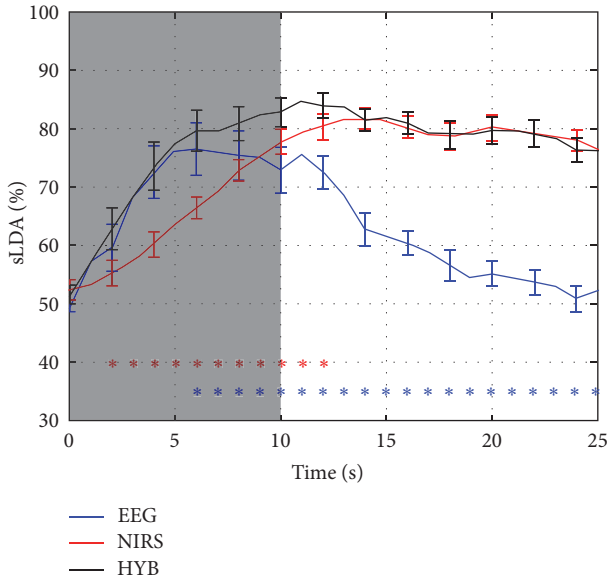

Figure 6: Grand average time-dependent NIRS (red), EEG (blue), and hybrid (HYB; black) classification accuracies. The gray shaded region shows a task period (t = 0–10 s). The red and blue asterisks below indicate the time periods in which the accuracies of HYB were significantly higher than those of NIRS (red) and EEG (blue), respectively. Error bars along with the solid lines show the standard errors.

4. Discussion

We aimed to establish a lightweight hybrid BCI system by combining a portable NIRS with an economical EEG system. The classification results verified that the simultaneous use of EEG and NIRS data was beneficial to improve classification performance. In particular, all subjects (except one: VP001) showed increased performance when the hybrid modality was used (see Table 1). Some previous studies have already confirmed that a hybrid BCI system combining NIRS with EEG can improve system performance, but they used stationary and bulky devices, thereby limiting application outside the laboratory setting [32, 37]. Since our hybrid system was implemented by combining a portable NIRS with an economical EEG system, it can be widely used and easy to handle not only in laboratory settings but also in out-of-lab scenarios.

Even though we verified the feasibility of the hybrid neuroimaging system in a typical BCI scenario, it may also be used for neurorehabilitation purposes, such as restoring motor functions lost in neurological disorders. In this study, MA was selected as a cognitive task to demonstrate the usability of our system because it is one of the stable and consistent cognitive tasks that can produce distinct task-relevant brain activation. As the light and convenient NIRS optodes can easily be reorganized to configure the channels, they are able to measure signals from different brain areas such as motor or occipital areas. However, we must note that careful hair preparation is necessary to avoid interference with the signal acquisition in this case.

In this study, we implemented a MA-based BCI system to demonstrate the feasibility of our hybrid EEG-NIRS neuroimaging device. This device generally showed low operation speed (10 s is theoretically required for producing one command) compared to other paradigms, such as P300 and steady-state visual evoked potential (SSVEP) [62]. However, as the EEG electrodes and NIRS optodes of our hybrid device can be easily reorganized, BCI systems employing other brain areas or paradigms could also be implemented using our hybrid neuroimaging device. For example, it is possible to develop an SSVEP-based BCI system by moving the recording sensors of our hybrid system to occipital areas. It has been well documented that an SSVEP-based BCI system shows high operation speed, and, in particular, a recent study demonstrated that the simultaneous use of EEG and NIRS can further increase the operation speed of an SSVEP-based BCI system [63]. Thus, our hybrid EEG-NIRS recording device may also be used to develop a high-speed BCI system for other BCI paradigms by appropriately modifying the configuration of recording sensors.

It is generally acknowledged that increased Δ[HbO] and decreased Δ[HbR] are induced in task-relevant brain areas during performance of the corresponding task. As seen in Figure 5(a), the opposite pattern to the typical NIRS signal pattern was observed, in that the increasing trend of Δ[HbR] was synchronized with the decreasing trend of Δ[HbO] from the task onset. Note that these opposite patterns are also frequently shown in the literature [64, 65]. Particularly, significant Δ[HbO] decrease and Δ[HbR] increase were observed during MA tasks in frontal areas [64–66].

As mentioned previously, system performance improvement with respect to the classification accuracy was not accomplished by HYB after t = 14 s. This likely results from the lack of task-relevant EEG signals after task termination, and, therefore, EEG does not contribute to the enhancement of system performance at this time. Moreover, before t = 6 s, because of inferior temporal responsiveness of NIRS due to inherent hemodynamic delay, the system performance improvement is also not observed. It is worth mentioning that, because of the delayed responses of NIRS, it would be hard to implement a high-speed BCI system using solely NIRS; nevertheless, NIRS is helpful as a second modality when incorporated in a hybrid BCI with EEG. Based on changing performance over time, an optimal task time length can be determined between 6 and 12 s for HYB. However, for t = 6 s, the degree of performance improvement is less than that for t = 12 s, while 12 s may degrade the usability of the NIRS system owing to the relatively long task time. The tradeoff between the time period to make a decision and performance should be considered based on whether system speed or performance is preferred.

5. Conclusion

Recently, various easily wearable commercial EEG devices have been released [67–70]. These devices have lightweight and easy-to-use configurations. They are used in the field of rehabilitation as well as in entertainment. In this study, we

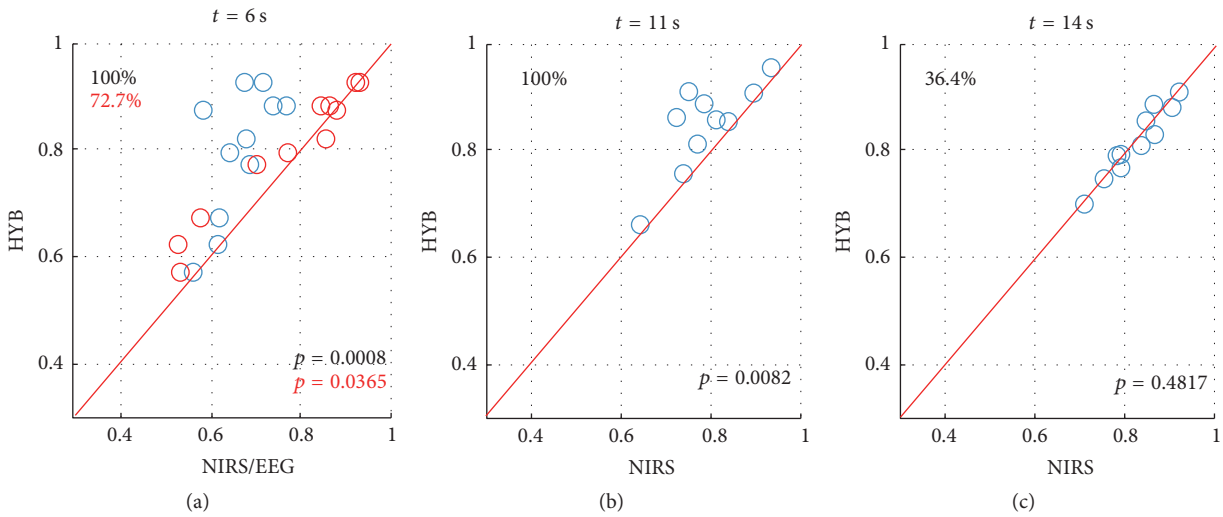

FIGURE 7: Comparisons of classification performances between NIRS and HYB (blue circles) at $t = 6$ (a), 11 (b), and 14 s (c). At $t = 6$, comparison of classification performances between EEG and HYB (red circles) and between NIRS and HYB (blue circles) is provided. The three time points are selected when EEG, hybrid, and NIRS show the highest classification accuracies according to the results shown in Figure 6. Circles above the red diagonal indicate that the performance is improved by HYB compared with NIRS/EEG. Percentage values indicate the percent of subjects showing performance improvement by HYB compared with NIRS (black) or EEG (red). p values indicate significance of the performance improvement by HYB compared with NIRS (black) or EEG (red).

verified the usefulness of a lightweight hybrid BCI system by combining a portable NIRS and a cost-effective EEG system. Our hybrid EEG-NIRS system allowed for improved classification performance. Despite probable doubt with respect to system stability and reliability of the economical EEG system, we verified that the proposed system is capable of stably enhancing the system performance. The concurrent use of the portable NIRS and EEG systems can help us to use the combined system more practically in a cost-effective way. Therefore the proposed system has a high potential for future BCI research in out-of-lab scenarios at low cost.

Competing Interests

The authors declare that there is no conflict of interests regarding the publication of this paper.

Acknowledgments

This research was mainly supported by Business for Cooperative R&D between Industry, Academy, and Research Institute funded Korea Small and Medium Business Administration in 2016 (Grants no. S2380249). The research was also supported in part by the Basic Science Research Program through the National Research Foundation of Korea (NRF) funded by the Ministry of Education (NRF-2014R1A6A3A03057524) and the Ministry of Science, ICT & Future Planning (NRF-2015R1C1A1A02037032) and by the BK21 program of NRF and by US/NIH Grant 1R21NS067278. Additionally we acknowledge funding by BMBF 01GQ0831 and BMBF 01GQ0850 and the German Research Foundation (DFG, KU 1453-1). Some equipment was generously provided by NIRx Medizintechnik GmbH, Berlin.

References

[1] B. Z. Allison, S. Dunne, R. Leeb, J. d. R. Millán, and A. Nijholt, "Recent and upcoming BCI progress: oerview, analysis, and recommendations," in *Towards Practical Brain-Computer Interfaces*, pp. 1–13, Springer, Berlin, Germany, 2012.

[2] B. Blankertz, M. Tangermann, C. Vidaurre et al., "The Berlin brain-computer interface: non-medical uses of BCI technology," *Frontiers in Neuroscience*, vol. 4, no. 1, article 198, 2010.

[3] G. Pfurtscheller, G. R. Müller-Putz, R. Scherer, and C. Neuper, "Rehabilitation with brain-computer interface systems," *Computer*, vol. 41, no. 10, pp. 58–65, 2008.

[4] K.-R. Müller, M. Tangermann, G. Dornhege, M. Krauledat, G. Curio, and B. Blankertz, "Machine learning for real-time single-trial EEG-analysis: from brain-computer interfacing to mental state monitoring," *Journal of Neuroscience Methods*, vol. 167, no. 1, pp. 82–90, 2008.

[5] D. Marshall, D. Coyle, S. Wilson, and M. Callaghan, "Games, gameplay, and BCI: the state of the art," *IEEE Transactions on Computational Intelligence and AI in Games*, vol. 5, no. 2, pp. 82–99, 2013.

[6] B. Blankertz, L. Acqualagna, S. Dähne et al., "The Berlin brain-computer interface: progress beyond communication and control," *Frontiers in Neuroscience*, vol. 10, no. 1, article 530, 2016.

[7] N. Naseer and K.-S. Hong, "fNIRS-based brain-computer interfaces: a review," *Frontiers in Human Neuroscience*, vol. 9, no. 1, article no. 3, 2015.

[8] J. R. Wolpaw, N. Birbaumer, W. J. Heetderks et al., "Brain-computer interface technology: a review of the first international meeting," *IEEE Transactions on Rehabilitation Engineering*, vol. 8, no. 2, pp. 164–173, 2000.

[9] R. Sitaram, N. Weiskopf, A. Caria, R. Veit, M. Erb, and N. Birbaumer, "fMRI brain-computer interfaces," *IEEE Signal Processing Magazine*, vol. 25, no. 1, pp. 95–106, 2008.

[10] J. Mellinger, G. Schalk, C. Braun et al., "An MEG-based brain-computer interface (BCI)," *NeuroImage*, vol. 36, no. 3, pp. 581–593, 2007.

[11] G. Schalk and E. C. Leuthardt, "Brain-computer interfaces using electrocorticographic signals," *IEEE Reviews in Biomedical Engineering*, vol. 4, no. 1, pp. 140–154, 2011.

[12] E. W. Sellers and E. Donchin, "A P300-based brain-computer interface: initial tests by ALS patients," *Clinical Neurophysiology*, vol. 117, no. 3, pp. 538–548, 2006.

[13] R. Ortner, B. Z. Allison, G. Korisek, H. Gaggl, and G. Pfurtscheller, "An SSVEP BCI to control a hand orthosis for persons with tetraplegia," *IEEE Transactions on Neural Systems and Rehabilitation Engineering*, vol. 19, no. 1, pp. 1–5, 2011.

[14] A. Ramos-Murguialday, D. Broetz, M. Rea et al., "Brain-machine interface in chronic stroke rehabilitation: a controlled study," *Annals of Neurology*, vol. 74, no. 1, pp. 100–108, 2013.

[15] T. Kaufmann, A. Herweg, and A. Kübler, "Toward brain-computer interface based wheelchair control utilizing tactually-evoked event-related potentials," *Journal of NeuroEngineering and Rehabilitation*, vol. 11, no. 1, article 7, 2014.

[16] J. Raethjen, M. Lindemann, M. Dümpelmann et al., "Corticomuscular coherence in the 6–15 Hz band: is the cortex involved in the generation of physiologic tremor?" *Experimental Brain Research*, vol. 142, no. 1, pp. 32–40, 2002.

[17] T.-P. Jung, S. Makeig, C. Humphries et al., "Removing electroencephalographic artifacts by blind source separation," *Psychophysiology*, vol. 37, no. 2, pp. 163–178, 2000.

[18] S. Makeig, A. J. Bell, T.-P. Jung, and T. J. Sejnowski, "Independent component analysis of electroencephalographic data," in *Proceedings of the Advances in Neural Information Processing Systems 8*, NIPS Proceedings, pp. 145–151, Denver, Colo, USA, 1996.

[19] R. N. Vigário, "Extraction of ocular artefacts from EEG using independent component analysis," *Electroencephalography and Clinical Neurophysiology*, vol. 103, no. 3, pp. 395–404, 1997.

[20] R. Sitaram, H. Zhang, C. Guan et al., "Temporal classification of multichannel near-infrared spectroscopy signals of motor imagery for developing a brain-computer interface," *NeuroImage*, vol. 34, no. 4, pp. 1416–1427, 2007.

[21] F. C. Robertson, T. S. Douglas, and E. M. Meintjes, "Motion artifact removal for functional near infrared spectroscopy: a comparison of methods," *IEEE Transactions on Biomedical Engineering*, vol. 57, no. 6, pp. 1377–1387, 2010.

[22] H. Obrig, "NIRS in clinical neurology—a 'promising' tool?" *NeuroImage*, vol. 85, part 1, pp. 535–546, 2014.

[23] S. K. Piper, A. Krueger, S. P. Koch et al., "A wearable multi-channel fNIRS system for brain imaging in freely moving subjects," *NeuroImage*, vol. 85, part 1, pp. 64–71, 2014.

[24] T. Nagaoka, K. Sakatani, T. Awano et al., "Development of a new rehabilitation system based on a brain-computer interface using near-infrared spectroscopy," *Advances in Experimental Medicine and Biology*, vol. 662, pp. 497–503, 2010.

[25] R. Sitaram, A. Caria, and N. Birbaumer, "Hemodynamic brain-computer interfaces for communication and rehabilitation," *Neural Networks*, vol. 22, no. 9, pp. 1320–1328, 2009.

[26] G. Strangman, R. Goldstein, S. L. Rauch, and J. Stein, "Near-infrared spectroscopy and imaging for investigating stroke rehabilitation: test-retest reliability and review of the literature," *Archives of Physical Medicine and Rehabilitation*, vol. 87, no. 12, pp. 12–19, 2006.

[27] X. Cui, S. Bray, and A. L. Reiss, "Speeded near infrared spectroscopy (NIRS) response detection," *PLoS ONE*, vol. 5, no. 11, Article ID e15474, 2010.

[28] J. R. Wolpaw, N. Birbaumer, D. J. McFarland, G. Pfurtscheller, and T. M. Vaughan, "Brain-computer interfaces for communication and control," *Clinical Neurophysiology*, vol. 113, no. 6, pp. 767–791, 2002.

[29] S. Fazli, S. Dähne, W. Samek, F. Bießmann, and K.-R. Müller, "Learning from more than one data source: data fusion techniques for sensorimotor rhythm-based brain-computer interfaces," *Proceedings of the IEEE*, vol. 103, no. 6, pp. 891–906, 2015.

[30] G. Pfurtscheller, B. Z. Allison, C. Brunner et al., "The hybrid BCI," *Frontiers in Neuroscience*, vol. 4, article 42, 2010.

[31] S. Amiri, R. Fazel-Rezai, and V. Asadpour, "A review of hybrid brain-computer interface systems," *Advances in Human-Computer Interaction*, vol. 2013, Article ID 187024, 8 pages, 2013.

[32] S. Fazli, J. Mehnert, J. Steinbrink et al., "Enhanced performance by a hybrid NIRS-EEG brain computer interface," *NeuroImage*, vol. 59, no. 1, pp. 519–529, 2012.

[33] V. Kaiser, G. Bauernfeind, A. Kreilinger et al., "Cortical effects of user training in a motor imagery based brain-computer interface measured by fNIRS and EEG," *NeuroImage*, vol. 85, part 1, pp. 432–444, 2014.

[34] B. Koo, H.-G. Lee, Y. Nam et al., "A hybrid NIRS-EEG system for self-paced brain computer interface with online motor imagery," *Journal of Neuroscience Methods*, vol. 244, no. 1, pp. 26–32, 2015.

[35] S. Dähne, F. Bießmann, W. Samek et al., "Multivariate machine learning methods for fusing multimodal functional neuroimaging data," *Proceedings of the IEEE*, vol. 103, no. 9, pp. 1507–1530, 2015.

[36] J. Shin, K.-R. Müller, and H.-J. Hwang, "Near-infrared spectroscopy (NIRS)-based eyes-closed brain-computer interface (BCI) using prefrontal cortex activation due to mental arithmetic," *Scientific Reports*, vol. 6, article 36203, 2016.

[37] A. P. Buccino, H. O. Keles, and A. Omurtag, "Hybrid EEG-fNIRS asynchronous brain-computer interface for multiple motor tasks," *PLoS ONE*, vol. 11, no. 1, Article ID e0146610, 2016.

[38] A. von Lühmann, H. Wabnitz, T. Sander, and K.-R. Müller, "M3BA: a mobile, modular, multimodal biosignal acquisition architecture for miniaturized EEG-NIRS based hybrid BCI and monitoring," *IEEE Transactions on Biomedical Engineering*, 2016.

[39] S. D. Power, A. Kushki, and T. Chau, "Automatic single-trial discrimination of mental arithmetic, mental singing and the no-control state from prefrontal activity: toward a three-state NIRS-BCI," *BMC Research Notes*, vol. 5, no. 1, article 141, 2012.

[40] K. Stytsenko, E. Jablonskis, and C. Prahm, "Evaluation of consumer EEG device Emotiv EPOC," in *Proceedings of the MEi:CogSci Conference*, Ljubljana, Slovenia, 2011.

[41] Y. Liu, X. Jiang, T. Cao et al., "Implementation of SSVEP based BCI with Emotiv EPOC," in *Proceedings of the IEEE International Conference on Virtual Environments Human-Computer Interfaces and Measurement Systems (VECIMS '12)*, pp. 34–37, Tianjin, China, 2012.

[42] N. A. Badcock, P. Mousikou, Y. Mahajan, P. de Lissa, J. Thie, and G. McArthur, "Validation of the Emotiv EPOC® EEG gaming systemfor measuring research quality auditory ERPs," *PeerJ*, vol. 1, no. 1, article e38, 2013.

[43] R. Lievesley, M. Wozencroft, and D. Ewins, "The Emotiv EPOC neuroheadset: an inexpensive method of controlling assistive

technologies using facial expressions and thoughts?" *Journal of Assistive Technologies*, vol. 5, no. 2, pp. 67–82, 2011.

[44] H. Ekanayake, "P300 and Emotiv EPOC: does Emotiv EPOC capture real EEG?" http://neurofeedback.visaduma.info/emotiv-research.htm.

[45] M. Duvinage, T. Castermans, M. Petieau, T. Hoellinger, G. Cheron, and T. Dutoit, "Performance of the Emotiv Epoc headset for P300-based applications," *BioMedical Engineering Online*, vol. 12, no. 1, article 56, 2013.

[46] A. Campbell, T. Choudhury, S. Hu et al., "NeuroPhone: brain-mobile phone interface using a wireless EEG headset," in *Proceedings of the ACM SIGCOMM Workshop on Networking, Systems, and Applications on Mobile Handhelds*, pp. 3–8, New Delhi, India, 2010.

[47] P. Aspinall, P. Mavros, R. Coyne, and J. Roe, "The urban brain: analysing outdoor physical activity with mobile EEG," *British Journal of Sports Medicine*, vol. 49, no. 4, pp. 272–276, 2015.

[48] A. Vourvopoulos and F. Liarokapis, "Brain-controlled NXT Robot: tele-operating a robot through brain electrical activity," in *Proceedings of the International Conference on Games and Virtual Worlds for Serious Applications (VS-GAMES '11)*, pp. 140–143, Athens, Greece, 2011.

[49] T. D. Pham and D. Tran, "Emotion recognition using the emotiv epoc device," in *Neural Information Processing: 19th International Conference, ICONIP 2012, Doha, Qatar, November 12–15, 2012, Proceedings, Part V*, vol. 7667 of *Lecture Notes in Computer Science*, pp. 394–399, Springer, Berlin, Germany, 2012.

[50] S. Debener, F. Minow, R. Emkes, K. Gandras, and M. de Vos, "How about taking a low-cost, small, and wireless EEG for a walk?" *Psychophysiology*, vol. 49, no. 11, pp. 1617–1621, 2012.

[51] R. Oostenveld and P. Praamstra, "The five percent electrode system for high-resolution EEG and ERP measurements," *Clinical Neurophysiology*, vol. 112, no. 4, pp. 713–719, 2001.

[52] B. Blankertz, S. Lemm, M. Treder, S. Haufe, and K.-R. Müller, "Single-trial analysis and classification of ERP components—a tutorial," *NeuroImage*, vol. 56, no. 2, pp. 814–825, 2011.

[53] A. Delorme and S. Makeig, "EEGLAB: an open source toolbox for analysis of single-trial EEG dynamics including independent component analysis," *Journal of Neuroscience Methods*, vol. 134, no. 1, pp. 9–21, 2004.

[54] N. Kollias and W. Gratzer, "Tabulated molar extinction coefficient for hemoglobin in water," http://omlc.org/spectra/hemoglobin/summary.html.

[55] L. Kocsis, P. Herman, and A. Eke, "The modified Beer-Lambert law revisited," *Physics in Medicine and Biology*, vol. 51, no. 5, pp. N91–N98, 2006.

[56] B. Blankertz, R. Tomioka, S. Lemm, M. Kawanabe, and K.-R. Müller, "Optimizing spatial filters for robust EEG single-trial analysis," *IEEE Signal Processing Magazine*, vol. 25, no. 1, pp. 41–56, 2008.

[57] S. Lemm, B. Blankertz, T. Dickhaus, and K.-R. Müller, "Introduction to machine learning for brain imaging," *NeuroImage*, vol. 56, no. 2, pp. 387–399, 2011.

[58] L. Holper and M. Wolf, "Single-trial classification of motor imagery differing in task complexity: a functional near-infrared spectroscopy study," *Journal of NeuroEngineering and Rehabilitation*, vol. 8, no. 1, article 34, 2011.

[59] O. Ledoit and M. Wolf, "A well-conditioned estimator for large-dimensional covariance matrices," *Journal of Multivariate Analysis*, vol. 88, no. 2, pp. 365–411, 2004.

[60] J. Schäfer and K. Strimmer, "A Shrinkage approach to large-scale covariance matrix estimation and implications for functional genomics," *Statistical Applications in Genetics and Molecular Biology*, vol. 4, no. 1, article 32, 2005.

[61] J. Perelmouter and N. Birbaumer, "A binary spelling interface with random errors," *IEEE Transactions on Rehabilitation Engineering*, vol. 8, no. 2, pp. 227–232, 2000.

[62] H.-J. Hwang, S. Kim, S. Choi, and C.-H. Im, "EEG-based brain-computer interfaces: a thorough literature survey," *International Journal of Human-Computer Interaction*, vol. 29, no. 12, pp. 814–826, 2013.

[63] Y. Tomita, F.-B. Vialatte, G. Dreyfus, Y. Mitsukura, H. Bakardjian, and A. Cichocki, "Bimodal BCI using simultaneously NIRS and EEG," *IEEE Transactions on Biomedical Engineering*, vol. 61, no. 4, pp. 1274–1284, 2014.

[64] G. Pfurtscheller, G. Bauernfeind, S. C. Wriessnegger, and C. Neuper, "Focal frontal (de)oxyhemoglobin responses during simple arithmetic," *International Journal of Psychophysiology*, vol. 76, no. 3, pp. 186–192, 2010.

[65] G. Bauernfeind, R. Leeb, S. C. Wriessnegger, and G. Pfurtscheller, "Development, set-up and first results for a one-channel near-infrared spectroscopy system," *BioMedical Engineering*, vol. 53, no. 1, pp. 36–43, 2008.

[66] H.-J. Hwang, J.-H. Lim, D.-W. Kim, and C.-H. Im, "Evaluation of various mental task combinations for near-infrared spectroscopy-based brain-computer interfaces," *Journal of Biomedical Optics*, vol. 19, no. 7, Article ID 077005, 2014.

[67] Neurosky, http://neurosky.com/biosensors/eeg-sensor/.

[68] Emotiv, https://emotiv.com/insight.php.

[69] Mindo, http://mindo.com.tw/.

[70] Brainbit, http://www.brainbit.co/.

Hindawi
BioMed Research International
Volume 2017, Article ID 4185939, 11 pages
https://doi.org/10.1155/2017/4185939

Research Article

Patient-Centered Robot-Aided Passive Neurorehabilitation Exercise Based on Safety-Motion Decision-Making Mechanism

Lizheng Pan,[1,2] Aiguo Song,[2] Suolin Duan,[1] and Zhuqing Yu[1]

[1]*School of Mechanical Engineering, Changzhou University, Changzhou 213164, China*
[2]*Remote Measurement and Control Key Lab of Jiangsu Province, School of Instrument Science and Engineering, Southeast University, Nanjing 210096, China*

Correspondence should be addressed to Lizheng Pan; plz517@sina.com.cn

Received 25 August 2016; Revised 6 December 2016; Accepted 22 December 2016; Published 16 January 2017

Academic Editor: Janne M. Hahne

Safety is one of the crucial issues for robot-aided neurorehabilitation exercise. When it comes to the passive rehabilitation training for stroke patients, the existing control strategies are usually just based on position control to carry out the training, and the patient is out of the controller. However, to some extent, the patient should be taken as a "cooperator" of the training activity, and the movement speed and range of the training movement should be dynamically regulated according to the internal or external state of the subject, just as what the therapist does in clinical therapy. This research presents a novel motion control strategy for patient-centered robot-aided passive neurorehabilitation exercise from the point of the safety. The safety-motion decision-making mechanism is developed to online observe and assess the physical state of training impaired-limb and motion performances and regulate the training parameters (motion speed and training rage), ensuring the safety of the supplied rehabilitation exercise. Meanwhile, position-based impedance control is employed to realize the trajectory tracking motion with interactive compliance. Functional experiments and clinical experiments are investigated with a healthy adult and four recruited stroke patients, respectively. The two types of experimental results demonstrate that the suggested control strategy not only serves with safety-motion training but also presents rehabilitation efficacy.

1. Introduction

According to the report of World Health Organization (WHO), in recent years, the proportion of the elderly population continues to increase, and many countries of the world are gradually coming into the aged society [1]. Stroke is one of the leading disabling or lethal diseases among the elderly population in the world and usually causes hemorrhagic or ischemic brain damage, which results in some functional deficits, such as motor, sensory, and cognitive limitations [2, 3]. On clinic, majority (more than 69%) of the stroke patients suffer motion disability with upper extremity in some degree [4]. Approximately 610,000 and 2,000,000 people suffer new stroke each year in the United State and China, respectively [5, 6]. The statistical results (in 2013) present that the limb-motion functional disabilities were a key body among all functional deficits; there were 15.64 million persons with the limb disabilities in China, which occupied 59% of the total disabilities. Long-term limitations of function not only impact the quality of daily life but also cause great physical and psychological suffering to patients. Fortunately, clinical medicine has verified that intensive motion training contributes to the recovery of motor neural function.

Recently, all kinds of motion-rehabilitation training robots have been developed to help stroke patients improve the impaired nervous system and motor control, according to the neural plasticity. Meanwhile, many investigations have verified that robot-aided rehabilitation training presents a positive impact in promoting the motion function. Due to the outstanding advantages for robot-aided rehabilitation in high intensity, automated repetition, and recording the data of the training process, the new neurorehabilitation technology with robots has attracted more attention and been rapidly developed. In terms of the upper-limb rehabilitation robots, many researches have done a great contribution in the fields of mechanism design [7], control algorithm [8–10],

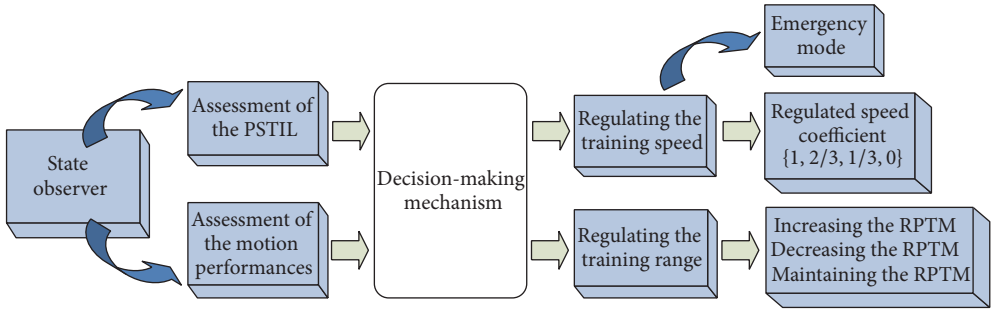

Figure 1: Safety-motion decision-making mechanism.

rehabilitation evaluation, and clinical trial [11]. Motion-rehabilitation training robots are developed in order to help stoke patients or other limb-motion function disorders to relearn motion skills or normal daily functions with robot-aided motion training. It means that the design of rehabilitation system has to follow the rehabilitation movement mechanism. So, safety and effectiveness of rehabilitation are been strongly addressed during the whole process of rehabilitation system design.

Due to the particularity of the service object, safety plays an important role in the rehabilitation system design, which is to be taken for granted. There are various techniques developed to match this issue from the point of hardware or software design. Barkana et al. have developed a quick-release device, same function to the safety mechanism applied in ADLER [12] and GENTLE/s [13], when the physical safety-related event happens, quickly removing the patient's limb out of the rehabilitation robot [14]. This safety mechanism usually works or serves after the event, not online. It cannot supply effective protection to the training subject under the external collision or sudden twitch. In [15], a new reflex mechanism structure was present, which was developed just like the human conditioned response to the external collision. In addition, some other schemes for the hardware design were also utilized to match the operational safety, for instance, making the end-effector work in a small space [16] or driving with pneumatic muscle [17]. The software-based procedure usually applies different detection and analysis techniques to monitor the operating areas and avoid collision with the outside obstacles, such as the estimated danger index [18], mapped virtual reality (MVR) [19], and verbal feedback [14]. In a summary, the existing safety-based designs with hardware or software mainly focus on the external collision, but not the safety motion of the rehabilitation training.

Furthermore, in clinical rehabilitation treatment, different motion-rehabilitation training is usually adopted according to the characteristics of disease and the stage of the recovery. At the early recovery phase, the limb of the stroke patient without any motion ability, passive rehabilitation exercise is usually employed to improve the motion perception and motor nerve system. In terms of the robot-aided passive neurorehabilitation exercise, one position controller is usually designed to serve the training limb tracking the reference trajectories. Due to the "inactive" peculiarity of passive training mode, many investigations pay more attention to developing the position-based tracking control strategies without considering the subject (another part of the rehabilitation system), and the supplied rehabilitation motion exercise is robot-in-charge mode. According to the principles of clinical training, patient-centered service should be well supplied at each stage of the rehabilitation. Patient is a part of the rehabilitation system, which is dynamic. Therefore, to the robot-aided passive training, the motion training should be adaptively regulated in the motion speed and training region for the safety according to the online condition of the patient, but not just tracking the predefined trajectories. However, the existing designed control systems for robot-aided passive rehabilitation exercise pay little attention to the safety from the point of the patient-centered motion training.

Thus, this research presents a novel motion control strategy for patient-centered robot-aided passive neurorehabilitation exercise from the point of the safety. The safety-motion decision-making mechanism is developed to online observe and assess the physical state of training impaired-limb (PSTIL) and motion performances and regulate the training parameters (motion speed and training region), ensuring the safety of the supplied rehabilitation exercise. The patient is taken as a part of the rehabilitation system, and the training movement is carried out with the patient's cooperation to some extent, which is just as what the therapist does.

2. Safety-Motion Decision-Making Mechanism

In clinical therapy, especially at the early stage of the recovery, the safety is strongly addressed when it comes to the passive rehabilitation exercise, because the impaired limb is easy to be hurt. During the traditional hand-to-hand rehabilitation exercise, the therapist usually in real time assesses the PSTIL and motion performances and then draws the impaired limb moving with appropriate speed and training range. The process may be described as observing-and-assessing and decision-making. In this research, the safety-motion decision-making mechanism is developed to play this role, which includes two parts (Figure 1), namely, state observer section and decision-making section. The state observer section in real time assesses the PSTIL and motion performances, and the decision-making section regulates the parameters of motion training to serve with safety rehabilitation.

2.1. State Observer. During the passive training, two factors influence the decision for regulating motion parameters. One is the real-time PSTIL, which determines what speed is selected to undergo the current movement. For example, when the patient causes some internal disturbance, such as position-pose changing, and coughing, the training speed should be cut down. The other is the whole motion performances, which reflects the state of the following motion and determines that training range is suitable to the subject. Thus, the state observer is designed to possess the function of assessing the PSTIL and motion performances.

2.1.1. Assessment of the PSTIL. During the robot-aided passive rehabilitation exercise, the impaired limb is relaxed and completely driven by the robot, without applying any active movement. However, the subject is a dynamic part of the cooperation movement, and the PSTIL is usually affected by the internal disturbance of the subject, such as position-pose changing, laughing, talking, and sudden twitch, or by the external disturbance (applying disturbance or collision). In terms of robot-aided passive rehabilitation exercise, it is a typical human-machine interaction activity. It means that, in a sense, the recording data of tracking motion presents the interaction process and further reflects the PSTIL.

During the robot-aided therapy, the motion parameters (position and velocity) are usually recorded. In our previous research [20], the tracking features of position and velocity are extracted and adopted to assess the PSTIL with fuzzy logic reasoning. In order to reflect the dynamic tracking movement effectively, a sliding window is employed to observe the movement information in real time, and the tracking features are extracted with subsection sliding mean square (SMSE). Meanwhile, the variation of the tracking error is also employed with the abstracted feature of subsection SMSE. The final abstracted feature includes the information of the tracking error and the feature abstracted with subsection SMSE, which is described as follows:

$$\begin{aligned} \chi &= \alpha_k + \lambda \cdot f\left(e_{\max}, e_{\min}\right), \\ \alpha_k &= \sqrt{\frac{\sum_{i=1}^{n}\left(\overline{x}_k - x_{k-i}\right)^2}{n-1}}, \\ \overline{x}_k &= \frac{1}{n}\sum_{i=1}^{n} x_{k-i}, \\ f\left(e_{\max}, e_{\min}\right) &= \sqrt{\left|\left(e_{\max} - \overline{e}\right) \times \left(e_{\min} - \overline{e}\right)\right|}, \end{aligned} \tag{1}$$

where α_k is the abstracted feature of the tracking error corresponding to the kth sample data with subsection SMSE, $f(e_{\max}, e_{\min})$ is a function to display the information of the tracking error, λ is proportional coefficient, x_{k-i} and $\overline{x}_k$ are the value of $(k-i)$th sample data and the mean of kth subsection, and n is the length of the subsection window.

According to the abstracted features of position and velocity tracking information, the PSTIL is evaluated with fuzzy logic reasoning. The two features (χ_p and χ_v represent position and velocity tracking, resp.) are managed as the inputs, and the output with fuzzy reasoning reflects the PSTIL.

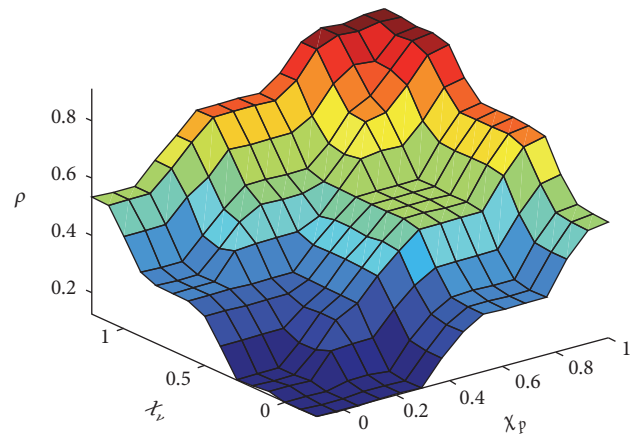

Figure 2: Fuzzy reasoning surface map for assessment of the PSTIL.

In this research, the inputs and output are fuzzified and defuzzfied with five trigonometry membership functions, respectively. According to the designed fuzzy reasoning rules, the overall input-output relationship surface map is shown as in Figure 2.

2.1.2. Assessment of the Motion Performance. Motion performance is the external manifestation of the patient to follow the designed rehabilitation training. It synthetically presents the internal state of the illness, current period status of the patient, and the rationality of the designed task, to a certain extent. Motion performance is associated with the designed exercises. In general, the range of passive training movement (RPTM) is more beyond the patient's capacity more discomfort disturbances caused. In other words, during the passive rehabilitation, motion performance really reflects whether the planed training range is suitable to the patient at that time or not. Therefore, observing the process of following movement and assessing the motion performance play an important role to realize the patient-centered passive rehabilitation exercise. In this research, the motion performances of the current two cycles are observed and assessed online and adopted to guide adjusting the RPTM.

2.2. Decision-Making Mechanisms. During the traditional hand-to-hand passive training session, the therapist usually dynamically adjusts the training exercise according to the specific case of the subject at any time. The motion speed and RPTM are two important parameters for rehabilitation training. As mentioned above, the assessments of the PSTIL and motion performance present the impaired-limb state at the execution time and following performance within current period, respectively. Safety is also demonstrated in the rationality and scientificity of the training strategy. When it comes to the robot-aided passive rehabilitation exercise, the movement speed and RPTM should be adaptively adjusted from the viewpoint of safety. Thus, the decision-making mechanisms are formulated to regulate the training motion

Table 1: Scheme for regulating RPTM.

Horizontal exercise	Planning points	360	→	260	→	210	→	262 (0.8v)	→	212 (0.8v)
	RPTM	[0.45, −0.45]		[0.4, −0.4]		[0.35, −0.35]		[0.35, −0.35]		[0.3, −0.3]
Vertical exercise	Planning points	268	→	203	→	136	→	170 (0.8v)	→	156 (0.8v)
	RPTM	[−5.37, −3.8]		[−5.3, −3.9]		[−5.2, −4.0]		[−5.2, −4.0]		[−5.1, −4.1]

Note: 0.8v represents that the global speed is 80% of the predefined speed.

parameters and realize the patient-centered rehabilitation exercise.

2.2.1. Regulating Motion Speed. During the traditional hand-to-hand motion training, the therapist usually dynamically regulates the stretching speed by evaluating the internal and external condition of the patient, in order to make the training safe. Patient as a part of the rehabilitation training is a dynamic system, which sometimes causes some disturbances for internal or external events. In terms of the robot-aided rehabilitation, when some events (talking, coughing, position-pose changing, sudden twitching, etc.) make the PSTIL changed, it may do some damage to the impaired limb if still stretching the limb with the same speed. Combining the clinical practice, as closely as the therapist, the training speed should be regulated with different degree according to the evaluated PSTIL at that time. When it comes to the emergency events, the robot must do no harm to the patient. In this research, an emergency mode is designed, in which the manipulator moves under full gravity compensation, floating with the arm without any interactive force.

The speed regulation abides by the following rules:

(1) The speed parameter is employed with four grades, namely, $\{1, 2/3, 1/3, 0\}$.

(2) In emergency mode, the manipulator moves under full gravity compensation, not stopping.

Online regulating the movement speed according to the evaluated PSTIL effectively enhances the safety of the rehabilitation training.

2.2.2. Regulating Motion Range. In clinical therapy, when the patient undergoes the training motion with suitable RPTM, the therapeutic effect is the best. As mentioned in Section 2.1.2, we can draw a conclusion whether the supplied RPTM is suitable or not by observing and assessing the motion performances of the current two cycles. In this research, in order to serve the patient with more suitable RPTM, the role of the global speed is also considered, when designing the regulating mechanisms. The rules for regulating the RPTM are present as follows.

① During current training cycle, being paused more than 3 times, it means that the undergoing RPTM is beyond the patient's current period capacity and then the RPTM is turned down.

② The global speed planning is also taken into account in the designed regulating mechanisms. When the RPTM is less than [0.35, −0.35] rad in the horizontal exercise or [−5.2, −4.0] rad in the vertical exercise, it means that the patient is in serious condition, and then the global predefined speed should be decreased. The regulating schemes in decreasing RPTM for horizontal and vertical motion exercises are shown in Table 1.

③ In two consecutive motion cycles, there is not any speed regulating or pausing; it means that the RPTM is less than the patient's current period capacity; then the RPTM is increased in the next cycle. Increasing RPTM is in the reverse direction to ②.

④ In other cases, the RPTM is the same as the previous cycle.

3. Rehabilitation System and Control System Design

3.1. Upper-Limb Rehabilitation System. The Barrett WAM with four degrees of freedom (DOF) is adopted as the main platform to construct the upper-limb rehabilitation system. Barrett WAM has been wildly accepted as experiment platform in the medical field, due to its outstanding dexterity and safety. The WAM is developed with cable-driven technology, which presents good performance in back drivability. Meanwhile, the WAM provides two control panels to do emergency. When pressing the stop button, the end-effector drops not sharply but slowly under gravity, which let the guardian have enough time to deal with the emergency. During the running, the position of each rotary joint is measured and recorded in real time, and the joint can be driven by setting the control torque. The WAM provides an ideal hardware platform to do motion training.

According to the requirement of the upper-limb rehabilitation system, a 3D force sensor is developed and installed on the end-effector to detect the interactive force between the impaired-limb and the robot. Meanwhile, in order to support the impaired limb for the seriously ill patients to undergo the passive rehabilitation training, an arm-support device is designed, which could be assembled and disassembled conveniently on the left or right side according to affected side of the subject. The constructed WAM upper-limb rehabilitation system is shown as Figure 3, which mainly consists of the Barrett WAM, external PC, self-developed force sensor, and arm-support device.

The software of the rehabilitation system is developed on the extern PC with Linux system. In order to improve the instantaneity, the real-time module Xenomai is employed.

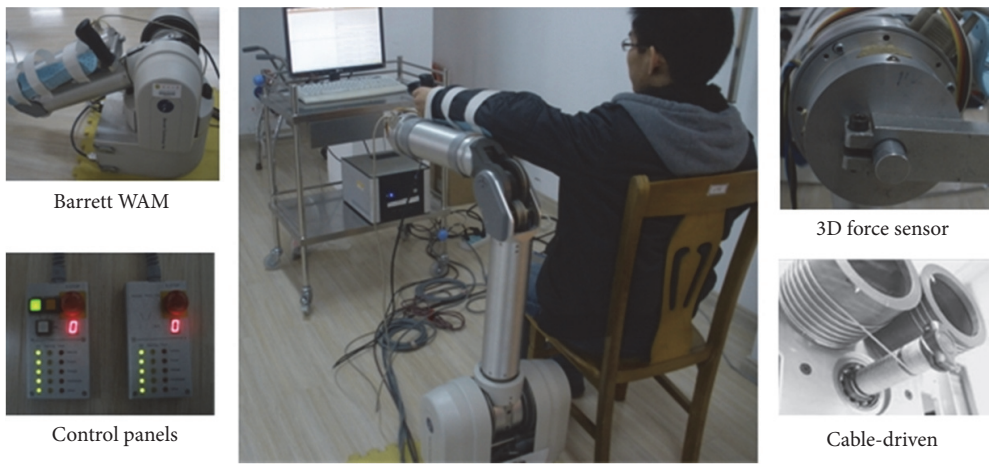

Figure 3: Hardware of the WAM upper-limb rehabilitation system.

Meanwhile, the tasks of the system are divided into real-time and nonreal-time according to its characteristics, and multithread mechanism is also adopted to manage the tasks.

3.2. Control System Design for Patient-Centered Rehabilitation Strategy. Motor learning is widely consented to be a promising method to regain the daily motion abilities for the stroke patient according to the neural plasticity. Passive rehabilitation training is usually introduced to the patient seriously damaged without any motion ability at the early stage of the recovery. The developed robot-aided rehabilitation training should rely on the recovery mechanism [21]. In terms of robot-aided passive rehabilitation, various trajectory tracking control methods are employed to draw the impaired limb following the predefined trajectory. The existing control strategies are usually just based on position control to carry out the training, and the patient is out of the controller. However, to some extent, the patient should be taken as a "cooperator" of the training activity from the viewpoint of patient-centered rehabilitant. Patients with central nerve system (CNS) injured are more vulnerable to injury during the process of movement. Thus, more attention must be paid on the interactive compliance and rationality of the training strategy during the control system design.

Impedance control is firstly developed by Hogan, which describes a relationship between the force and the deviation of the position and velocity [6]. Impedance control is widely adopted to realize the interactive compliance. In this study, the position-based impedance control is selected to execute the compliant following movement.

According to [22, 23] and combining our previous researches [20, 24], the impedance relationship of force and deviation is built with a mass-damper-spring model, described as follows:

$$\Delta F = M_d \Delta \ddot{X} + B_d \Delta \dot{X} + K_d \Delta X,$$
$$\Delta X = X_d - X,$$
$$\Delta \dot{X} = \dot{X}_d - \dot{X},$$
$$\Delta \ddot{X} = \ddot{X}_d - \ddot{X}, \quad (2)$$

where ΔF is the variance in force, X, $\dot{X}$, and $\ddot{X}$ are the actual parameters for position, velocity, and acceleration, X_d, $\dot{X}_d$, and $\ddot{X}_d$ are the corresponding desired parameters, and M_d, B_d, and K_d are the desired inertia, damping, and stiffness matrix, respectively.

The position-based impedance control is a method combining the impedance control and position control. The impedance control manages the interactive compliance, and the proportional-integral-derivation (PID) position control guides the upper limb to move along certain paths.

As mentioned in Section 2.2.1, when there is a sudden emergency, the robot works in emergency mode. For this working mode, the manipulator moves under the full gravity compensation, like a feather floating with the arm, not stopping, which effectively protects the training arm under the emergency.

In order to realize the patient-centered rehabilitation, the movement speed and RPTM should be dynamically regulated according to the PSTIL and motion performance, just as what the therapist does in clinical therapy. The safety-motion decision mechanism is developed in Section 2, which plays an important role to serve the subject with safety motion.

The control system with the proposed safety-motion decision mechanism is designed as Figure 4. It mainly includes two sections, namely, the position-based impedance controller and safety-motion decision mechanism. The safety-motion decision mechanism online observes the position-velocity information and assesses the PSTIL at that time and the motion ability at the current period and then regulates the movement speed and RPTM according to the designed regulating mechanisms, supplying decision-making for safety-motion training. The position-based impedance controller

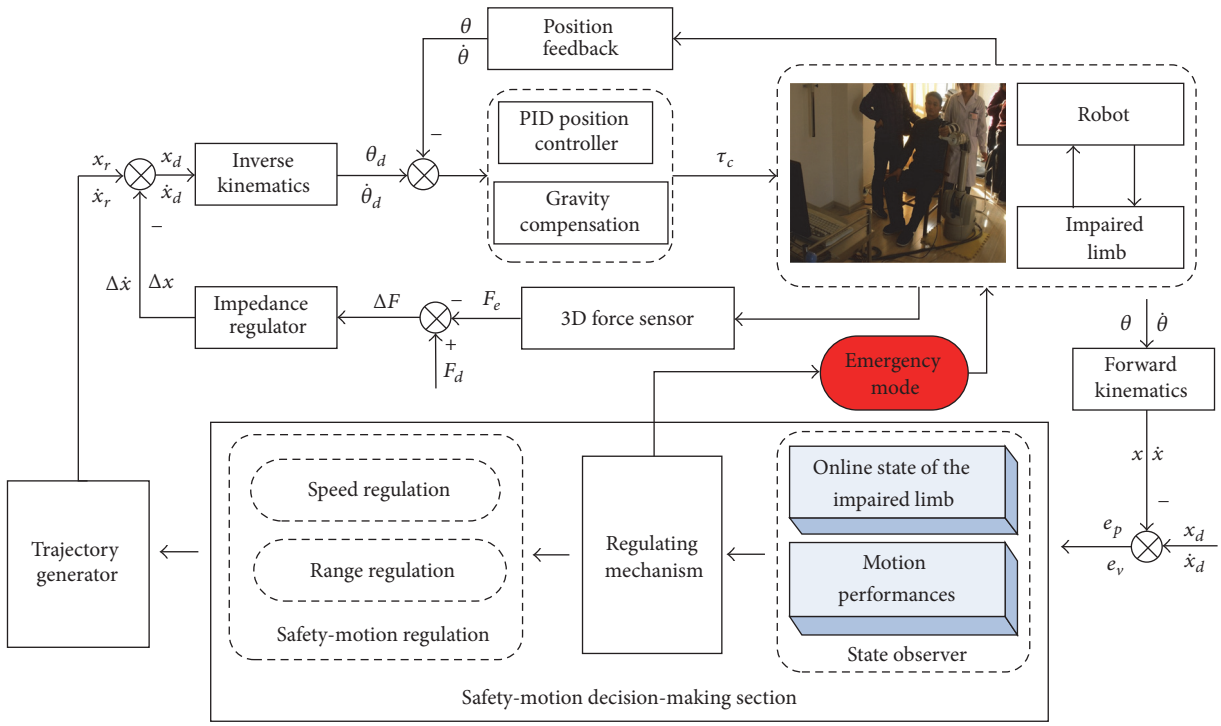

Figure 4: Block diagram of the control system.

Table 2: Information of the stroke patients.

Patient code	Age	Gender	Time since stroke (months)	Impaired limb
1	56	Male	2	Right
2	68	Female	6	Left
3	61	Female	8	Left
4	58	Male	15	Right

is employed to realize the trajectory tracking motion with interactive compliance.

4. Experiments and Results

4.1. Experiment Scheme. In order to verify the effectiveness and efficacy of the proposed control strategy with the developed safety-motion decision-making mechanisms, the functional experiments and clinical experiments were schemed. A healthy volunteer was guided to carry out the functional experiments. In functional experiments, the subject was asked to deliberately cause some disturbance and make the limb being different PSTIL, to test the regulating function of the developed safety-motion decision-making mechanisms for serving with safety-motion training. Moreover, four stroke patients are recruited to undergo the clinical experiments for investigating the rehabilitation efficacy. The information of the patients is presented in Table 2.

According to the clinical practice, two movement trajectories were predefined, namely, shoulder extension/flexion in horizontal and elbow extension/flexion in vertical. Each type of experiments was carried out with the predefined exercises.

4.2. Functional Experiments. The aim of the function experiments is to test the designed control system with safety motion decision-making mechanism whether it could adaptively regulate the motion parameters (motion speed and RPTM) according to the assessment results online or not. In this type of experiments, the subject is asked to deliberately cause some disturbance just as what may happen in clinical therapy, making the limb being different PSTIL. The disturbance is caused within presenting different regulation function (described in Section 2.2.2). As described in Section 2.2.2, the regulation of the RPTM is based on observing the process of the following motion, which is mainly presented with the speed regulation. Thus, the regulation of the RPTM synthetically reflects the adaptive regulation function in motion speed and RPTM. During the experiments, the corresponding information is recorded to verify the designed functions, such as the number of points in the cycle, the predefined and adjusted trajectories, the speed adjustment or pausing times, number of ideal exercise cycles, and the global coefficient for speed. The functional experimental results of regulating the RPTM in horizontal and vertical exercises are shown in Figures 5 and 6, respectively.

By analyzing the Figures 5 and 6, the designed control system presents a good performance in adaptive regulation

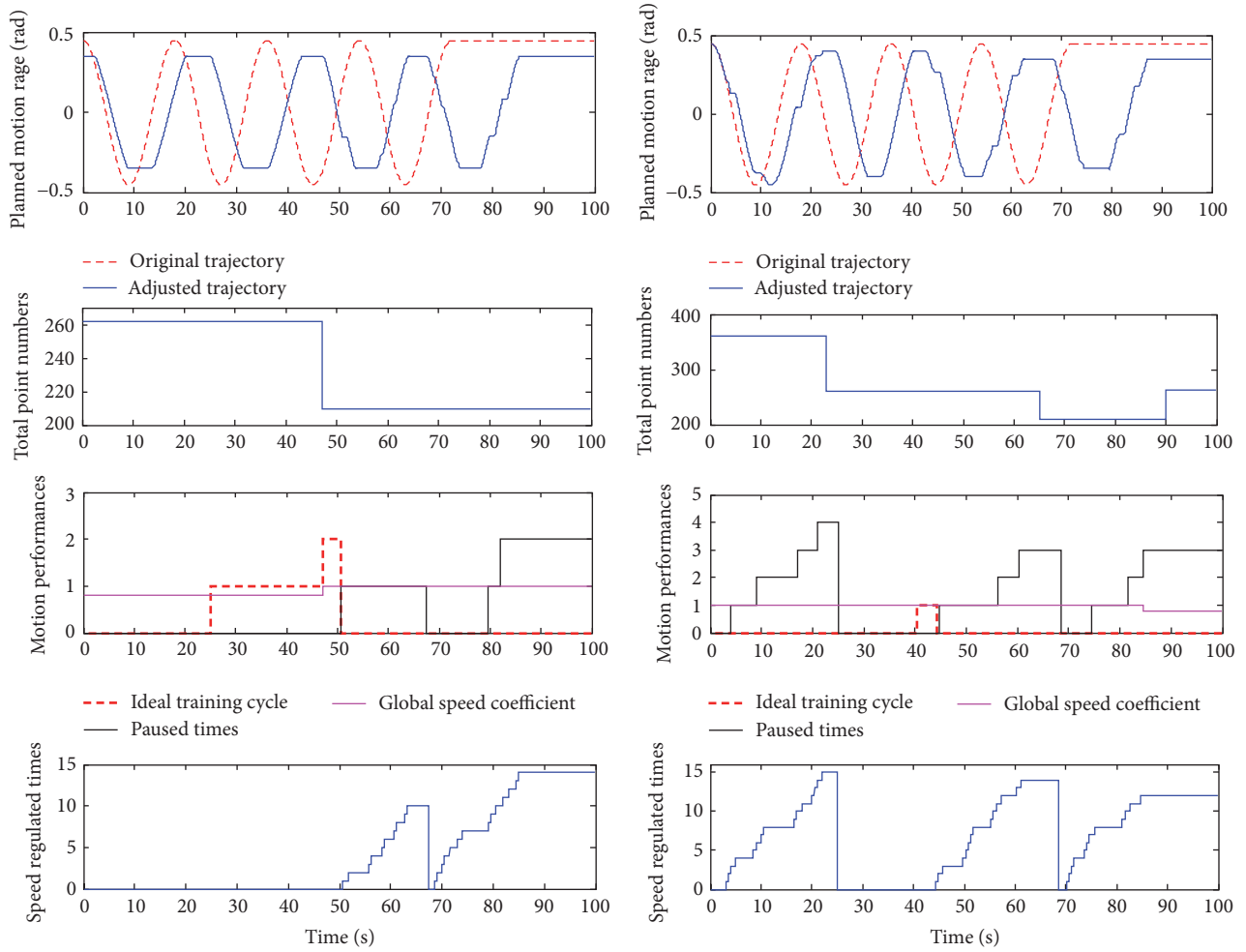

Figure 5: Functional experiments in horizontal exercise.

the RPTM and global speed coefficient. In Figure 5(a), undergoing two ideal cyclic exercises, it means that the supplied RPTM is less than the subject's capacity, and then the global speed coefficient is increased from 0.8 to 1.0. In Figure 6(b) for vertical exercise, during the first cycle, times of pausing are more than 3, and then the RPTM is regulated down from 203 points to 136 points in the next cycle. Moreover, in Figure 6(b), the predetermined global speed coefficient is regulated from 1.0 to 0.8 in the fourth cycle according to the designed regulating mechanism. In summary, the designed control strategy with safety-motion decision-making mechanism could regulate the motion speed according to the PSTIL and well manage the regulating of the RPTM and the global exercise speed. The safety-motion decision-making mechanism plays an important role in serving with safety-motion training, as what the therapist does in clinical hand-to-hand rehabilitation.

4.3. Clinical Experiments. The aim of clinical experiments is to verify the rehabilitation of the proposed control strategy. Clinical experiments with four recruited stoke patients are carried out with designed patient-centered passive rehabilitation exercise last for one month (22 training days). Each patient undergoes one session in horizontal and vertical exercises, respectively, 30 min/session, one training day. Then comparing RPTM of the patients for pretraining and postraining is shown as in Figure 7. By analyzing Figure 7, each patient regains an increased RPTM, whether in horizontal and vertical exercises or not, and the RPTM of Patient 1 and Patient 3 increase more obviously.

Figure 8 presents the recorded information (times for speed regulating and pausing) of Patient 1 during one session. Because the designed regulation mechanism makes the subject exercise with the maximum suitable RPTM, the times of speed regulating or pausing cannot directly reflect the patient's motion performance. In general, smaller RPTM presents less speed regulating or pausing. The RPTM and global coefficient for speed are determined to the motion performances, so they reflect the motion performances of

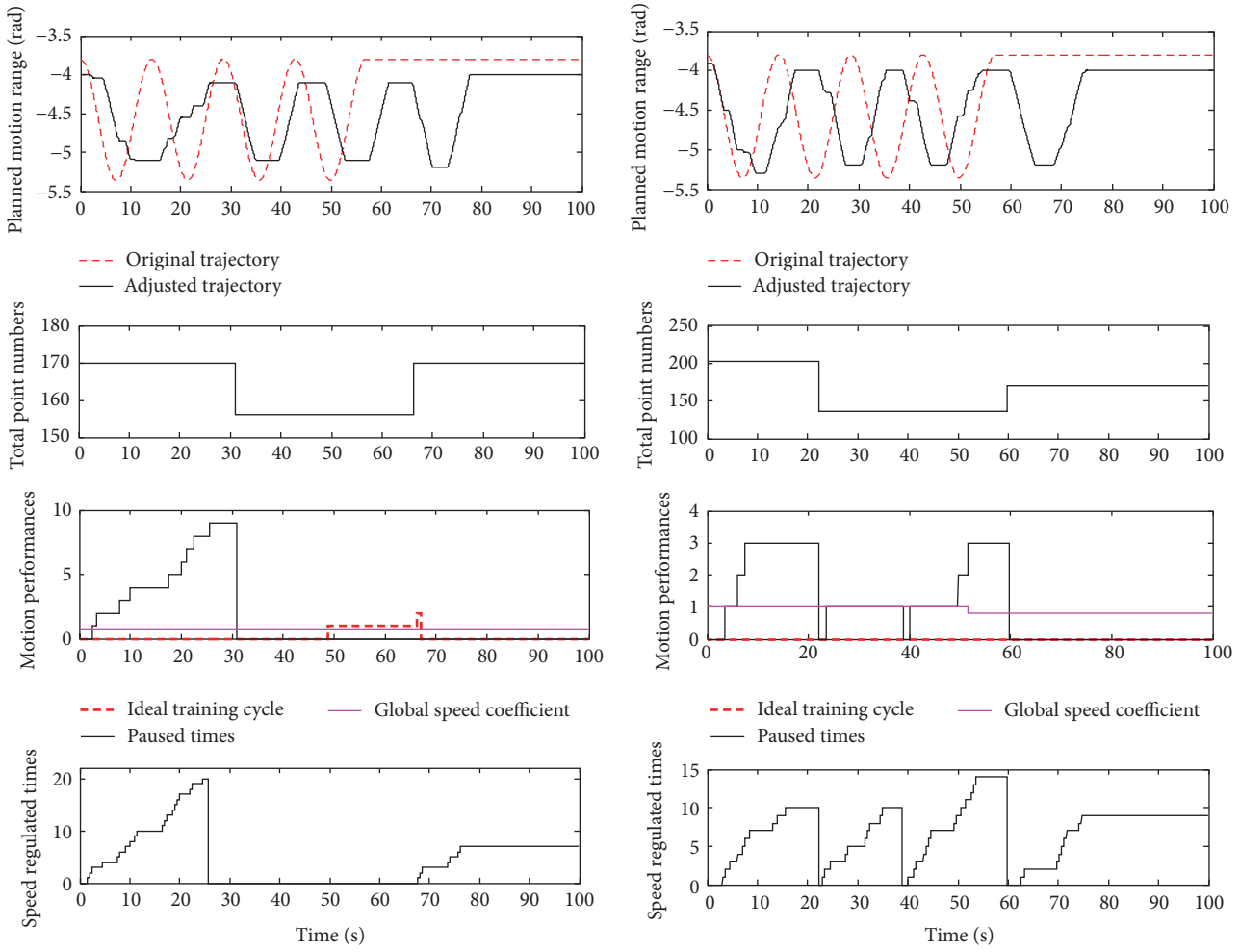

(a) Increasing the RPTM

(b) Decreasing the RPTM

Figure 6: Functional experiments in vertical exercise.

the impaired limb to some extent. Due to the fact that the RPTM and global coefficient for speed are regulated online, each mean of the parameters is adopted as the comparative indicators. According to the regulation mechanisms in Section 2.2.2, the RPTM is divided into 4 degrees labeled 1~4 and global coefficient for speed into 2 degrees labeled 1 and 2, respectively. Each mean of the RPTM and global coefficient for speed of each training day was described with 22 training days as in Figure 9. By analyzing the Figure 9, a conclusion can be made that the each mean of the RPTM and global coefficient for speed presents rising tendency; in other words, the motion performances of the impaired limb are improved to a certain extent.

5. Conclusion and Discussion

In this investigation, a control strategy with safety-motion decision-making mechanism was proposed to realize patient-centered passive neurorehabilitation exercise, serving with safety-and-efficacy robot-aided motion. The safety-motion decision-making mechanism was developed to observe and assess the PSTIL and motion performances in real time and regulate the training parameters according to the internal and external state of the subject, ensuring the safety of the supplied rehabilitation exercise. During the training, the PSTIL was online assessed by fuzzy logic reasoning with the extracted features of the position-velocity tracking information. The movement speed was regulated according to the assessed PSTIL with the designed mechanisms. In terms of safety for the emergency events, an emergency mode was developed, in which the manipulator moved with full gravity compensation. Moreover, the motion performances of the current two cycles were observed and assessed online and adopted to guide adjusting the RPTM according to the designed regulating mechanisms. In order to improve the interactive compliance, the position-based impedance controller was employed to execute the following motion training. Two types of experiments, functional experiments and clinical experiments were schemed and investigated with a healthy adult and four recruited stroke patients, respectively. The experimental results demonstrated that the suggested control strategy not only serves with safety-motion training but also presents rehabilitation efficacy. The developed safety-motion decision mechanism played an important

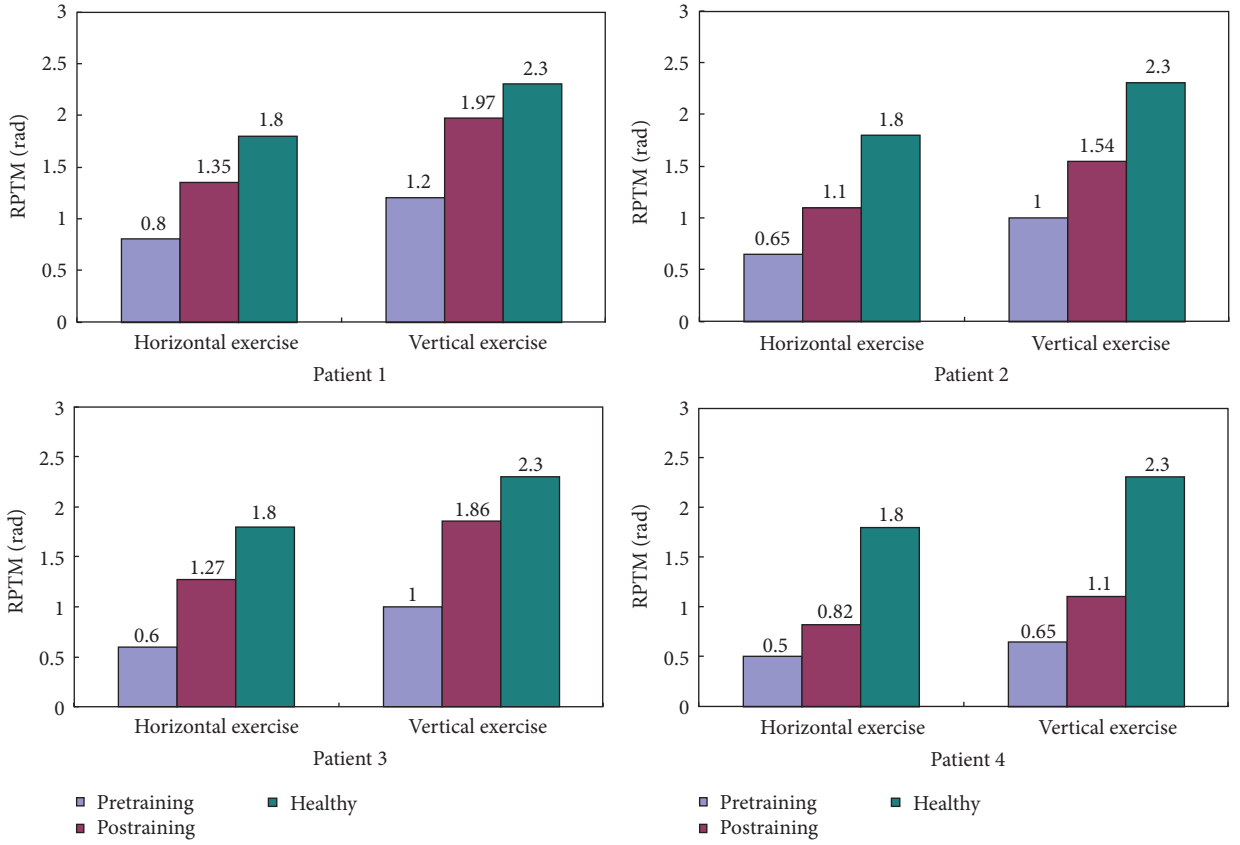

Figure 7: Compared RPTM of the patients for pretraining and postraining.

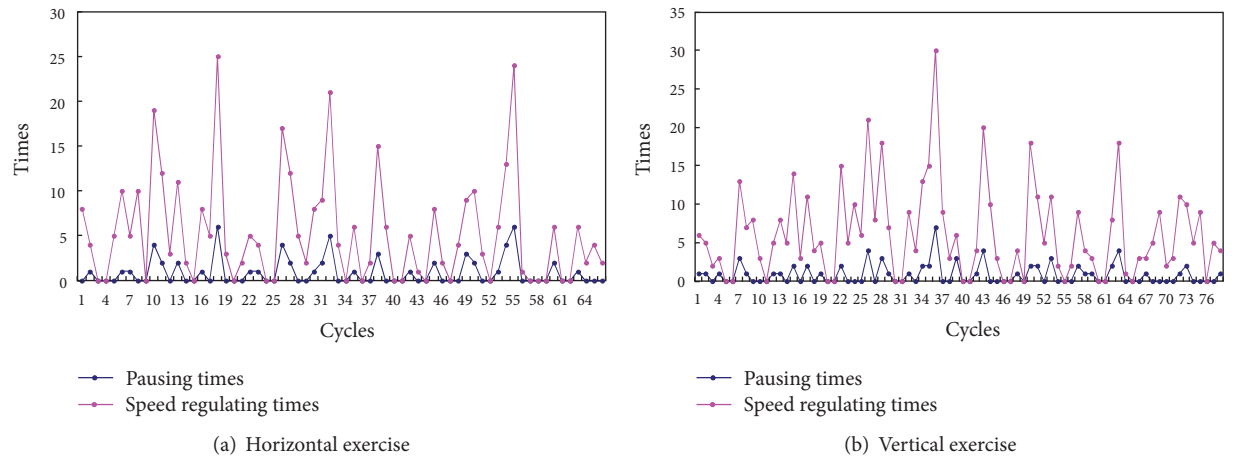

(a) Horizontal exercise

(b) Vertical exercise

Figure 8: Recorded information of Patient 1 during one session.

role to serve the subject with safety motion, as closely as what the therapist did. In next work, we will design a series of spatial trajectories, adopt some feedback strategies, and further investigate the rehabilitation efficacy with controlled experiments.

Competing Interests

The authors declare that there is no conflict of interests regarding the publication of this article and regarding the funding that they have received.

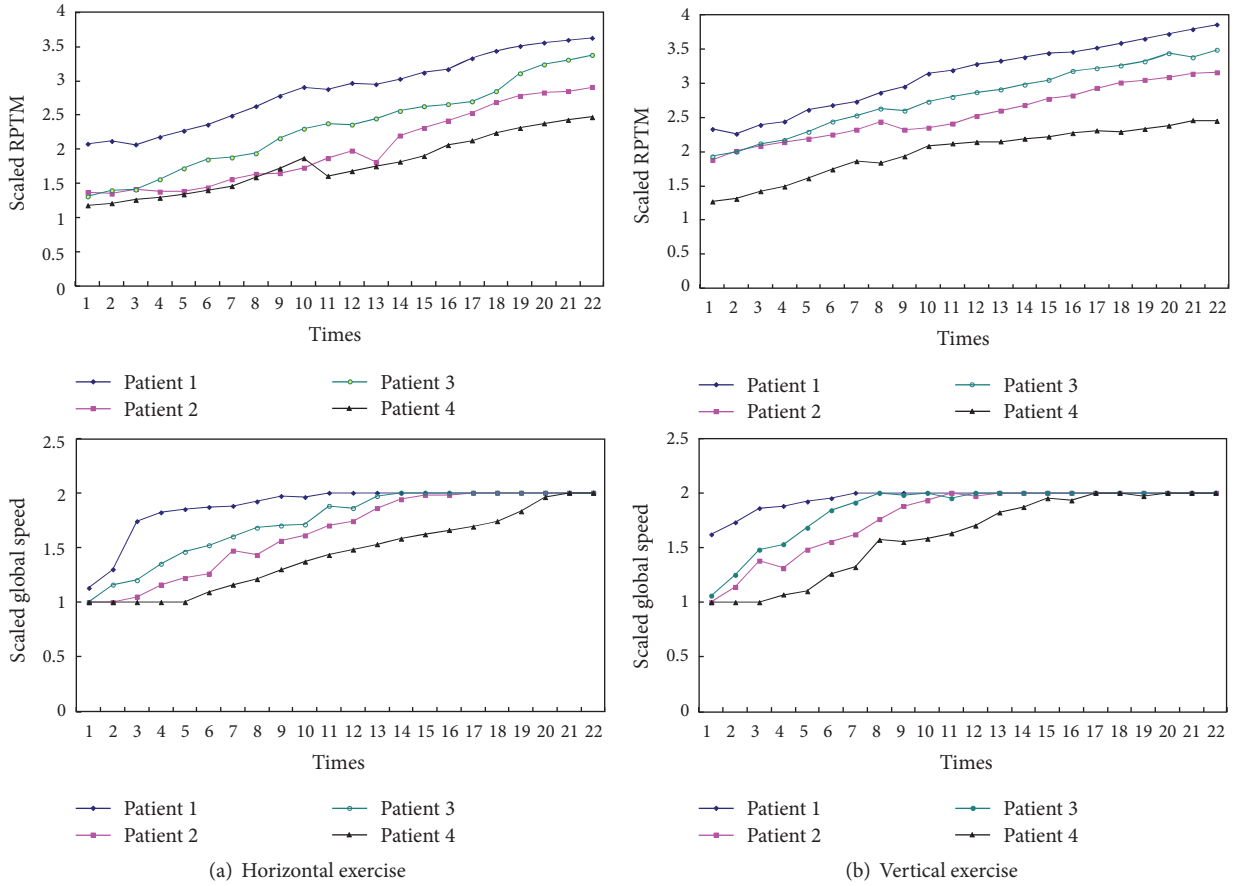

Figure 9: Recorded each mean of the RPTM and global speed (scaled results).

Acknowledgments

This work was funded by Jiangsu Ordinary University Science Research Project (14KJB510002), Open Foundation of Remote Measurement and Control Key Lab of Jiangsu Province (YCCK201303), and Foundation of Changzhou University (ZMF13020048).

References

[1] W. Meng, Q. Liu, Z. Zhou, Q. Ai, B. Sheng, and S. Xie, "Recent development of mechanisms and control strategies for robot-assisted lower limb rehabilitation," *Mechatronics*, vol. 31, pp. 132–145, 2015.

[2] C. Duret, O. Courtial, A.-G. Grosmaire, and E. Hutin, "Use of a robotic device for the rehabilitation of severe upper limb paresis in subacute stroke: exploration of patient/robot interactions and the motor recovery process," *BioMed Research International*, vol. 2015, Article ID 482389, 7 pages, 2015.

[3] J. Zhang and C. C. Cheah, "Passivity and stability of human-robot interaction control for upper-limb rehabilitation robots," *IEEE Transactions on Robotics*, vol. 31, no. 2, pp. 233–245, 2015.

[4] Z. Qian and Z. Bi, "Recent Development of Rehabilitation Robots," *Advances in Mechanical Engineering*, vol. 7, no. 2, Article ID 563062, 2015.

[5] Chinese Ministry of Health, http://www.moh.gov.cn/public/.

[6] J. Cao, S. Q. Xie, R. Das, and G. L. Zhu, "Control strategies for effective robot assisted gait rehabilitation: the state of art and future prospects," *Medical Engineering & Physics*, vol. 36, no. 12, pp. 1555–1566, 2014.

[7] L. Marchal-Crespo and D. J. Reinkensmeyer, "Review of control strategies for robotic movement training after neurologic injury," *Journal of NeuroEngineering and Rehabilitation*, vol. 6, article 20, 2009.

[8] M. Mendoza, I. Bonilla, E. González-Galván, and F. Reyes, "Impedance control in a wave-based teleoperator for rehabilitation motor therapies assisted by robots," *Computer Methods and Programs in Biomedicine*, vol. 123, pp. 54–67, 2016.

[9] M. Caimmi, E. Visani, F. Digiacomo et al., "Predicting functional recovery in chronic stroke rehabilitation using event-related desynchronization-synchronization during robot-assisted movement," *BioMed Research International*, vol. 2016, Article ID 7051340, 11 pages, 2016.

[10] N. Nordin, S. Q. Xie, and B. Wünsche, "Assessment of movement quality in robot-assisted upper limb rehabilitation after stroke: a review," *Journal of NeuroEngineering and Rehabilitation*, vol. 11, article 137, 2014.

[11] M. H. Rahman, M. J. Rahman, O. L. Cristobal, M. Saad, J. P. Kenné, and P. S. Archambault, "Development of a whole arm wearable robotic exoskeleton for rehabilitation and to assist upper limb movements," *Robotica*, vol. 33, no. 1, pp. 19–39, 2015.

[12] M. J. Johnson, "Recent trends in robot-assisted therapy environments to improve real-life functional performance after stroke,"

Journal of NeuroEngineering and Rehabilitation, vol. 3, no. 1, article 29, 6 pages, 2006.

[13] R. Loureiro, F. Amirabdollahian, M. Topping, B. Driessen, and W. Harwin, "Upper limb robot mediated stroke therapy—GENTLE/s approach," *Autonomous Robots*, vol. 15, no. 1, pp. 35–51, 2003.

[14] D. E. Barkana, J. Das, F. Wang, T. E. Groomes, and N. Sarkar, "Incorporating verbal feedback into a robot-assisted rehabilitation system," *Robotica*, vol. 29, no. 3, pp. 433–443, 2011.

[15] N. Tejima and D. Stefanov, "Fail-safe components for rehabilitation robots—a reflex mechanism and fail-safe force sensor," in *Proceedings of the IEEE 9th International Conference on Rehabilitation Robotics (ICORR '05)*, pp. 456–460, IEEE, Chicago, Ill, USA, July 2005.

[16] Y. Choi, J. Gordon, D. Kim, and N. Schweighofer, "An adaptive automated robotic task-practice system for rehabilitation of arm functions after stroke," *IEEE Transactions on Robotics*, vol. 25, no. 3, pp. 556–568, 2009.

[17] R. Morales, F. J. Badesa, N. García-Aracil, J. M. Sabater, and C. Pérez-Vidal, "Pneumatic robotic systems for upper limb rehabilitation," *Medical & Biological Engineering & Computing*, vol. 49, no. 10, pp. 1145–1156, 2011.

[18] A. Pervez and J. Ryu, "Safe physical human-robot interaction of mobility assistance robots: evaluation index and control," *Robotica*, vol. 29, no. 5, pp. 767–785, 2011.

[19] S. M. Grigorescu, T. Lüth, C. Fragkopoulos, M. Cyriacks, and A. Gräser, "A BCI-controlled robotic assistant for quadriplegic people in domestic and professional life," *Robotica*, vol. 30, no. 3, pp. 419–431, 2012.

[20] L. Z. Pan, A. G. Song, G. Z. Xu, H. Li, B. Xu, and P. Xiong, "Hierarchical safety supervisory control strategy for robot-assisted rehabilitation exercise," *Robotica*, vol. 31, no. 5, pp. 757–766, 2013.

[21] Y. Ma, S. Q. Xie, and Y. X. Zhang, "A patient-specific EMG-driven neuromuscular model for the potential use of human-inspired gait rehabilitation robots," *Computers in Biology and Medicine*, vol. 70, pp. 88–98, 2016.

[22] M. M. Fateh and R. Babaghasabha, "Impedance control of robots using voltage control strategy," *Nonlinear Dynamics*, vol. 74, no. 1-2, pp. 277–286, 2013.

[23] N. Hogan, "Impedance control: an approach to manipulation: part 1—theory, part 2—implementation, and part 3—application," *ASME Journal of Dynamic Systems, Measurement, and Control*, vol. 107, pp. 1–24, 1985.

[24] G. Z. Xu, A. G. Song, and H. J. Li, "Adaptive impedance control for upper-limb rehabilitation robot using evolutionary dynamic recurrent fuzzy neural network," *Journal of Intelligent & Robotic Systems*, vol. 62, no. 3-4, pp. 501–525, 2011.

Hindawi Publishing Corporation
BioMed Research International
Volume 2016, Article ID 2618265, 11 pages
http://dx.doi.org/10.1155/2016/2618265

Research Article

Vowel Imagery Decoding toward Silent Speech BCI Using Extreme Learning Machine with Electroencephalogram

Beomjun Min, Jongin Kim, Hyeong-jun Park, and Boreom Lee

Department of Biomedical Science and Engineering (BMSE), Institute of Integrated Technology (IIT), Gwangju Institute of Science and Technology (GIST), Gwangju, Republic of Korea

Correspondence should be addressed to Boreom Lee; leebr@gist.ac.kr

Received 30 September 2016; Revised 4 November 2016; Accepted 17 November 2016

Academic Editor: Han-Jeong Hwang

The purpose of this study is to classify EEG data on imagined speech in a single trial. We recorded EEG data while five subjects imagined different vowels, /a/, /e/, /i/, /o/, and /u/. We divided each single trial dataset into thirty segments and extracted features (mean, variance, standard deviation, and skewness) from all segments. To reduce the dimension of the feature vector, we applied a feature selection algorithm based on the sparse regression model. These features were classified using a support vector machine with a radial basis function kernel, an extreme learning machine, and two variants of an extreme learning machine with different kernels. Because each single trial consisted of thirty segments, our algorithm decided the label of the single trial by selecting the most frequent output among the outputs of the thirty segments. As a result, we observed that the extreme learning machine and its variants achieved better classification rates than the support vector machine with a radial basis function kernel and linear discrimination analysis. Thus, our results suggested that EEG responses to imagined speech could be successfully classified in a single trial using an extreme learning machine with a radial basis function and linear kernel. This study with classification of imagined speech might contribute to the development of silent speech BCI systems.

1. Introduction

People communicate with each other by exchanging verbal and visual expressions. However, paralyzed patients with various neurological diseases such as amyotrophic lateral sclerosis and cerebral ischemia have difficulties in daily communications because they cannot control their body voluntarily. In this context, brain-computer interface (BCI) has been studied as a tool of communication for these types of patients. BCI is a computer-aided control technology based on brain activity data such as EEG, which is appropriate for BCI systems because of its noninvasive nature and convenience of recording [1, 2].

The classification of EEG signals recorded during the motor imagery paradigm has been widely studied as a BCI controller [3–5]. According to these studies, different imagined tasks induce different EEG patterns on the contralateral hemisphere mainly in mu (7.5–12.5 Hz) and beta (13–30 Hz) frequency bands. Many researchers have successfully constructed BCI systems based on the limb movement imagination paradigm such as right hand, left hand, and foot movement [5–7]. However, EEG signals recorded during imagination of speech without any movement of either mouth or tongue are still difficult to classify; however, this topic has become an interesting issue for researchers because speech imagination has high similarity to real voice communication. For example, Deng et al. proposed a method to classify imagined syllables, /ba/ and /ku/, in three different rhythms using Hilbert spectrum methods, and the classification results were significantly greater than the chance level [8]. In addition, DaSalla et al. classified /a/ and /u/ as vowel speech imagery for EEG-based BCI [9]. Furthermore, a study to discriminate syllables embedded in spoken and imagined words using an electrocorticogram (ECoG) was conducted [10].

Obviously, for the BCI system, the use of optimized classification algorithms that categorize a set of data into different classes is essential, and these algorithms are usually

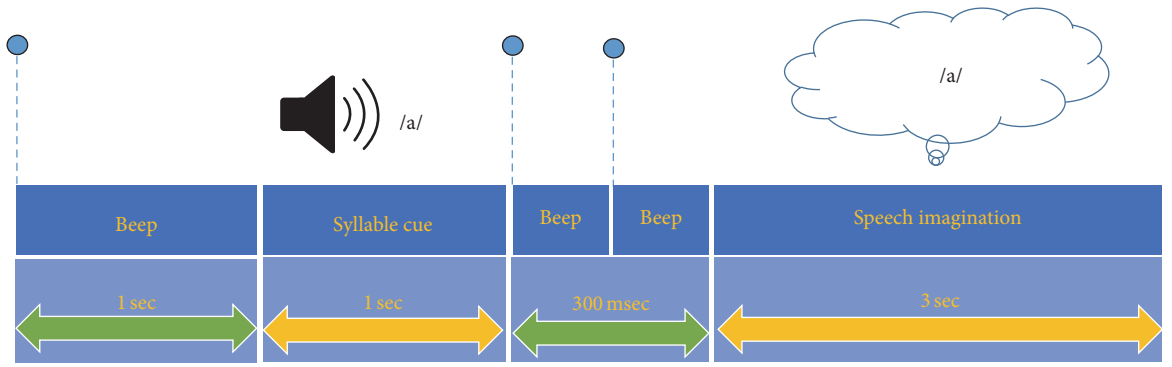

- Syllable cue: vowels /a/, /e/, /i/, /o/, /u/ and mute are randomly presented.
- Beep: beep sound for preparation of listening the sound or covert vowel articulation.
- Speech Imagination: covert vowel articulation (to imagine the vowel).

Figure 1: Schematic sequence of the experimental paradigm. Vowels /a/, /e/, /i/, /o/, /u/, and mute were randomly presented 1 s after the beginning of each trial. After the third beep sound, the subject imagines the same vowel heard at the beginning of the trial. The EEG data acquired during the speech imagination period were used for signal processing and classification in this study.

divided into five groups: linear classifiers, neural networks, nonlinear Bayesian classifiers, nearest neighbor classifiers, and combinations of classifiers [11]. For instance, various algorithms for speech classification have been used, such as k-nearest neighbor classifier (KNN) [12], support vector machine (SVM) [9, 13], and linear discriminant analysis (LDA) [8].

The extreme learning machine (ELM) is a type of feedforward neural network for classification, proposed by Huang et al. [14]. ELM has high speed and good generalization performance compared to the classic gradient-based learning algorithms. There is growing interest in the application of ELM and its variants in the biomedical field, such as epileptic EEG pattern recognition [15, 16], MRI study [17], and BCI [18].

In this study, we measured the EEG activities of speech imagination and attempted to classify those signals using the ELM algorithm and its variants with kernels. In addition, we compared the results to the support vector machine with a radial basis function (SVM-R) kernel and linear discriminant analysis (LDA). As far as we know, applications of ELM as a classifier for EEG data of imagined speech have been rarely studied. In the present study, we will examine the validity of using ELM and its variants in the classification of imagined speech and the possibility of our method for applications in BCI systems based on silent speech.

2. Materials and Methods

2.1. Participants. Five healthy human participants (5 males; mean age: 28.25 ± 2.71, range: 26–32) participated in this study. All participants were native Koreans with normal hearing and right-handedness. None of the participants had any known neurological disorders or other significant health problems. All participants gave written informed consent, and the experimental protocol was approved by the Institutional Review Board (IRB) of the Gwangju Institute of Science and Technology (GIST). The approval process of the IRB complies with the declaration of Helsinki.

2.2. Experimental Paradigm. Participants were seated in a comfortable armchair and wore earphones (er-4p, Etymotic research, Inc., IL 60007, United States of America) providing auditory stimuli. Five types of Korean syllables—/a/, /e/, /i/, /o/, and /u/, as well as a mute (zero volume) sound—were utilized in the experiment. Figure 1 describes the overall experimental paradigm. At the beginning of each trial, a beep sound was presented to prepare the participants for perception of the target syllable. These six auditory cues (including the mute sound) were recorded using Goldwave software (GoldWave, Inc., St. John's, Newfoundland, Canada), and the source audio was from Oddcast's online (http://www.oddcast.com/home/demos/tts/tts_example.php?sitepa). The five vowels and mute sound were randomly presented. Another 1 s after the onset of the target syllable, two beep sounds were given sequentially, with a 300 ms interval between them. After the two beep sounds, participants were instructed to imagine the same syllable heard at the beginning of the trial. The time for imagination was 3 s for each trial. Participants performed 5 sessions, with each session consisting of 10 trials for each syllable. Resting times were given between sessions for 1 min. Therefore, 50 trials were recorded for each syllable and the mute sound, and the total time for the experiment was approximately 10 min. All sessions were carried out in a day.

The experimental procedure was designed with e-Prime 2.0 software (Psychology Software Tools, Inc., Sharpsburg, PA, USA). A HydroCel Geodesic Sensor Net with 64 channels and Net Amps 300 amplifiers (Electrical Geodesics, Inc.,

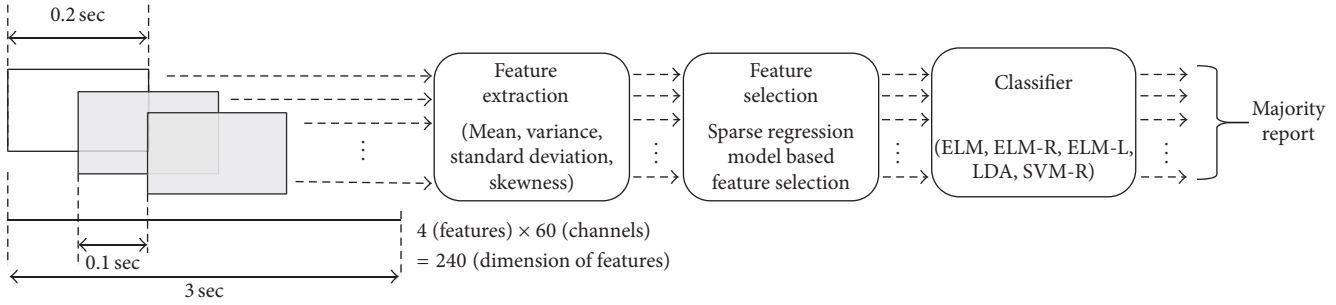

Figure 2: Overall signal processing procedure for classification. First, each trial was divided into thirty blocks with a 0.2 s length and 0.1 s overlap. Mean, variance, standard deviation, and skewness were extracted from all blocks and channels. Sequentially, sparse-regression-model-based feature selection was employed to reduce the dimension of the features. All features were used as the input of the trained classifier. Because each trial includes thirty blocks, thirty classifier outputs were acquired; therefore, the label of each trial was determined by selecting the most frequent output of the thirty classifier outputs.

Eugene, OR, USA) were used to record the EEG signals, using a 1000 Hz sampling rate (Net Station version 4.5.6).

2.3. Data Processing and Classification Procedure

2.3.1. Preprocessing. First, we resampled the acquired EEG data into 250 Hz for fast preprocessing procedure. The EEG data was bandpass filtered with 1–100 Hz. Sequentially, an IIR notch filter (Butterworth; order: 4; bandwidth: 59–61 Hz) was applied to remove the power line noise.

In general, EEG classification has problems in terms of poor generalization performance and the overfitting phenomenon because the number of samples is much smaller than the dimension of the features. Therefore, to obtain enough samples for learning and testing the classifier, we divided each imagination trial for 3 s into 30 time segments with a 0.2 s length and 0.1 s overlap. Therefore, we obtained a total of 9000 segments = (6 (conditions) × 50 (trials per each condition) × 30 segments) to learn and test the classifier. We calculated the mean, variance, standard deviation, and skewness from each segment to acquire the feature vector for the classifier. The dimension of the feature vector is 240 (4 (types of features) × 60 (the number of channels)). Additionally, to reduce the dimension of the feature vector, we applied a feature selection algorithm based on the sparse regression model. The selected set of features extracted from all segments was employed to learn and test the classifier. Because a trial consists of thirty segments, a trial has thirty outputs of the classifier. Therefore, the label of the test trial was determined by selecting the most frequent output among the outputs of the thirty segments. The training and testing of the classifier model are conducted using the segments extracted only from training data and testing data, respectively. Finally, to accurately estimate the classification performance, we applied 10-fold cross-validation. The classification accuracies of ELM, extreme learning machine with linear function (ELM-L), extreme learning machine with radial basis function (ELM-R), and SVM-R for all five subjects were compared to select the optimal classifier to discriminate the vowel imagination. The overall signal processing procedures are briefly described in Figure 2.

2.3.2. Sparse-Regression-Model-Based Feature Selection. Tibshirani developed a sparse regression model known as the Lasso estimate [19]. In this study, we employed the sparse regression model to select the discriminative set of features to classify the EEG responses to covert articulation. The formula for selecting discriminative features based on the sparse regression model can be described as follows:

$$\mathbf{z}^* = \underset{\mathbf{z}}{\operatorname{argmin}} \left\| \mathbf{F}\mathbf{z} - \bar{\mathbf{t}} \right\|_2^2 + \lambda \left\| z \right\|_1, \tag{1}$$

where $\| \cdot \|_p$ denotes the l_p-norm, $\mathbf{z}$ is a sparse vector to be learned, and $\mathbf{z}^*$ indicates an optimal sparse vector. $\bar{\mathbf{t}} \in \Re^{N_t \times 1}$ is a vector about the true class label for the number of training samples, N_t, and λ is a positive regularization parameter that controls the sparsity of $\mathbf{z}$. $\mathbf{F}$ is the matrix that consists of the mean, variance, standard deviation, and skewness for each channel

$$\mathbf{F} = \left[\mathbf{f}_1, \mathbf{f}_2, \ldots, \mathbf{f}_{240} \right], \tag{2}$$

where $\mathbf{f}_p \in \Re^{N_t \times 1}$ is the pth column vector of $\mathbf{F}$. The coordinate descent algorithm is adopted to solve the optimization problem in (1) [20].

The column vectors in $\mathbf{F}$ corresponding to the zero entries in $\mathbf{z}$ are excluded to form an optimized feature set, $\tilde{\mathbf{F}}$, that is of lower dimensionality than $\mathbf{F}$.

2.3.3. Extreme Learning Machine. Conventional feedforward neural networks require weights and biases for all layers to be adjusted by the gradient-based learning algorithms. However, the procedure for tuning the parameters of all layers is very slow because it is repeated many times, and its solutions easily fall into local optima. For this reason, Huang et al. proposed ELM, which randomly assigns the input weights and analytically calculates only the output

weights. Therefore, the learning speed of ELM is much faster than conventional learning algorithms and has outstanding generalization performance [21–23]. If we assume the N_t training samples $\{(\mathbf{v}_k, \mathbf{l}_k)\}_{k=1}^{N_t}$, where $\mathbf{v}_k$ is an n-dimensional feature vector, $\mathbf{v}_k = [v_{k,1}, v_{k,2}, \ldots, v_{k,n}]^T$, and $\mathbf{l}_k$ is the true labels, which consists of m-classes, $\mathbf{l}_k = [l_{k1}, l_{k2}, \ldots, l_{km}]^T$, a standard SLFN with N_h hidden neurons and activation function $a(\cdot)$ can be formulated as follows:

$$\sum_{j=1}^{N_h} \mathbf{w}_j^h a\left(\mathbf{w}_j^i \cdot \mathbf{v}_k + \mathbf{b}_j\right) = \mathbf{o}_k, \quad k = 1, \ldots, N_t, \tag{3}$$

where $\mathbf{w}_j^i = [w_{j,1}^i, w_{j,2}^i, \ldots, w_{j,n}^i]^T$ is the weight vector for the input layer between the jth hidden neuron and the input neurons, $\mathbf{w}_j^h = [w_{j,1}^h, w_{j,2}^h, \ldots, w_{j,m}^h]^T$ is the weight vector for the hidden layer between the jth hidden neuron and the output neurons, $\mathbf{o}_k = [o_{k,1}, o_{k,2}, \ldots, o_{k,m}]^T$ is the output vector of the network, and $\mathbf{b}_j$ is the bias of the jth hidden neuron. The operator $\cdot$ indicates the inner product. We can now reformulate the equation into matrix form as follows

$$\mathbf{A}\mathbf{W}^h = \mathbf{O}, \tag{4}$$

where

$$\mathbf{A} = \begin{bmatrix} a\left(\mathbf{w}_1^i \cdot \mathbf{v}_1 + \mathbf{b}_1\right) & \cdots & a\left(\mathbf{w}_{N_h}^i \cdot \mathbf{v}_1 + \mathbf{b}_{N_h}\right) \\ \vdots & \cdots & \vdots \\ a\left(\mathbf{w}_1^i \cdot \mathbf{v}_{N_t} + \mathbf{b}_1\right) & \cdots & a\left(\mathbf{w}_{N_h}^i \cdot \mathbf{v}_{N_t} + \mathbf{b}_{N_h}\right) \end{bmatrix}_{N_t \times N_h}, \tag{5}$$

$$\mathbf{W}^h = \begin{bmatrix} \mathbf{w}_1^h & \cdots & \mathbf{w}_{N_h}^h \end{bmatrix}_{N_h \times m}^T,$$

$$\mathbf{O} = \begin{bmatrix} \mathbf{o}_1 & \cdots & \mathbf{o}_{N_t} \end{bmatrix}_{N_t \times m}^T,$$

where matrix $\mathbf{A}$ is the output matrix of the hidden layer and the operator ^{T} indicates the transpose of the matrix. Because the ELM algorithm randomly selects the input weights $\mathbf{w}_j^i$ and biases $\mathbf{b}_j$, we can find weights for the hidden layer, $\mathbf{w}_j^h$, by solving the following optimization problem:

$$\min_{\mathbf{w}_j^h} \quad \left\|\mathbf{A}\mathbf{W}^h - \mathbf{L}\right\|^2, \tag{6}$$

where $\mathbf{L}$ is the matrix of true labels for training samples

$$\mathbf{L} = \begin{pmatrix} \mathbf{l}_1 & \cdots & \mathbf{l}_{N_t} \end{pmatrix}_{N_t \times m}^T. \tag{7}$$

The above problem is known as a linear system optimization problem, and its unique least-squares solution with a minimum norm is as follows:

$$\widehat{\mathbf{W}^h} = \mathbf{A}^\dagger \mathbf{L}, \tag{8}$$

where $\mathbf{A}^\dagger$ is the Moore–Penrose generalized inverse of the matrix $\mathbf{A}$. According to the analysis of Bartlett and Huang, the ELM algorithms achieve not only the minimum square training error but also the best generalization performance on novel test samples [14, 24].

In this paper, the activation function $a(\cdot)$ was determined to be a sigmoidal function, and the probability density function for assigning the input weights and biases was set to be a uniform distribution function.

3. Results and Discussion

3.1. Time-Frequency Analysis for Imagined Speech EEG Data. We computed the time-frequency representation (TFR) of imagined speech EEG data for every subject to identify speech-related brain activities. TFR of each trial was calculated using a Morlet wavelet and averaged over all trials. Among the five subjects, we plotted TFRs of subjects 2 and 5 which showed notable patterns in gamma frequency. As shown in Figure 3, much of the gamma band (30–70 Hz) powers of five vowel conditions (/a/, /e/, /i/, /o/, and /u/) in the left temporal area are totally distinct and much higher than those of the control condition (mute sound). In addition, topographical head plot of subject 5 was presented in Figure 4. Increased gamma activities were observed in both temporal regions when the subject imagined vowels.

3.2. Classification Results. Figure 5 shows the classification accuracies averaged over all pairwise classifications for five subjects using ELM, ELM-L, ELM-R, SVM-R, and LDA. We also conducted SVM and SVM with a linear kernel, but the results of SVM and SVM with a linear kernel are excluded because these classifiers could not be converged during many iterations (100,000 times). All classification accuracies are estimated by 10 × 10-fold cross-validation. In the cases of subjects 1, 3, and 4, ELM-L shows the best classification performance compared to the other four classifiers. However, ELM-R shows the best classification accuracies in subjects 2 and 5. In the cases of all subjects, the classification accuracies of ELM, ELM-L, and ELM-R are much better than those of SVM-R, which are approximately the chance level of 50%. To identify the best classifier to discriminate the vowel imagination, we conducted paired t-tests between the classification accuracies of ELM-R and those of the other three classifiers. As a result, the classification performance of ELM-R is significantly better than those of ELM ($p < 0.01$), LDA ($p < 0.01$), and SVM-R ($p < 0.01$). However, there is no significant difference between the classification accuracies of ELM-R and ELM-L ($p = 0.46$).

Table 1 describes the classification accuracies of subject 2, which shows the highest overall accuracies among all subjects, after 10 × 10-fold cross-validation, for all pairwise combinations. In almost all pairwise combinations, ELM-R has better classification performance than the other four classifiers for subject 2. The most discriminative pairwise combination for subject 2 is vowels /a/ and /i/, which shows 100% classification accuracy using ELM-R for subject 2.

Table 2 contains the results of ELM-R for the pairwise combinations and shows the top five classification performances for each subject. There is no pairwise combination to be selected from all subjects; however, /a/ versus mute and

Table 1: Classification accuracies in % employing SVM-R, ELM, ELM-L, ELM-R, and LDA for subject 2. The highest classification accuracy among the four classifiers is marked in bold for pairwise combination. Classification accuracies are expressed as mean and associated standard deviation. SVM-R, ELM, ELM-L, ELM-R, and LDA denote the support vector machine with radial basis function, extreme learning machine, extreme learning machine with a linear kernel, extreme learning machine with a radial basis function, and linear discriminant analysis, respectively.

Classifier	/a/ versus /e/	/a/ versus /i/	/a/ versus /o/	/a/ versus /u/	/e/ versus /i/	/e/ versus /o/	/e/ versus /u/	/i/ versus /o/	/i/ versus /u/	/o/ versus /u/	/a/ versus /mute/	/e/ versus /mute/	/i/ versus /mute/	/o/ versus /mute/	/u/ versus /mute/
SVM-R	50.24 ± 1.01	55.32 ± 2.15	51.41 ± 0.51	50.22 ± 0.60	50.31 ± 0.19	49.18 ± 0.23	52.41 ± 1.57	52.47 ± 0.71	51.11 ± 0.22	51.02 ± 1.32	49.48 ± 0.70	50.35 ± 0.22	51.22 ± 1.22	50.14 ± 1.60	51.23 ± 0.23
ELM	81.41 ± 1.18	94.23 ± 1.02	62.42 ± 2.15	73.34 ± 3.21	**90.55 ± 1.78**	69.76 ± 12.94	56.23 ± 3.48	96.32 ± 0.18	97.47 ± 0.76	66.81 ± 3.83	92.85 ± 2.43	82.31 ± 2.16	**99.41 ± 0.12**	88.16 ± 3.74	80.28 ± 2.87
ELM-L	81.32 ± 0.47	98.15 ± 0.67	67.11 ± 1.04	82.22 ± 2.40	88.31 ± 1.73	78.25 ± 2.23	53.14 ± 3.10	98.16 ± 0.37	**98.23 ± 2.12**	68.36 ± 1.63	92.28 ± 0.83	80.49 ± 3.70	99.12 ± 0.33	93.14 ± 2.21	87.25 ± 1.12
ELM-R	**86.28 ± 1.12**	**99.02 ± 0.76**	**73.03 ± 4.62**	83.14 ± 1.02	89.08 ± 0.14	**78.27 ± 0.16**	**58.36 ± 3.41**	**98.15 ± 0.22**	97.07 ± 1.42	**73.38 ± 2.73**	**95.09 ± 1.03**	**89.28 ± 3.13**	99.01 ± 0.14	**93.25 ± 0.73**	**93.01 ± 1.12**
LDA	79.25 ± 1.62	90.32 ± 2.61	60.57 ± 2.13	**84.12 ± 1.14**	88.23 ± 1.67	70.04 ± 1.43	56.38 ± 1.41	97.07 ± 0.39	96.28 ± 1.62	65.14 ± 1.73	91.26 ± 1.43	80.38 ± 4.70	98.07 ± 1.32	90.39 ± 1.62	82.25 ± 1.27

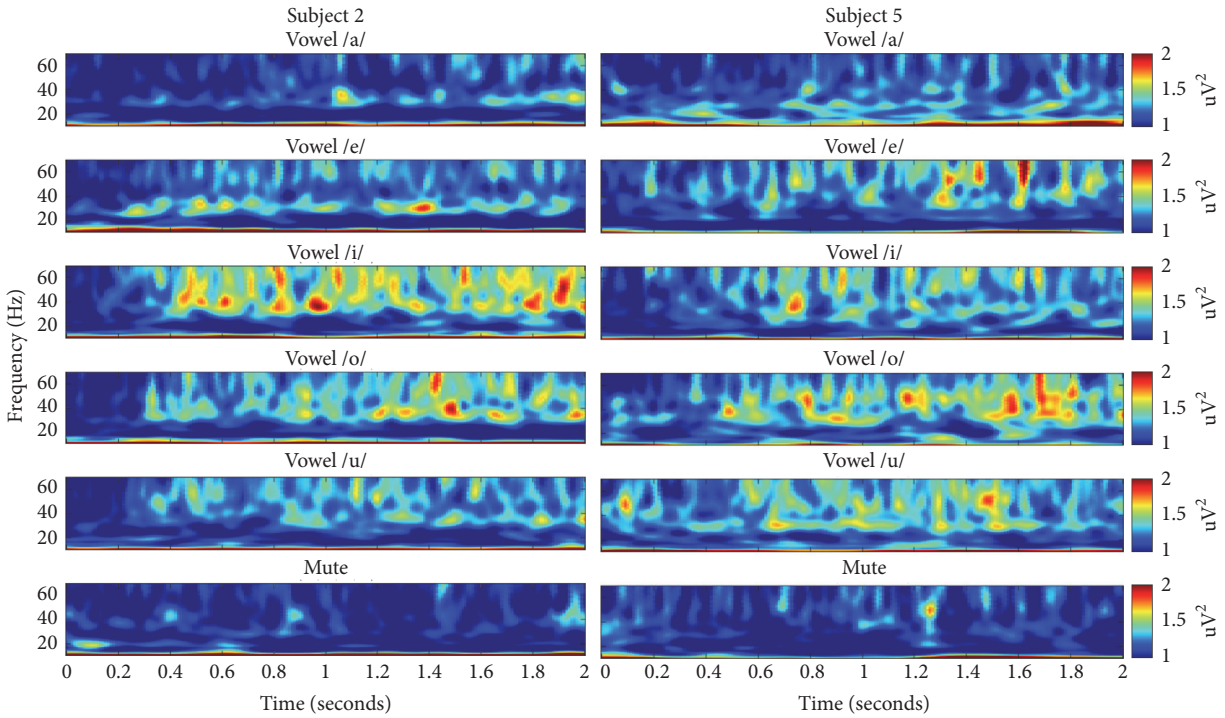

Figure 3: Time-frequency representation (TFR) of EEG signals averaged over all trials for subjects 2 and 5. The EEG signals were obtained from eight electrodes in the left temporal areas during each of the six experimental conditions (vowels /a/, /e/, /i/, /o/, /u/, and mute). The EEG data were bandpass filtered with 1–100 Hz, and a Morlet mother wavelet transform was used to calculate the TFR. The TFRs are plotted for the first 2 s after final beep sound and for the frequency range of 10–70 Hz.

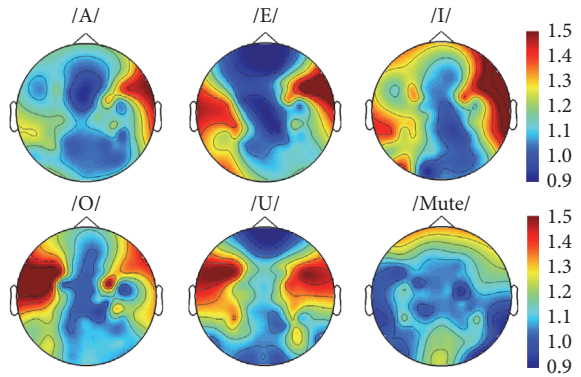

Figure 4: Topographical distribution of gamma activities during vowel imagination for subject 5. Increased activities were observed in both temporal areas when the subject imagined vowels. Time interval for the analysis is 0–3 sec.

/i/ versus mute are selected from four subjects, and /a/ versus /i/ is selected from three subjects.

Table 3 indicates the confusion matrix for all pairwise combinations and subjects using ELM, ELM-L, ELM-R, SVM-R, and LDA. In terms of sensitivity and specificity, ELM-L is the best classifier for our EEG data. Although SVM-R shows higher specificity than those of the other three classifiers in this table, SVM-R classified almost all conditions as positive and resulted in poor sensitivity; therefore, the high specificity of the SVM-R is possibly invalid. Thus, SVM-R might be an unsuitable classifier for our study.

3.3. Discussion. Overall, ELM, ELM-L, and ELM-R showed better performance than the SVM-R and LDA algorithms in this study. In several previous studies, ELM achieved similar or better classification accuracy rates with much less training time compared to other algorithms using EEG data [16, 25–27]. However, we could not find studies on classification of imagined speech using ELM algorithms. Deng et al. reported classification rates using LDA for imagined speech with 72.67% of the highest accuracy, but the average results were not much better than the chance level [8]. DaSalla et al. using SVM showed approximately 82% of the best accuracy and

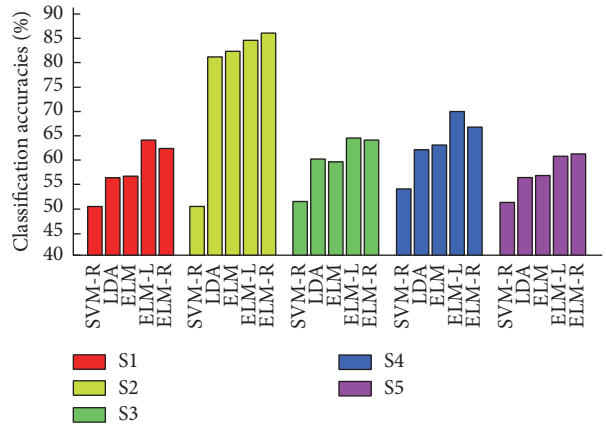

Figure 5: Averaged classification accuracies over all pairwise classification using a support vector machine with a radial basis function kernel (SVM-R), extreme learning machine (ELM), extreme learning machine with a linear kernel (ELM-L), and extreme learning machine with a radial basis function kernel (ELM-R) for all five subjects.

Table 2: Classification accuracies in % employing ELM-R for the pairwise combinations, which shows the top five classification performances for each subject. Classification accuracies are expressed as mean and associated standard deviation.

Subjects					
S1	86.47 ± 1.07	81.21 ± 1.03	80.01 ± 3.73	73.35 ± 3.17	72.44 ± 1.71
	(/a/ versus /i/)	(/a/ versus mute)	(/a/ versus /u/)	(/a/ versus /e/)	(/i/ versus /o/)
S2	99.02 ± 0.76	99.30 ± 0.14	98.22 ± 0.22	95.14 ± 1.03	93.01 ± 0.73
	(/a/ versus /i/)	(/i/ versus mute)	(/i/ versus /o/)	(/a/ versus mute)	(/o/ versus mute)
S3	92.08 ± 1.08	90.19 ± 0.63	89.15 ± 1.37	87.27 ± 0.71	70.38 ± 1.38
	(/e/ versus mute)	(/i/ versus mute)	(/u/ versus mute)	(/o/ versus mute)	(/a/ versus /i/)
S4	93.33 ± 0.31	92.27 ± 1.03	92.24 ± 2.13	91.12 ± 0.54	90.05 ± 1.83
	(/i/ versus mute)	(/u/ versus mute)	(/a/ versus mute)	(/e/ versus mute)	(/o/ versus mute)
S5	96.32 ± 2.31	94.01 ± 0.17	92.29 ± 1.14	90.07 ± 0.58	88.06 ± 1.23
	(/e/ versus mute)	(/i/ versus mute)	(/o/ versus mute)	(/a/ versus mute)	(/u/ versus mute)

73% of the average result overall [9], whereas Huang et al. reported that ELM tends to have a much higher learning speed and comparable generalization performance in binary classification [21]. In another study, Huang argued that ELM has fewer optimization constraints owing to its special separability feature and results in simpler implementation, faster learning, and better generalization performance [23]. Thus, our results showed consistent characters with others' previous research using ELM and even similar or better classification results for imagined speech compared to other research using different algorithms. Recently, ELM algorithms have been extensively applied in many other medical and biomedical studies [28–31]. More detailed information about ELM can be found in a recent review [32].

In this study, each trial was divided into the thirty time segments of 0.2 s in length and a 0.1 s overlap. Each time segment was considered as a sample for training the classifier, and the final label of the test sample was determined by selecting the most frequent output (see Figure 2). We also compared the classification accuracy of our method with those of a conventional method that does not divide the trials into multiple time segments. As a result, our method showed superior performance in terms of classification accuracy to the conventional method. In our opinion, by dividing the trials, some effects such as increasing number of trials for classifier training might occur, and each time segment with a 0.2 s length is likely to retain enough information for discrimination of EEG vowel imagination. Generally, EEG classification has problems in terms of poor generalization performance and the overfitting phenomenon because of the deficiency of the number of samples for the classifier. Therefore, an increased number of samples by dividing trials could mitigate the aforementioned problems. However, further analyses are required to prove our assumptions in subsequent studies.

To reduce the dimension of the feature vector, we employed a feature selection algorithm based on the sparse regression model. In the sparse-regression-model-based feature selection algorithm, the regularization parameter, λ, of equation (1) must be carefully selected because λ determines the dimension of the optimized feature parameter. For example, when the selected λ is too large, the algorithm excludes discriminative features from an optimal feature set, $\widetilde{\mathbf{F}}$. However, when users set λ too small, redundant features are not excluded from an optimal feature set $\widetilde{\mathbf{F}}$. Therefore, the optimal value for λ was selected by cross-validation on

Table 3: Confusion matrix for all pairwise combinations and subjects using ELM, ELM-L, ELM-R, SVM-R, and LDA.

	Classifiers									
	ELM		ELM-L		ELM-R		SVM-R		LDA	
	Condition positive	Condition negative	Condition positive	Condition negative	Condition positive	Condition negative	Condition positive	Condition negative	Condition positive	Condition positive
Test positive	2516	1234	2649	1101	2635	1115	3675	75	2556	1194
Test negative	1509	2241	1261	2489	1297	2453	3525	225	1398	2352
	Sensitivity = 0.6251	Specificity = 0.6449	Sensitivity = 0.6775	Specificity = 0.6933	Sensitivity = 0.6701	Specificity = 0.6875	Sensitivity = 0.5104	Specificity = 0.7500	Sensitivity = 0.6464	Specificity = 0.6633

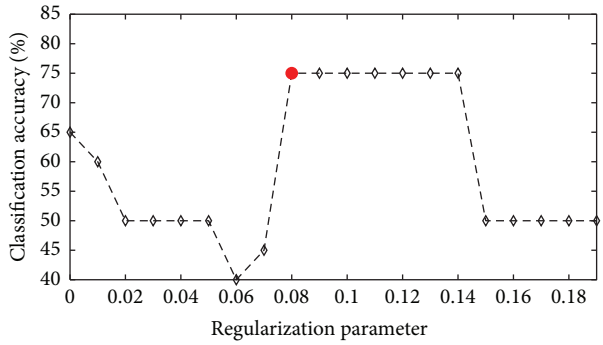

Figure 6: Effects of varying the regularization parameter on the classification accuracies obtained by ELM-R with sparse-regression-model-based feature selection for subject 2. The parameter value giving the highest accuracy is highlighted with a red circle.

the training session in our study. For example, the change of classification accuracy caused by varying λ for subject 1 is illustrated in Figure 6. In the case of /a/ and /i/ using ELM-R, the best classification accuracy reached a plateau at λ = 0.08 and declined after 0.14. However, the optimal values of λ are totally different among the pairwise combinations and all subjects.

Furthermore, our optimized results were achieved in the gamma frequency band (30–70 Hz). We also tested the other frequency ranges, such as beta (13–30 Hz), alpha (8–13 Hz), and, theta (4–8 Hz); however, the classification rates of those bands were not much better than the chance level in every subject and pairwise combination of syllables. In addition, the results of our TFR and topographical analysis (Figures 3 and 4) could support some relationship between gamma activities and imagined speech processing. As far as we know, in the EEG classification of imagined speech, there have been only a few studies that examined the differences between multiple frequency bands including gamma frequency [33, 34]. Therefore, our study might be the first report that the gamma frequency band could play an important role as features for the EEG classification of imagined speech. Moreover, several studies using ECoG reported quite good results in the gamma frequency for imagined speech classification [35, 36], and these findings are consistent with our results. However, several studies have been conducted that suggested the role of gamma frequency band for speech processing in neurophysiological perspectives [37–39]. However, those studies usually used intracranial recordings and focused on the analysis for the high gamma (70–150 Hz) frequency band. Thus, suggesting a relevance between those results and our classification study is not easy. However, a certain relation between some information in low gamma frequencies as a feature for classification and its implication from a neurophysiological view will be specified in future studies.

Currently, communication systems with various BCI technologies have been developed for disabled people [40]. For instance, the P300 speller is one of the most widely researched BCI technologies to decode verbal thoughts from EEG [41]. Despite many efforts toward better and faster performance, the P300 speller is still insufficient for use in normal conversation [42, 43], whereas, independent of the P300 component, efforts toward extraction and analysis of EEG or ECoG induced by imagined speech have been conducted [44, 45]. In this context, our results of high performance from the application of ELM and its variants have potential to advance BCI research using silent speech communication. However, the pairwise combinations with the highest accuracies (see Table 2) differed in each subject. After experiment, each participant reported different patterns of vowel discrimination. For example, one subject reported that he could not discriminate /e/ from /i/, and the other subject reported the other pair was not easy to distinguish. Although those reports were not exactly matched to the results of classification, these discrepancies of subjective sensory perception might be related to process of imagining speech and classification results. Besides, we have not tried multiclass classification in this study, yet some attempts in multiclass classification of imagined speech have been performed by others [8, 46, 47]. These issues related to intersubject variability and multiclass systems should be considered for our future study to develop more practical and generalized BCI systems using silent speech.

4. Conclusions

In the present study, we used classification algorithms for EEG data of imagined speech. Particularly, we compared ELM and its variants to SVM-R and LDA algorithms and observed that ELM and its variants showed better performance than other algorithms with our data. These results might lead to the development of silent speech BCI systems.

Competing Interests

The authors declare that there is no conflict of interests regarding the publication of this paper.

Authors' Contributions

Beomjun Min and Jongin Kim equally contributed to this work.

Acknowledgments

This research was supported by the GIST Research Institute (GRI) in 2016 and the Pioneer Research Center Program through the National Research Foundation of Korea funded by the Ministry of Science, ICT & Future Planning (Grant no. 2012-0009462).

References

[1] H.-J. Hwang, S. Kim, S. Choi, and C.-H. Im, "EEG-based brain-computer interfaces: a thorough literature survey," *International Journal of Human-Computer Interaction*, vol. 29, no. 12, pp. 814–826, 2013.

[2] U. Chaudhary, N. Birbaumer, and A. Ramos-Murguialday, "Brain–computer interfaces for communication and rehabilitation," *Nature Reviews Neurology*, vol. 12, no. 9, pp. 513–525, 2016.

[3] M. Hamedi, S.-H. Salleh, and A. M. Noor, "Electroencephalographic motor imagery brain connectivity analysis for BCI: a review," *Neural Computation*, vol. 28, no. 6, pp. 999–1041, 2016.

[4] C. Neuper, R. Scherer, S. Wriessnegger, and G. Pfurtscheller, "Motor imagery and action observation: modulation of sensorimotor brain rhythms during mental control of a brain-computer interface," *Clinical Neurophysiology*, vol. 120, no. 2, pp. 239–247, 2009.

[5] H.-J. Hwang, K. Kwon, and C.-H. Im, "Neurofeedback-based motor imagery training for brain–computer interface (BCI)," *Journal of Neuroscience Methods*, vol. 179, no. 1, pp. 150–156, 2009.

[6] G. Pfurtscheller, C. Brunner, A. Schlögl, and F. H. Lopes da Silva, "Mu rhythm (de)synchronization and EEG single-trial classification of different motor imagery tasks," *NeuroImage*, vol. 31, no. 1, pp. 153–159, 2006.

[7] M. Ahn and S. C. Jun, "Performance variation in motor imagery brain-computer interface: a brief review," *Journal of Neuroscience Methods*, vol. 243, pp. 103–110, 2015.

[8] S. Deng, R. Srinivasan, T. Lappas, and M. D'Zmura, "EEG classification of imagined syllable rhythm using Hilbert spectrum methods," *Journal of Neural Engineering*, vol. 7, no. 4, Article ID 046006, 2010.

[9] C. S. DaSalla, H. Kambara, M. Sato, and Y. Koike, "Single-trial classification of vowel speech imagery using common spatial patterns," *Neural Networks*, vol. 22, no. 9, pp. 1334–1339, 2009.

[10] X. Pei, D. L. Barbour, E. C. Leuthardt, and G. Schalk, "Decoding vowels and consonants in spoken and imagined words using electrocorticographic signals in humans," *Journal of Neural Engineering*, vol. 8, no. 4, Article ID 046028, 2011.

[11] F. Lotte, M. Congedo, A. Lécuyer, F. Lamarche, and B. Arnaldi, "A review of classification algorithms for EEG-based brain-computer interfaces," *Journal of Neural Engineering*, vol. 4, no. 2, article R01, pp. R1–R13, 2007.

[12] K. Brigham and B. V. K. V. Kumar, "Imagined speech classification with EEG signals for silent communication: a preliminary investigation into synthetic telepathy," in *Proceedings of the 4th International Conference on Bioinformatics and Biomedical Engineering (iCBBE '10)*, Chengdu, China, June 2010.

[13] J. Kim, S.-K. Lee, and B. Lee, "EEG classification in a single-trial basis for vowel speech perception using multivariate empirical mode decomposition," *Journal of Neural Engineering*, vol. 11, no. 3, Article ID 036010, 2014.

[14] G.-B. Huang, Q.-Y. Zhu, and C.-K. Siew, "Extreme learning machine: theory and applications," *Neurocomputing*, vol. 70, no. 1-3, pp. 489–501, 2006.

[15] Y. Song and J. Zhang, "Automatic recognition of epileptic EEG patterns via Extreme Learning Machine and multiresolution feature extraction," *Expert Systems with Applications*, vol. 40, no. 14, pp. 5477–5489, 2013.

[16] Q. Yuan, W. Zhou, S. Li, and D. Cai, "Epileptic EEG classification based on extreme learning machine and nonlinear features," *Epilepsy Research*, vol. 96, no. 1-2, pp. 29–38, 2011.

[17] M. N. I. Qureshi, B. Min, H. J. Jo, and B. Lee, "Multiclass classification for the differential diagnosis on the ADHD subtypes using recursive feature elimination and hierarchical extreme learning machine: structural MRI study," *PLoS ONE*, vol. 11, no. 8, Article ID e0160697, 2016.

[18] L. Gao, W. Cheng, J. Zhang, and J. Wang, "EEG classification for motor imagery and resting state in BCI applications using multi-class Adaboost extreme learning machine," *Review of Scientific Instruments*, vol. 87, no. 8, Article ID 085110, 2016.

[19] R. Tibshirani, "Regression shrinkage and selection via the Lasso Robert Tibshirani," *Journal of the Royal Statistical Society: Series B (Statistical Methodology)*, vol. 58, no. 1, pp. 267–288, 2007.

[20] J. Friedman, T. Hastie, and R. Tibshirani, "Regularization paths for generalized linear models via coordinate descent," *Journal of Statistical Software*, vol. 33, no. 1, pp. 1–22, 2010.

[21] G.-B. Huang, H. Zhou, X. Ding, and R. Zhang, "Extreme learning machine for regression and multiclass classification," *IEEE Transactions on Systems, Man, and Cybernetics Part B: Cybernetics*, vol. 42, no. 2, pp. 513–529, 2012.

[22] J. Cao, Z. Lin, and G.-B. Huang, "Composite function wavelet neural networks with extreme learning machine," *Neurocomputing*, vol. 73, no. 7-9, pp. 1405–1416, 2010.

[23] G.-B. Huang, X. Ding, and H. Zhou, "Optimization method based extreme learning machine for classification," *Neurocomputing*, vol. 74, no. 1-3, pp. 155–163, 2010.

[24] P. L. Bartlett, "The sample complexity of pattern classification with neural networks: the size of the weights is more important than the size of the network," *Institute of Electrical and Electronics Engineers. Transactions on Information Theory*, vol. 44, no. 2, pp. 525–536, 1998.

[25] L.-C. Shi and B.-L. Lu, "EEG-based vigilance estimation using extreme learning machines," *Neurocomputing*, vol. 102, pp. 135–143, 2013.

[26] Y. Peng and B.-L. Lu, "Discriminative manifold extreme learning machine and applications to image and EEG signal classification," *Neurocomputing*, vol. 174, pp. 265–277, 2014.

[27] N.-Y. Liang, P. Saratchandran, G.-B. Huang, and N. Sundararajan, "Classification of mental tasks from EEG signals using extreme learning machine," *International Journal of Neural Systems*, vol. 16, no. 1, pp. 29–38, 2006.

[28] J. Kim, H. S. Shin, K. Shin, and M. Lee, "Robust algorithm for arrhythmia classification in ECG using extreme learning machine," *Biomedical Engineering OnLine*, vol. 8, article 31, 2009.

[29] S. Karpagachelvi, M. Arthanari, and M. Sivakumar, "Classification of electrocardiogram signals with support vector machines and extreme learning machine," *Neural Computing and Applications*, vol. 21, no. 6, pp. 1331–1339, 2012.

[30] W. Huang, Z. M. Tan, Z. Lin et al., "A semi-automatic approach to the segmentation of liver parenchyma from 3D CT images with Extreme Learning Machine," in *Proceedings of the IEEE*

Annual International Conference of the IEEE Engineering in Medicine and Biology Society (EMBC' 12), pp. 3752–3755, Buenos Aires, Argentina, September 2012.

[31] R. Barea, L. Boquete, S. Ortega, E. López, and J. M. Rodríguez-Ascariz, "EOG-based eye movements codification for human computer interaction," *Expert Systems with Applications*, vol. 39, no. 3, pp. 2677–2683, 2012.

[32] G. Huang, G.-B. Huang, S. Song, and K. You, "Trends in extreme learning machines: a review," *Neural Networks*, vol. 61, pp. 32–48, 2015.

[33] B. M. Idrees and O. Farooq, "Vowel classification using wavelet decomposition during speech imagery," in *Proceedings of the International Conference on Signal Processing and Integrated Networks (SPIN '16)*, pp. 636–640, Noida, India, Feburary 2016.

[34] A. Riaz, S. Akhtar, S. Iftikhar, A. A. Khan, and A. Salman, "Inter comparison of classification techniques for vowel speech imagery using EEG sensors," in *Proceedings of the 2nd International Conference on Systems and Informatics (ICSAI '14)*, pp. 712–717, IEEE, Shanghai, China, November 2014.

[35] S. Martin, P. Brunner, I. Iturrate et al., "Word pair classification during imagined speech using direct brain recordings," *Scientific Reports*, vol. 6, Article ID 25803, 2016.

[36] X. Pei, J. Hill, and G. Schalk, "Silent communication: toward using brain signals," *IEEE Pulse*, vol. 3, no. 1, pp. 43–46, 2012.

[37] A.-L. Giraud and D. Poeppel, "Cortical oscillations and speech processing: emerging computational principles and operations," *Nature Neuroscience*, vol. 15, no. 4, pp. 511–517, 2012.

[38] V. L. Towle, H.-A. Yoon, M. Castelle et al., "ECoG γ activity during a language task: differentiating expressive and receptive speech areas," *Brain*, vol. 131, no. 8, pp. 2013–2027, 2008.

[39] S. Martin, P. Brunner, C. Holdgraf et al., "Decoding spectrotemporal features of overt and covert speech from the human cortex," *Frontiers in Neuroengineering*, vol. 7, article 14, 2014.

[40] J. S. Brumberg, A. Nieto-Castanon, P. R. Kennedy, and F. H. Guenther, "Brain-computer interfaces for speech communication," *Speech Communication*, vol. 52, no. 4, pp. 367–379, 2010.

[41] L. A. Farwell and E. Donchin, "Talking off the top of your head: toward a mental prosthesis utilizing event-related brain potentials," *Electroencephalography and Clinical Neurophysiology*, vol. 70, no. 6, pp. 510–523, 1988.

[42] D. J. Krusienski, E. W. Sellers, F. Cabestaing et al., "A comparison of classification techniques for the P300 Speller," *Journal of Neural Engineering*, vol. 3, no. 4, article 007, pp. 299–305, 2006.

[43] E. Yin, Z. Zhou, J. Jiang, F. Chen, Y. Liu, and D. Hu, "A novel hybrid BCI speller based on the incorporation of SSVEP into the P300 paradigm," *Journal of Neural Engineering*, vol. 10, no. 2, Article ID 026012, 2013.

[44] C. Herff and T. Schultz, "Automatic speech recognition from neural signals: a focused review," *Frontiers in Neuroscience*, vol. 10, article 429, 2016.

[45] S. Chakrabarti, H. M. Sandberg, J. S. Brumberg, and D. J. Krusienski, "Progress in speech decoding from the electrocorticogram," *Biomedical Engineering Letters*, vol. 5, no. 1, pp. 10–21, 2015.

[46] K. Mohanchandra and S. Saha, "A communication paradigm using subvocalized speech: translating brain signals into speech," *Augmented Human Research*, vol. 1, no. 1, article 3, 2016.

[47] O. Ossmy, I. Fried, and R. Mukamel, "Decoding speech perception from single cell activity in humans," *NeuroImage*, vol. 117, pp. 151–159, 2015.

Hindawi Publishing Corporation
BioMed Research International
Volume 2016, Article ID 2826905, 8 pages
http://dx.doi.org/10.1155/2016/2826905

Research Article

Integrative Evaluation of Automated Massage Combined with Thermotherapy: Physical, Physiological, and Psychological Viewpoints

Do-Won Kim,[1,2] Dae Woon Lee,[3] Joergen Schreiber,[4] Chang-Hwan Im,[5] and Hansung Kim[3,6]

[1]*Department of Biomedical Engineering, Chonnam National University, 50 Daehak-ro, Yeosu-si 59626, Republic of Korea*
[2]*Berlin Institute of Technology, Machine Learning Group, Marchstraße 23, 10587 Berlin, Germany*
[3]*Yonsei Fraunhofer IZFP Medical Device Lab, Yonsei University, Medical Industry Techo Tower 205, Wonju 220-710, Republic of Korea*
[4]*Fraunhofer Institute for Ceramic Technologies and Systems, Maria-Reiche-Straße 2, 01109 Dresden, Germany*
[5]*Department of Biomedical Engineering, Hanyang University, 17 Haengdang-dong, Seongdong-gu, Seoul 133-791, Republic of Korea*
[6]*Department of Biomedical Engineering, Yonsei University, Medical Industry Techno Tower 307, Wonju 220-710, Republic of Korea*

Correspondence should be addressed to Hansung Kim; hanskim@yonsei.ac.kr

Received 7 July 2016; Revised 18 September 2016; Accepted 28 September 2016

Academic Editor: Ashraf S. Gorgey

Various types of massages are reported to relieve stress, pain, and anxiety which are beneficial for rehabilitation; however, more comprehensive studies are needed to understand the mechanism of massage therapy. In this study, we investigated the effect of massage therapy, alone or in combination with infrared heating, on 3 different aspects: physical, physiological, and psychological. Twenty-eight healthy university students were subjected to 3 different treatment conditions on separate days, one condition per day: control, massage only, or massage with infrared heating. Physical (trunk extension [TE]; maximum power of erector spinae), physiological (heart-rate variability [HRV]; electroencephalogram [EEG]), and psychological (state-trait anxiety inventory [STAI]; visual analogue scale [VAS]) measurements were evaluated and recorded before and after each treatment condition. The results showed that massage therapy, especially when combined with infrared heating, significantly improved physical functioning, increased parasympathetic response, and decreased psychological stress and anxiety. In the current study, we observed that massage therapy contributes to various physical, physiological, and psychological changes, where the effect increases with thermotherapy.

1. Introduction

Massage therapy is a systematic manipulation of soft tissues with rhythmical pressure and stroking which contributes to relieving various types of body distress [1, 2]. Massage therapy is often used as a complimentary therapy to support pharmacological treatment with sedatives and analgesics for reducing stress, pain, or anxiety of the patients. However, controlled studies investigating the mechanisms underlying the benefits of massage therapy were absent until recently [3].

Over the past two decades, investigators have shown the effects of massage therapy on various physiological features, such as blood pressure [4, 5], heart-rate variability (HRV) [6], and electroencephalogram (EEG) [3, 7], and also in terms of psychological abilities, such as mental operations and psychological record [8–11]. In most studies, researchers have reported that massage therapy relieves psychological or physiological stress, for instance, chronic pain (e.g., headache and low back pain) [12–14], muscle fatigue, anxiety [15, 16], or depression [7, 17, 18]. Therefore, massage therapy is often used for rehabilitation purposes, often in combination with other rehabilitation methods to maximize the effect.

However, despite various attempts to find the underlying mechanism of massage therapy, it is still unclear how exactly massage therapy affects our body. Researchers suggested that massage therapy activates the parasympathetic nervous

Table 1: Demographic data of the participants.

Male : female	15 : 13
Age (years)	25.00 ± 2.66
Weight (kg)	64.46 ± 12.92
Height (cm)	168.29 ± 7.68
BMI	22.20 ± 3.15

BMI: body mass index.

system, which in turn decreases blood pressure, heart rate, and muscle fatigue and increases muscle oxygenation [6, 19–22], whereas others show activation of the sympathetic nervous system [23–25]. This inconsistency might be because of differences in massage technique, treatment time, or operator skill level which are not standardized between studies. Therefore, the need for systematic studies has been suggested [8, 26].

One way to overcome inconsistent outcomes with massage treatment is to use an automated massage device. The automated massage device has some advantages compared to the traditional massage methods performed by the therapist. First, it does not depend on the therapists' physical condition and always delivers a consistent pressure. Also, the massage pressure and location can be controlled precisely depending on the subjects' physical condition. Third, the automated massage can easily be combined with thermotherapy, where recent studies have suggested that massage accompanied with skin heating may have positive effects, such as increased skin blood flow [27] and decreased plasma cortisol and norepinephrine [28].

The current study evaluated the effect of automated massage therapy from three perspectives: physical, physiological, and psychological. We have used trunk extension (TE) and electromyography (EMG) as physical measures; heart-rate variability (HRV) and EEG as physiological measures; and state anxiety inventory (STAI-X-1) and visual analogue scale (VAS) as psychological measures. The massage therapy was controlled using an automatic chiropractic massage bed to minimize the performance of the massages. We also tested the effect of a combined massage program that consisted of pressure massage and thermotherapy.

2. Materials and Methods

2.1. Participants. Twenty-eight healthy participants (15 men and 13 women) were recruited through on-campus advertisements, bulletin boards, or verbal requests. An initial screening interview was conducted to check for history of psychiatric disease, mood disorder, brain injury, cardiovascular disease, or if he/she was on medications that might influence their response to treatment. The participants' demographic data are given in Table 1. All participants were right-handed and had normal or corrected-normal vision. The mean age of the male participants was 26.2 ± 2.68 years, and their average mean body mass index (BMI) was 24.69 ± 1.82; the mean age of the female participants was 23.26 ± 1.82 years, and their average BMI was 19.33 ± 1.34. There were statistical differences between genders in age ($p = 0.009$). All experimental procedures were approved by Yonsei University Wonju Campus Human Studies Committee (approval number: 2011-15).

2.2. Test Conditions and Procedure. Upon enrollment, the participants were scheduled for 3 different visits in a week. During each visit, the participants were treated with either chiropractic (single massage [SM]), chiropractic with infrared heating stimulation (combined massage [CM]), or control (CON) treatment. For SM, the participants laid on an automatic spine massage bed (NM-5000; Nuga Medical, Wonju, Korea) and underwent a 20 min preprogrammed chiropractic massage sequence (Figure 1). In this sequence, a roller massages the muscles along the spine by moving up and down from cervical vertebrae to coccygeal vertebra (Figure 2). For CM, a heat source was added to the 20 min massage program. The heat was delivered using the heating light source located inside the roller. The temperature of the light source was set to 60°C (140°F). For CON, the participant laid on the massage bed without any massage/heat stimulation. All participants were asked to close their eyes, yet to keep themselves alert during the experiment.

2.3. Psychological, Physical, and Physiological Evaluations

2.3.1. Physical Evaluation. To evaluate the physical changes before and after each treatment, EMG signals were measured during TE. The performer first lies prone on the floor and interlaces the fingers behind the head, which is the rest position. While the assistant secures the performer's hip against the floor, on the instruction "go," the performer has to raise the chest and head from the floor as far as possible. TE was measured by the distance between the participants' chin and floor during trunk extension, indicating the flexibility of the trunk and also the fatigue and strength of the back muscle [29, 30]. The performance was measured by the average height of three attempts.

The EMG signal of erector spinae was recorded during TE, by attaching two electrodes of 4 cm horizontally centered on the participants' L3. The signal was recorded using EMG100C amplifier (Biopac Systems, Inc., USA) with sampling frequency of 1000 Hz. The EMG signal was filtered online using a 10–500 Hz band pass filter. Then, the root mean square (RMS) of the EMG signal during TE was averaged, which indicated the maximum strength of erector spinae muscles [31, 32].

2.3.2. Physiological Evaluation. Physiological changes between pre- and posttreatment were evaluated using the ratio between high frequency and low frequency (LF/HF); heart rate (HR) derived from electrocardiogram (ECG); and spectral power of delta (1–4 Hz), theta (5–7 Hz), alpha (8–12 Hz), beta (13–30 Hz) band of EEG recordings. ECG and EEG were recorded for 5 min before and after the treatment. The participants were asked to lie on the massage bed and relax with their eyes closed to prevent any motor or ocular artifacts during measurement.

The ECG was measured using MP150 data acquisition system (Biopac Systems, Inc., USA) sampled at 1000 Hz

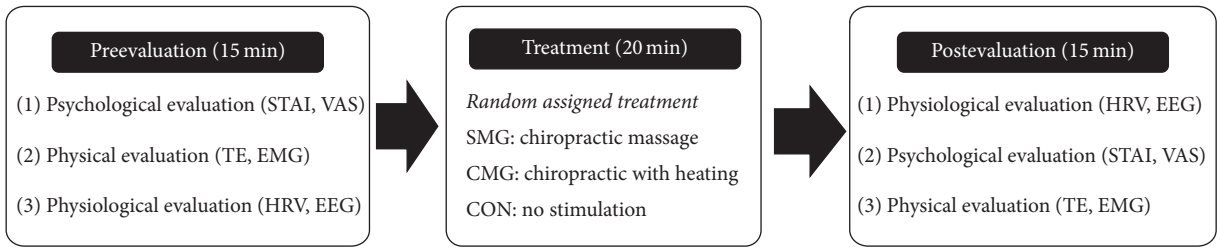

Figure 1: Overall procedure of the experiment. All subjects underwent 3 different treatment conditions in separate days (SM: single massage, CM: combined massage, and CON: control). The treatments were given to each participant in random order.

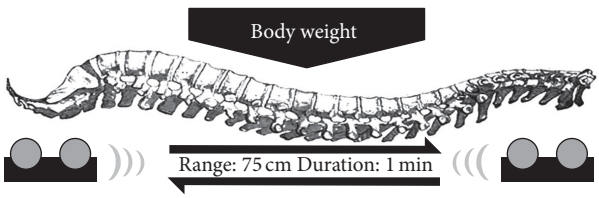

Figure 2: Schematic view of the automatic chiropractic massager. A pair of rollers massages the muscles along the spine by moving up and down from cervical vertebrae to coccygeal vertebra.

with 0.5–35 Hz band pass filter. The recordings were done following the standard limb leads method. HR was acquired using R-R interval series. The LF/HF ratio was calculated by dividing the average power of high frequency component (0.15–4 Hz) to low frequency component (0.04–0.15 Hz) of the R-R interval series. The power spectrum was calculated using fast Fourier transform (FFT) with Hamming window applied to the whole data. All HRV measures were calculated using Acknowledge 4.1 (Biopac Systems, Inc., USA) Software.

EEG was measured using an EEG acquisition system (WEEG-32; Laxtha Inc., Daejeon, Korea). Scalp readings were recorded in 2 frontal lobe locations (F3 and F4) referenced at Cz [33]. The sampling frequency was 512 Hz with a 0.5–64 Hz band pass filter applied to the recording. The recordings were then divided into 2 s epochs and were visually inspected to reject any epochs with artifacts (i.e., muscle artifacts). The spectrum was calculated using FFT for the artifact-free epochs and the spectrum was averaged for each band (delta, theta, alpha, and beta). All analysis procedure was done using an in-house coded program with MATLAB 2009a (Mathworks, Inc., USA).

2.3.3. Psychological Evaluation. Psychological changes before and after each treatment were evaluated using STAI and VAS. STAI is a self-report series of 20 items designed to evaluate state and trait anxiety in adults [34]. The level of stress was evaluated using VAS [35, 36]. The participants were provided with a paper with a 10 cm line, where the two ends of the line were marked to reflect extreme states of emotion. The participants were asked to report their current stress level by marking a spot on the line. The length between the left end of the line and the spot is proportional to stress.

3. Results

3.1. Physical Evaluation. TE significantly differed after treatment in SM (pre versus post; 32.04 ± 4.32 versus 34.06 ± 4.31, $p < 0.001$) and CM condition (32.97 ± 4.22 versus 36.60 ± 3.75, $p < 0.001$) but not in CON condition (33.20 ± 4.21 versus 33.13 ± 4.03, $p = 0.715$; Figure 3(a)). Posttreatment height differed significantly between treatments ($F(2) = 45.697$, $p < 0.001$). Post hoc analysis revealed significant differences in all condition pairs: CON versus SM ($p < 0.001$), CON versus CM ($p < 0.001$), and SM versus CM ($p < 0.001$).

Changes in EMG-RMS showed similar trend to those in TE: SM and CM showed significant differences (SM: 0.185 ± 0.032 versus 0.204 ± 0.037, $p < 0.001$; CM: 0.183 ± 0.035 versus 0.222 ± 0.041, $p < 0.001$) but not in CON (0.189 ± 0.022 versus 0.190 ± 0.023, $p = 0.675$; Figure 3(b)). Differences between treatments were statistically significant ($F(2) = 45.966$, $p < 0.001$). Post hoc analysis showed differences in all condition pairs: CON versus SM ($p < 0.001$), CON versus CM ($p < 0.001$), and SM versus CM ($p < 0.001$).

3.2. Physiological Evaluation. HR decreased significantly in SM and CM but not in CON (CON: 68.30 ± 7.97 versus 68.58 ± 8.74; SM: 69.65 ± 7.76 versus 66.29 ± 7.06, $p = 0.003$; CM: 68.93 ± 8.27 versus 64.95 ± 7.19, $p < 0.001$; Figure 4(a)). CON did not show significant change in HR between pre- and posttreatment ($p = 0.645$). The main effect on treatment was significant in HR ($F(2) = 9.091$, $p < 0.001$), where CON versus SM ($p = 0.005$) and CON versus CM ($p < 0.001$) showed significant changes in post hoc analysis. However, SM and CM did not show significant differences in posttreatment HR ($p = 1.000$).

Pre-post comparison between LF/HF ratio was significant in SM (1.36 ± 0.26 versus 1.02 ± 0.26, $p < 0.001$) and CM condition (1.38 ± 0.26 versus 0.82 ± 0.24, $p < 0.001$) but not in CON (1.36±0.33 versus 1.24±0.42, $p = 0.157$; Figure 4(b)). Significant differences in posttreatment LF/HF ratio were found ($F(2) = 17.185$, $p < 0.001$), and post hoc analysis showed significant differences between all conditions: CON versus SM ($p = 0.013$), CON versus CM ($p < 0.001$), and SM versus CM ($p = 0.014$).

Differences in EEG power were significant only in alpha and beta band between pre- and posttreatment in CM (alpha:

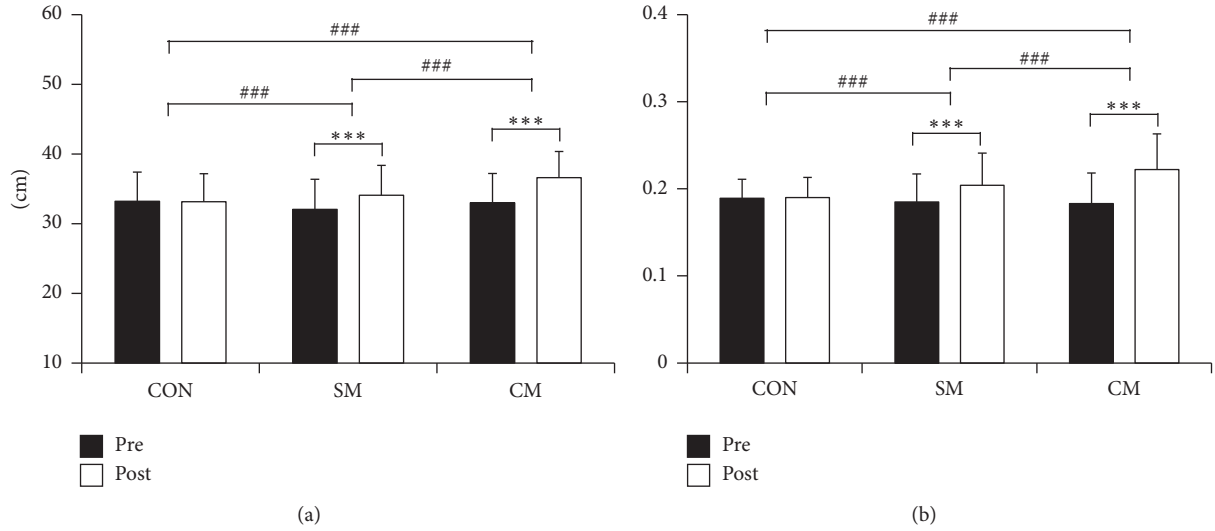

Figure 3: Physical changes of each treatment condition represented as (a) trunk extension (TE) and (b) electromyography root mean square (EMG-RMS) (CON: control, SM: single massage, and CM: combined massage; $^{*}p < 0.05$, $^{**}p < 0.01$, $^{***}p < 0.001$, $^{\#}p < 0.05$, $^{\#\#}p < 0.01$, $^{\#\#\#}p < 0.001$).

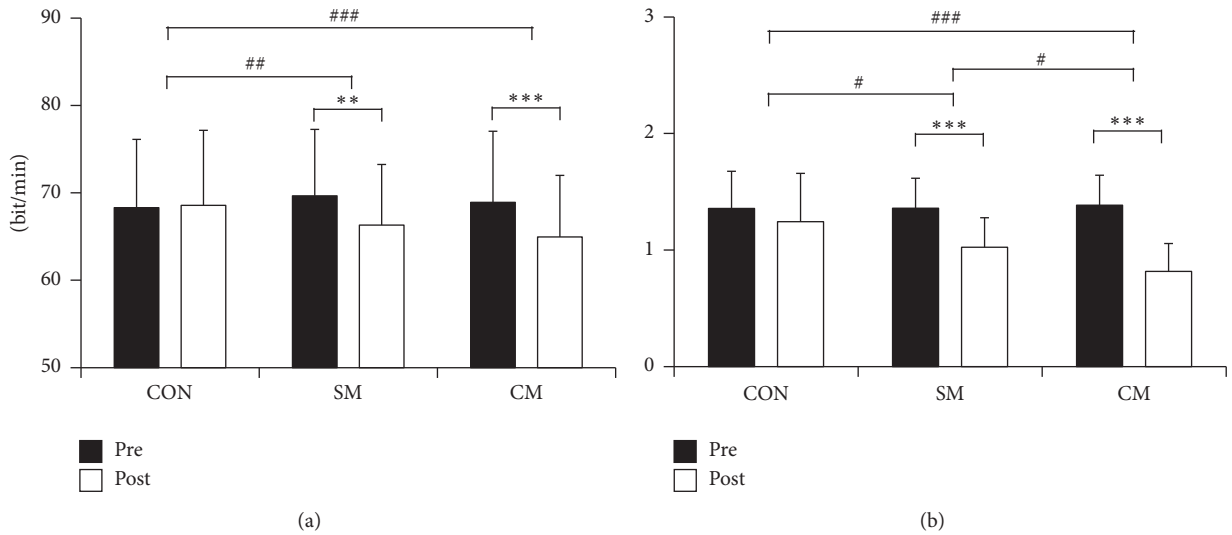

Figure 4: Physiological changes of each treatment condition in two heart-rate variability (HRV) related measures: (a) heart rate and (b) LF/HF ratio (CON: control, SM: single massage, and CM: combined massage; $^{*}p < 0.05$, $^{**}p < 0.01$, $^{***}p < 0.001$, $^{\#}p < 0.05$, $^{\#\#}p < 0.01$, $^{\#\#\#}p < 0.001$).

1.533 ± 0.569 versus 1.212 ± 0.395, $p = 0.004$; beta: 0.558 ± 0.129 versus 0.489 ± 0.106, $p = 0.007$; Figure 5). Posttreatment alpha power was significantly different between treatments ($F(2) = 5.853$, $p = 0.005$), and post hoc analysis revealed significant differences between CON and CM ($p = 0.003$).

3.3. Psychological Evaluation. Figure 6 represents the psychological changes of each treatment condition. All groups showed significant decrease in STAI-X-1 compared to pretreatment (CON: 36.89 ± 7.11 versus 33.61 ± 8.54, $p = 0.008$; SM: 35.86 ± 6.06 versus 30.61 ± 6.24, $p < 0.001$; CM: 36.21 ± 7.61 versus 29.21 ± 6.34, $p < 0.001$; Figure 6(a)). Posttreatment STAI-X-1 had a significant main effect in treatment ($F(2) = 4.321$, $p = 0.017$), and post hoc analysis revealed significant differences between CON and CM ($p = 0.013$).

VAS scores also showed significant decrease after each treatment (CON: 4.43 ± 1.67 versus 3.54 ± 1.77, $p = 0.001$; SM: 3.71 ± 2.31 versus 2.29 ± 1.67, $p < 0.001$; CM: 4.00 ± 2.24 versus 2.11 ± 1.79, $p < 0.001$; Figure 6(b)). These changes were significantly different between treatments ($F(2) = 7.481$, $p = 0.001$), with post hoc analysis revealing significant differences

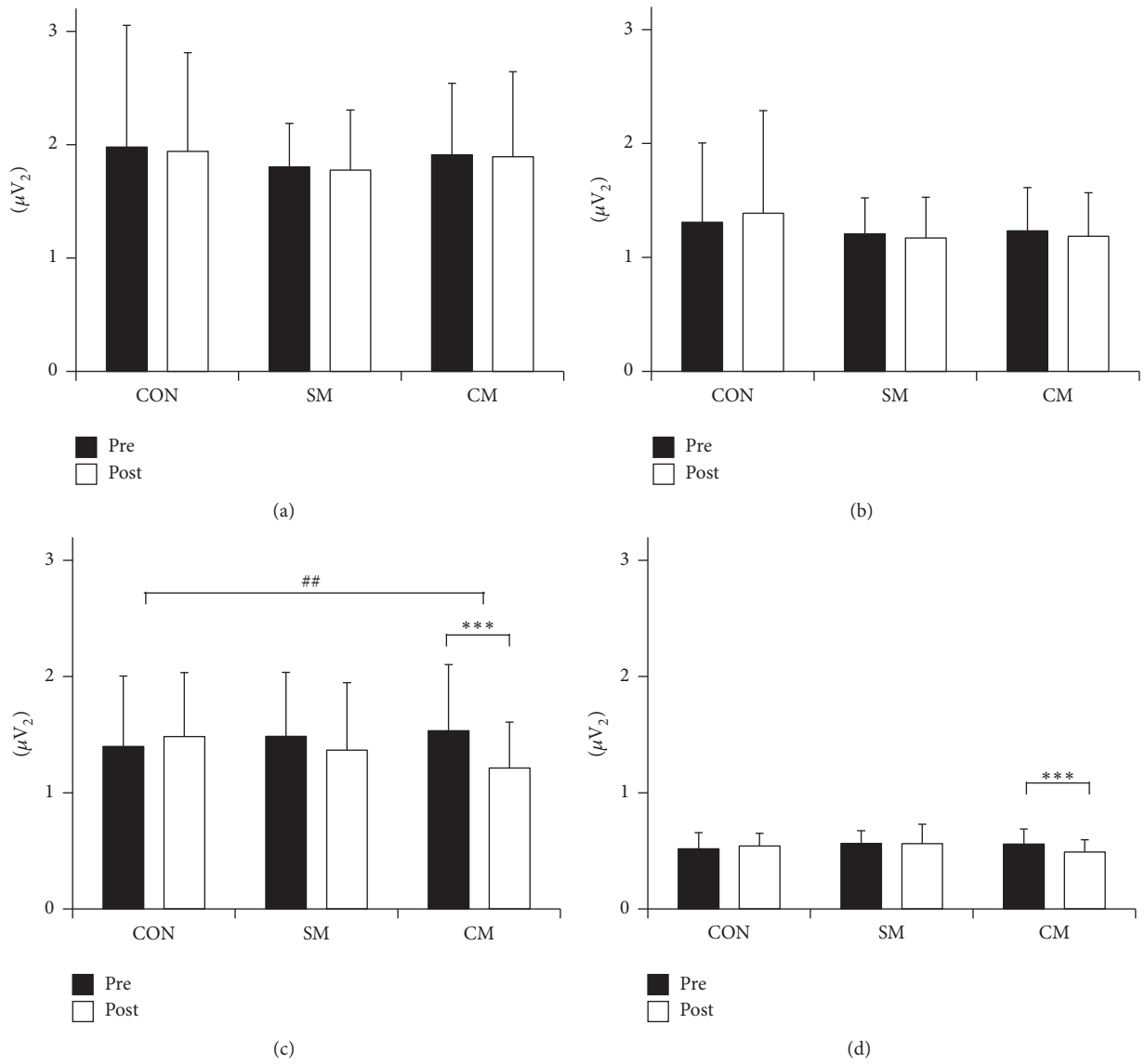

Figure 5: Physiological changes between pre- and posttreatment represented as power in four distinct frequency bands of EEG: (a) delta, (b) theta, (c) alpha, and (d) beta (CON: control, SM: single massage, and CM: combined massage; $^{*}p < 0.05$, $^{**}p < 0.01$, $^{***}p < 0.001$, $^{\#}p < 0.05$, $^{\#\#}p < 0.01$, $^{\#\#\#}p < 0.001$).

in posttreatment VAS scores between CON and SM ($p = 0.034$) and also between CON and CM ($p = 0.001$). However, there were no differences between SM and CM ($p = 0.719$).

4. Discussion

In the present study, we found that automated massage therapy has not only a significant physical effect, represented by increment of TE and EMG-RMS, but also a significant physiological effect, represented by decrement in HR, LF/HF ratio of HRV and reduced alpha and beta EEG power, and psychological effect, represented by decrement of STAI-X-1 and VAS scores. Most of the effects were more significant when massage therapy was combined with infrared heating.

Previous studies investigating the effects of massage therapy related to muscle characteristics have found positive effects such as increased muscle range of motion, maximum muscle strength, or flexibility [2, 26, 37]. For instance, Shambaugh [38] showed that pressure massage affects muscle recovery from physical stress or muscle fatigue, indicated as increased muscle flexibility and maximum muscle activation. Another previous study showed similar results of increased maximum strength and TE [21]. In the current study, both TE and EMG-RMS of SM and CM, but not of CON, were significantly increased after treatment. However, CM showed the most significant increment in both TE and EMG-RMS.

According to studies focusing on time domain analysis of HRV, massage therapy showed decreased stress response indicated as significantly decreased mean HR [3, 39, 40]. In the case of frequency domain analysis, massage therapy demonstrated an increase in HF leading to a decrease in

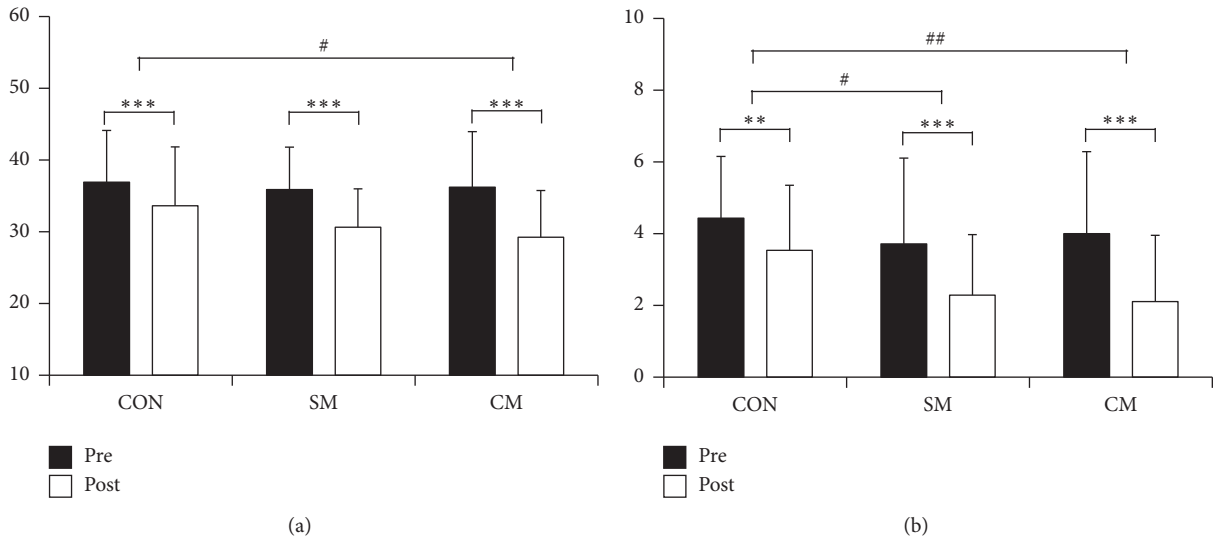

Figure 6: Psychological changes of each treatment condition represented as (a) state-trait anxiety inventory (STAI-X-1) and (b) visual analogue scale (VAS) (CON: control, SM: single massage, and CM: combined massage; $^{*}p < 0.05$, $^{**}p < 0.01$, $^{***}p < 0.001$, $^{\#}p < 0.05$, $^{\#\#}p < 0.01$, $^{\#\#\#}p < 0.001$).

LF/HF ratio [6]. Both mean HR and LF/HF ratio are associated with parasympathetic activity, with reduction of those values indicating an increase in parasympathetic activity [3, 6, 41–44]. Such increased parasympathetic activity owing to massage therapy appears to improve blood circulation through antagonistic activity of the autonomic nervous system, which helps to recover the physiological balance of tissues and organs of the human body [21, 45]. Therefore, the reduced LF/HF ratio or HR resulting from massage therapy alone seems to activate the parasympathetic nervous system, and adding infrared heating to massage therapy might increase the activation. Another physiological factor, EEG, showed decreased frontal alpha and beta band power between pre- and posttreatment, but only alpha band showed significant differences between treatment conditions. The results are coherent with studies using EEG to investigate the effect of moderate massage, which usually decreased frontal alpha and beta band power while increasing delta power, suggesting a relaxation response [3].

With regard to the psychological aspects, STAI and VAS were used to determine the change of participants' anxiety and stress level before and after the massage therapy. The results indicated that anxiety and stress are decreased regardless of treatment condition, which is consistent with previous reports of decreased STAI and VAS after pressure massage [46–48]. However, the posttreatment scores showed significant reduction in treatment condition, which revealed that anxiety and stress are more efficiently relieved by massage therapy with infrared heating than by massage therapy alone.

Integrating the results together, the current result supports the hypothesis that massage therapy activates the parasympathetic nervous system, thus leading the body to relax represented by physical, physiological, and psychological responses. Furthermore, we have revealed that the combination of infrared heating with massage therapy was more beneficial in terms of relaxation by more significant responses of the body.

Previous studies have evaluated the effectiveness of massage performed by a masseur. However, massage by the masseur might be a source of human errors [49]. In this study, it was possible to minimize human errors by employing uniform, automated massage for all participants. Through this experimental control, we considered to get a more clear assessment of the efficacy of massage.

The present study has some limitations. First, the measures used in this study were indirect measures for evaluation of the balance of the autonomic nervous system; more direct measurements related to parasympathetic/sympathetic might be preferable. For instance, biochemical measures such as cortisol [42] or oxytocin level [50] are hormonal responses related to the balance of the autonomic nervous system and also immune interactions. Especially, the cortisol level is able to estimate the hypothalamic-pituitary-adrenal axis which is another neural stress system [51, 52]. Second, the ages of participants of this study were limited. There are evidences that EEG [53] or HRV [54] vary according to age; thus, it would be necessary to investigate if the effect of the massage is consistent across ages.

5. Conclusion

In the current study, we observed that massage therapy contributed to psychological stability, improved trunk flexibility, maximal strength of the muscle, and activating parasympathetic nerves. When massage was combined with infrared heating, a more effective response was observed. Hence, the combination of pressure and heating massage could be offered as an alternative treatment method to help to prevent musculoskeletal pain and to relieve stress.

Competing Interests

The authors declare that there are no competing interests regarding the publication of this paper.

Authors' Contributions

Do-Won Kim and Dae Woon Lee contributed equally to this work as first author.

Acknowledgments

This research was supported by the Leading Foreign Research Institute Recruitment Program through the National Research Foundation of Korea (NRF) funded by the Ministry of Education, Science and Technology (MEST) (2010-00757).

References

[1] P. Weerapong, P. A. Hume, and G. S. Kolt, "The mechanisms of massage and effects on performance, muscle recovery and injury prevention," *Sports Medicine*, vol. 35, no. 3, pp. 235–256, 2005.

[2] S. Netchanok, M. Wendy, C. Marie, and O. D. Siobhan, "The effectiveness of Swedish massage and traditional Thai massage in treating chronic low back pain: a review of the literature," *Complementary Therapies in Clinical Practice*, vol. 18, no. 4, pp. 227–234, 2012.

[3] M. A. Diego, T. Field, C. Sanders, and M. Hernandez-Reif, "Massage therapy of moderate and light pressure and vibrator effects on EEG and heart rate," *International Journal of Neuroscience*, vol. 114, no. 1, pp. 31–44, 2004.

[4] M. Hernandez-Reif, T. Field, J. Krasnegor, Z. Hossain, H. Theakston, and I. Burman, "High blood pressure and associated symptoms were reduced by massage therapy," *Journal of Bodywork and Movement Therapies*, vol. 4, no. 1, pp. 31–38, 2000.

[5] M. Aourell, M. Skoog, and J. Carleson, "Effects of Swedish massage on blood pressure," *Complementary Therapies in Clinical Practice*, vol. 11, no. 4, pp. 242–246, 2005.

[6] M. A. Diego and T. Field, "Moderate pressure massage elicits a parasympathetic nervous system response," *International Journal of Neuroscience*, vol. 119, no. 5, pp. 630–638, 2009.

[7] T. Field, G. Ironson, F. Scafidi et al., "Massage therapy reduces anxiety and enhances EEG pattern of alertness and math computations," *International Journal of Neuroscience*, vol. 86, no. 3-4, pp. 197–205, 1996.

[8] L. Bazzichi, M. Dini, A. Rossi et al., "A combination therapy of massage and stretching increases parasympathetic nervous activity and improves joint mobility in patients affected by fibromyalgia," *Health*, vol. 02, no. 08, pp. 919–926, 2010.

[9] V. Buttagat, W. Eungpinichpong, D. Kaber, U. Chatchawan, and P. Arayawichanon, "Acute effects of traditional Thai massage on electroencephalogram in patients with scapulocostal syndrome," *Complementary Therapies in Medicine*, vol. 20, no. 4, pp. 167–174, 2012.

[10] H. Kunikata, K. Watanabe, M. Miyoshi, and T. Tanioka, "The effects measurement of hand massage by the autonomic activity and psychological indicators," *Journal of Medical Investigation*, vol. 59, no. 1-2, pp. 206–212, 2012.

[11] J. J. Newham, M. Westwood, J. D. Aplin, and A. Wittkowski, "State-trait anxiety inventory (STAI) scores during pregnancy following intervention with complementary therapies," *Journal of Affective Disorders*, vol. 142, no. 1–3, pp. 22–30, 2012.

[12] H. Walach, C. Güthlin, and M. König, "Efficacy of massage therapy in chronic pain: a pragmatic randomized trial," *The Journal of Alternative and Complementary Medicine*, vol. 9, no. 6, pp. 837–846, 2003.

[13] M. Hernandez-Reif, T. Field, J. Krasnegor, and H. Theakston, "Lower back pain is reduced and range of motion increased after massage therapy," *International Journal of Neuroscience*, vol. 106, no. 3-4, pp. 131–145, 2001.

[14] D. C. Cherkin, D. Eisenberg, K. J. Sherman et al., "Randomized trial comparing traditional Chinese medical acupuncture, therapeutic massage, and self-care education for chronic low back pain," *Archives of Internal Medicine*, vol. 161, no. 8, pp. 1081–1088, 2001.

[15] H. Mori, H. Ohsawa, T. H. Tanaka, E. Taniwaki, G. Leisman, and K. Nishijo, "Effect of massage on blood flow and muscle fatigue following isometric lumbar exercise," *Medical Science Monitor*, vol. 10, no. 5, pp. CR173–CR178, 2004.

[16] J. L. Durkin, A. Harvey, R. L. Hughson, and J. P. Callaghan, "The effects of lumbar massage on muscle fatigue, muscle oxygenation, low back discomfort, and driver performance during prolonged driving," *Ergonomics*, vol. 49, no. 1, pp. 28–44, 2006.

[17] T. Field, C. Morrow, C. Valdeon, S. Larson, C. Kuhn, and S. Schanberg, "Massage reduces anxiety in child and adolescent psychiatric patients," *Journal of the American Academy of Child and Adolescent Psychiatry*, vol. 31, no. 1, pp. 125–131, 1992.

[18] T. M. Field, N. Grizzle, F. Scafidi, and S. Schanberg, "Massage and relaxation therapies' effects on depressed adolescent mothers," *Adolescence*, vol. 31, no. 124, pp. 903–911, 1996.

[19] B. V. Reed and J. M. Held, "Effects of sequential connective tissue massage on autonomic nervous system of middle-aged and elderly adults," *Physical Therapy*, vol. 68, no. 8, pp. 1231–1234, 1988.

[20] T. Field, "Massage therapy facilitates weight gain in preterm infants," *Current Directions in Psychological Science*, vol. 10, no. 2, pp. 51–54, 2001.

[21] C. A. Moyer, J. Rounds, and J. W. Hannum, "A meta-analysis of massage therapy research," *Psychological Bulletin*, vol. 130, no. 1, pp. 3–18, 2004.

[22] T. Field, M. A. Diego, M. Hernandez-Reif, O. Deeds, and B. Figuereido, "Moderate versus light pressure massage therapy leads to greater weight gain in preterm infants," *Infant Behavior and Development*, vol. 29, no. 4, pp. 574–578, 2006.

[23] J. S. Barr and N. Taslitz, "The influence of back massage on autonomic functions," *Physical Therapy*, vol. 50, no. 12, pp. 1679–1691, 1970.

[24] B. D. Naliboff and K. H. Tachiki, "Autonomic and skeletal muscle responses to nonelectrical cutaneous stimulation," *Perceptual and Motor Skills*, vol. 72, no. 2, pp. 575–584, 1991.

[25] T. Hatayama, S. Kitamura, C. Tamura, M. Nagano, and K. Ohnuki, "The facial massage reduced anxiety and negative mood status, and increased sympathetic nervous activity," *Biomedical Research*, vol. 29, no. 6, pp. 317–320, 2008.

[26] V. Buttagat, W. Eungpinichpong, U. Chatchawan, and S. Kharmwan, "The immediate effects of traditional Thai massage on heart rate variability and stress-related parameters in patients with back pain associated with myofascial trigger points," *Journal of Bodywork and Movement Therapies*, vol. 15, no. 1, pp. 15–23, 2011.

[27] E. B. Lohman III, K. S. B. Sackiriyas, G. S. Bains et al., "A comparison of whole body vibration and moist heat on lower extremity skin temperature and skin blood flow in healthy older individuals," *Medical Science Monitor*, vol. 18, no. 7, pp. 415–424, 2012.

[28] Y.-H. Lee, B. N. R. Park, and S. H. Kim, "The effects of heat and massage application on autonomic nervous system," *Yonsei Medical Journal*, vol. 52, no. 6, pp. 982–989, 2011.

[29] D. Tomchuk, "Flexibility testing," in *Companion Guide to Measurement and Evaluation for Kinesiology*, pp. 23–44, Jones & Bartlett Learning, Bolingbrook, Ill, USA, 1st edition, 2010.

[30] N. S. Hannibal, S. A. Plowman, M. A. Looney, and J. Brandenburg, "Reliability and validity of low back strength/muscular endurance field tests in adolescents," *Journal of Physical Activity and Health*, vol. 3, no. s2, pp. S78–S89, 2006.

[31] B. Ghugare, P. Das, J. Ghate, K. Patond, M. Koranne, and R. Singh, "Assessment of nerve conduction in evaluation of radiculopathy among chronic low back pain patients without clinical neurodeficit," *Indian Journal of Physiology and Pharmacology*, vol. 54, no. 1, pp. 63–68, 2010.

[32] M. Harris and K. C. Richards, "The physiological and psychological effects of slow-stroke back massage and hand massage on relaxation in older people," *Journal of Clinical Nursing*, vol. 19, no. 7-8, pp. 917–926, 2010.

[33] U. Herwig, P. Satrapi, and C. Schönfeldt-Lecuona, "Using the international 10-20 EEG system for positioning of transcranial magnetic stimulation," *Brain Topography*, vol. 16, no. 2, pp. 95–99, 2003.

[34] C. D. Spielberger, "State-trait anxiety inventory," in *The Corsini Encyclopedia of Psychology*, I. B. Weiner and W. E. Craighead, Eds., vol. 4, John Wiley & Sons, Hoboken, NJ, USA, 2010.

[35] S. Grant, T. Aitchison, E. Henderson et al., "A comparison of the reproducibility and the sensitivity to change of visual analogue scales, Borg scales, and Likert scales in normal subjects during submaximal exercise," *Chest*, vol. 116, no. 5, pp. 1208–1217, 1999.

[36] J. Dyer, K. Thomas, C. Sandsund, and C. Shaw, "Is reflexology as effective as aromatherapy massage for symptom relief in an adult outpatient oncology population?" *Complementary Therapies in Clinical Practice*, vol. 19, no. 3, pp. 139–146, 2013.

[37] S. Y. Huang, M. Di Santo, K. P. Wadden, D. F. Cappa, T. Alkanani, and D. G. Behm, "Short-duration massage at the hamstrings musculotendinous junction induces greater range of motion," *The Journal of Strength & Conditioning Research*, vol. 24, no. 7, pp. 1917–1924, 2010.

[38] P. Shambaugh, "Changes in electrical activity in muscles resulting from chiropractic adjustment: a pilot study," *Journal of Manipulative and Physiological Therapeutics*, vol. 10, no. 6, pp. 300–304, 1987.

[39] A. A. McKechnie, F. Wilson, N. Watson, and D. Scott, "Anxiety states: a preliminary report on the value of connective tissue massage," *Journal of Psychosomatic Research*, vol. 27, no. 2, pp. 125–129, 1983.

[40] A. D. Kaye, A. J. Kaye, J. Swinford et al., "The effect of deep-tissue massage therapy on blood pressure and heart rate," *The Journal of Alternative and Complementary Medicine*, vol. 14, no. 2, pp. 125–128, 2008.

[41] M. V. Kamath and E. L. Fallen, "Power spectral analysis of heart rate variability: a noninvasive signature of cardiac autonomic function," *Critical Reviews in Biomedical Engineering*, vol. 21, no. 3, pp. 245–311, 1993.

[42] D. Acolet, N. Modi, X. Giannakoulopoulos et al., "Changes in plasma cortisol and catecholamine concentrations in response to massage in preterm infants," *Archives of Disease in Childhood*, vol. 68, no. 1, pp. 29–31, 1993.

[43] Y.-C. P. Arai, T. Ushida, T. Osuga et al., "The effect of acupressure at the extra 1 point on subjective and autonomic responses to needle insertion," *Anesthesia & Analgesia*, vol. 107, no. 2, pp. 661–664, 2008.

[44] A. Moraska, R. A. Pollini, K. Boulanger, M. Z. Brooks, and L. Teitlebaum, "Physiological adjustments to stress measures following massage therapy: a review of the literature," *Evidence-Based Complementary and Alternative Medicine*, vol. 7, no. 4, pp. 409–418, 2010.

[45] P. A. Iaizzo, "Autonomic nervous system," in *Handbook of Cardiac Anatomy, Physiology, and Devices*, K. Fitzgerald, R. F. Wilson, and P. A. Iaizzo, Eds., chapter 12, pp. 177–189, Springer, New York, NY, USA, 2nd edition, 2009.

[46] N. Bost and M. Wallis, "The effectiveness of a 15 minute weekly massage in reducing physical and psychological stress in nurses," *Australian Journal of Advanced Nursing*, vol. 23, no. 4, pp. 28–33, 2006.

[47] M.-P. Campeau, R. Gaboriault, M. Drapeau et al., "Impact of massage therapy on anxiety levels in patients undergoing radiation therapy: randomized controlled trial," *Journal of the Society for Integrative Oncology*, vol. 5, no. 4, pp. 133–138, 2007.

[48] T. Ogura, M. Tashiro, M. Masud et al., "Cerebral metabolic changes in men after chiropractic spinal manipulation for neck pain," *Alternative Therapies in Health and Medicine*, vol. 17, no. 6, pp. 12–17, 2011.

[49] D. C. Cherkin, K. J. Sherman, J. Kahn et al., "A comparison of the effects of 2 types of massage and usual care on chronic low back pain: a randomized, controlled trial," *Annals of Internal Medicine*, vol. 155, no. 1, pp. 1–9, 2011.

[50] K. Uvnäs-Moberg, "Oxytocin may mediate the benefits of positive social interaction and emotions," *Psychoneuroendocrinology*, vol. 23, no. 8, pp. 819–835, 1998.

[51] A. H. Marques, M. N. Silverman, and E. M. Sternberg, "Evaluation of stress systems by applying noninvasive methodologies: measurements of neuroimmune biomarkers in the sweat, heart rate variability and salivary cortisol," *NeuroImmunoModulation*, vol. 17, no. 3, pp. 205–208, 2010.

[52] S. Porges, "Stress and parasympathetic control," in *Stress Science: Neuroendocrinology*, G. Fink, Ed., pp. 306–312, Elsevier, Burlington, Vt, USA, 1st edition, 2010.

[53] R. E. Dustman, J. A. LaMarche, N. B. Cohn, D. E. Shearer, and J. M. Talone, "Power spectral analysis and cortical coupling of EEG for young and old normal adults," *Neurobiology of Aging*, vol. 6, no. 3, pp. 193–198, 1985.

[54] M. W. Agelink, R. Malessa, B. Baumann et al., "Standardized tests of heart rate variability: normal ranges obtained from 309 healthy humans, and effects of age, gender, and heart rate," *Clinical Autonomic Research*, vol. 11, no. 2, pp. 99–108, 2001.

Hindawi Publishing Corporation
BioMed Research International
Volume 2016, Article ID 1584947, 8 pages
http://dx.doi.org/10.1155/2016/1584947

Research Article

Effect of Anodal-tDCS on Event-Related Potentials: A Controlled Study

Ahmed Izzidien,[1] Sriharasha Ramaraju,[2] Mohammed Ali Roula,[2] and Peter W. McCarthy[3]

[1]*Social Cognition Laboratory, Harvard University, Cambridge, MA, USA*
[2]*Medical Electronics and Signal Processing Research Unit, University of South Wales, Treforest, UK*
[3]*Clinical Technology and Diagnostics Research Unit, University of South Wales, Treforest, UK*

Correspondence should be addressed to Mohammed Ali Roula; ali.roula@southwales.ac.uk

Received 24 June 2016; Revised 22 September 2016; Accepted 11 October 2016

Academic Editor: Do-Won Kim

We aim to measure the postintervention effects of A-tDCS (anodal-tDCS) on brain potentials commonly used in BCI applications, namely, Event-Related Desynchronization (ERD), Event-Related Synchronization (ERS), and P300. Ten subjects were given sham and 1.5 mA A-tDCS for 15 minutes on two separate experiments in a double-blind, randomized order. Postintervention EEG was recorded while subjects were asked to perform a spelling task based on the "oddball paradigm" while P300 power was measured. Additionally, ERD and ERS were measured while subjects performed mental motor imagery tasks. ANOVA results showed that the absolute P300 power exhibited a statistically significant difference between sham and A-tDCS when measured over channel Pz ($p = 0.0002$). However, the difference in ERD and ERS power was found to be statistically insignificant, in controversion of the the mainstay of the litrature on the subject. The outcomes confirm the possible postintervention effect of tDCS on the P300 response. Heightening P300 response using A-tDCS may help improve the accuracy of P300 spellers for neurologically impaired subjects. Additionally, it may help the development of neurorehabilitation methods targeting the parietal lobe.

1. Introduction

Transcranial Direct Current Stimulation (tDCS) is a noninvasive brain stimulation technique which has recently gained interest in neuroscientific research. Studies have reported improvements in cognitive functions [1, 2], motor processing [3], memory [4], and learning in healthy brains [5–7]. Additionally, tDCS has been studied in patients with neurodegenerative diseases, movement disorders, epilepsy, and poststroke language, attention, or executive deficits [8–13].

If shown to be reliable, tDCS may have several advantages that render it attractive for clinical use in comparison to invasive stimulation. The technique is, as stated, noninvasive and elicits only a slight tingling under the electrodes and can be applied continuously and safely for up to 20 minutes [14–17]. The device is also easy to use, small, and relatively inexpensive [5]. One area where noninvasive enhancement of neural function may be of benefit is Brain Computer Interfacing (BCI). In particular, its possible use in communication aids and in motor rehabilitation is considered in this paper.

BCI-based communication aids have been developed in the form of word spellers to help people with severe motor disabilities communicate with ease [18–20]. The concept of a BCI speller is based on a system that enables direct brain-to-character translation through the "oddball paradigm" [21]. However, P300 systems have had limited practical applications mostly because potential users may have reduced neural activity in one or multiple areas of the brain due to illness or damage. Ramaraju et al. [22] have looked at the effect of tDCS on P300 potentials and how tDCS may help facilitate better P300 responses. While not directly related, Antal et al. [23] reported measurable effects of tDCS on Visual Evoked Potentials (VEP) and Lee et al. [24] reported measurable effects of tDCS on latency and amplitude.

The other types of brain signals commonly used in BCI applications are the ones generated by motor imagery (MI). There too, potentially beneficial effects of tDCS have been reported such as in the rehabilitative motor training of patients who have suffered subacute strokes [25]. Results from a number of studies suggest that ERDs can be slightly and temporarily amplified to heighten responsiveness [16,

Table 1: List of papers which did not use randomized, double-blind, and sham-controlled protocols in their research.

Paper	Year	Randomized	Double-blind	Sham-controlled	p value
Kasashima et al. [31]	2012	Yes	No	No	0.018
Matsumoto et al. [7]	2010	Yes	No	No	0.001
Wei et al. [6]	2013	Yes	No	Yes	0.023
Notturno et al. [16]	2014	Yes	No	No	0.035
Roy et al. [17]	2014	Yes	No	Yes	0.001
Nitsche et al. [3]	2003	Yes	No	Yes	0.001
Lee et al. [24]	2014	No	No	No	<0.05

26–28]. tDCS has been reported to heighten the magnitude of alpha waves [29] and also be used in conjunction with BCI [30].

However, many studies that have shown a unidirectional change in the ERD level and an increase in ERD with A-tDCS did not use a tricombination of randomization of stimulations/cues, sham control, and a double-blind protocol as shown in Table 1. Thus, we set out in this work to measure the degree by which tDCS may elicit changes in ERD, ERS, and P300 using a robust experimental protocol which includes double-blinding, sham control, and randomization. Part of this work has been presented here were presented in a preliminary form as a conference paper [22].

2. Materials and Methods

2.1. Subject Selection. Ten right-handed subjects (aged 22 ± 3 years) participated in this study after giving written informed consent. No subject had any history of a neurological condition or had been receiving any acute or chronic medication affecting the central nervous system. This investigation has been given ethical approval by the University of South Wales.

2.2. A-tDCS Application Protocol. The tDCS device (HDC-Stim HS0023L02-73, Newronika S.r.l) with electrodes of size 5 cm × 5 cm was fitted according to the procedure used by DaSilva et al. [32] for anodal stimulation. The anodal electrode was placed over the left M1 and the cathodal electrode over the right supraorbital area. Subjects sat in an armless chair, and then using measurements of the distance between inion and nasion Cz was found, and then 20% of the distance from Cz to the left preauricular point was found. EEG high conductivity gel was then applied to this location, C3, and the temple. The tDCS pads were soaked in normal tap water, and high conductivity gel was applied. The pads were placed on C3 and right frontal lobe and both secured with a plastic band and netted cap.

Each subject underwent two experimental A-tDCS sessions, one real and one sham, separated by a one-week interval. The order of the A-tDCS presentation (sham or real) was randomized and double-blinded (neither the investigator nor the participants were made aware of what stimulation is being administered). Double-blinding was achieved by an independent investigator generating a sequence of random binary number pairs and associating them to real and sham in an undisclosed file. The A-tDCS option (real or sham) was selected for each participant by the independent investigator using the predetermined sequence: turning the sham button either "on" or "off" outside the view of the main researcher and the subject. The independent investigator did not interact with the experiment after applying the designated option. At the end of each session, the independent investigator verified that the researcher did not know whether the stimulation was applied to check the effectiveness of blinding. Furthermore, participants were not informed that the current intensity would be varied for each study (sham and real).

The real A-tDCS consisted of a 1.5 mA current applied for 15 minutes. The sham consisted of a dose of 1.5 mA ramping up from 0 mA to 1.5 mA over 10 s, followed by 8 s at 1.5 mA before the A-tDCS automatically turned off. This was done to mimic the transient skin sensation at the beginning of actual A-tDCS without producing any potential conditioning effects on the brain [33]. The complete study was run on each participant within one hour of removing the A-tDCS, which is within the time window reported previously for effects of tDCS to be detected [23, 34, 35].

The impedance value of the A-tDCS while operating was checked by the independent investigator and remained between 4 kΩ and 9 kΩ for all participants, which was the recommended window given in the A-tDCS device instructions.

2.3. EEG Measurement Protocol. After the application of real or sham stimulation, the EEG electrodes in the cap were connected, taking between 10 and 20 minutes to connect and apply conductive gel to the electrodes. Once connected, the impedance of each electrode remained at a maximum of 20 kΩ with a typical value being under 10 kΩ throughout the experiment. EEG signals were recorded from 14 Ag/AgCl disc electrodes (1 cm in diameter) with the ground at AFz and the reference electrodes at FCz. All the electrodes are placed according to the international 10–20 system. The signal was prefiltered (0.2–45 Hz) and a digital notch filter was applied at 50 Hz. The cap was centered on the scalp at Cz midway between the inion and nasion. Cz was checked for its equidistance to both left and right preauricular points.

Subjects sat in an armless chair with their eyes open facing a computer monitor placed approximately 0.7 m in front of them at eye level. Both arms dangled freely by their sides towards the ground. They were asked to avoid any further muscular activity including blinking. However,

they were informed not to be concerned about accidental blinking or flinching. Participants were told that the study would be repeated several times and that occasional artefact would be removed. This was aimed at preventing stress in the participants if they did accidentally blink or move, the stress of which may have affected the remaining results.

2.4. ERD/ERS Measurement Protocol. Subjects were shown a tennis ball on the computer screen and asked to use their right hand in an attempt to grab it and then to let go and return their hand to its original position dangling freely by their side. They would perform this routine physically, clasping their hand within 1 cm of the screen before bringing it back. They were then asked to keep their arm and hand dangling freely by their side and mentally simulate the performance of the same reach-and-grasp motion, without moving either their arm or hand. Initially, during the rehearsal phase of this part of the study, the researcher held the participant's arm and shoulder gently to detect any muscular contractions. This rehearsal phase for each subject was conducted for both sham and tDCS sessions. Subjects were asked to repeat the imagined reach-and-grasp procedure until no muscular movement was detectable by the investigator. It was made clear to participants that they were required to make the mental effort to grab the ball in the same manner they had practiced physically and not just to imagine a video playback of their hand grasping it.

Each trial consisted of two cues, a blank slide which appeared for 5 to 8 s (randomized) followed by a cue with a tennis ball centered on it. The blank cue signified the adoption of a rest state by the participant. When the tennis ball cue appeared, the participant was asked to make the mental effort of reaching out to the ball, grasping it, letting it go, and returning their arm to their side. These were all done with no time gaps in between each step. The presequence duration (blank-cue) appeared once at the start of the experiment. After this, the screen would display a tennis ball for 4 s followed by a blank screen. The blank screen was made up of three sequential blank slides. These three slides were used to allow for randomization in the length of time for which the blank black cue appeared before the tennis ball reappeared. They were made up of the interstimulus duration, the blank cue, and the postsequence duration. The interstimulus duration slide was on screen for between 1 and 3 seconds. All three blank slides appeared as one cue. From the perspective of the subject, they only saw two cues: a blank black cue and a tennis ball cue. A total of 6 trials per subject were conducted in each of the real and sham experiments totaling 120 trials overall. These steps are summarized in Figure 1.

All the EEG trials were visually inspected for any abnormal signals from the electrode contacts or muscular artifacts across C3 and C4 and these trials were omitted. C3 and C4 were selected as they produced the highest ERD/ERS response compared to all other channels. The EEG signal from C3 and C4 was filtered between 8 Hz and 13 Hz using a standard FIR filter. The epochs (−1 s to 3.5 s) were extracted, and baseline removal was run using the time window (−1 s to 0 s) on each channel's data. The epochs were averaged, and the power (μV^2) was found for the time windows before cue (−1 s to 0 s) and after cue (0.5 s to 3.5 s). The latter time window was selected to characterize the ERD signal from mentally reaching, clasping, and releasing the ball. The physical act took less than 3 seconds to complete. Both power values were normalized to the number of frequency points.

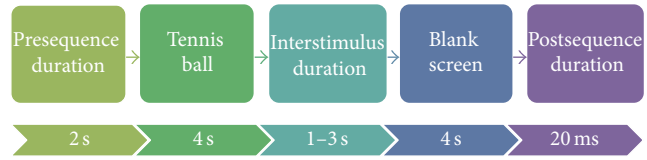

Figure 1: Cue timeline for ERD experiment.

ERS values for C3 and C4 were arrived at by filtering the original preprocessed signal between 13 Hz and 24 Hz followed by baseline removal using the time window (−1 s to 0 s). The time segment 1 s to 5 s was used for analysis. All processing was done using EEGLAB [36]. For both cases of sham and real, ERD and ERS were calculated across both channels C3 and C4. The blank-cue power was termed the neutral power. The tennis ball cue power was termed the motor imagery power. The following measures were used to calculate the effect of A-tDCS on the ERD and ERS potentials:

$$\mathrm{RPD} = P_{\mathrm{Neutral}} - P_{\mathrm{Imagery}}, \tag{1}$$

where RPD stands for Relative Power Difference. P_{Neutral} is blank-cue power, and P_{Imagery} is tennis ball cue (active motor imagery) power measured at the ERD (8 Hz–13 Hz) and ERS (13 Hz–24 Hz) bands, respectively. Both power values were normalized to the number of frequency points.

2.5. P300 Measurement Protocol. A P300 oddball speller, which contains all characters (A–Z), numbers from 0 to 9, and spacebar, was presented to the volunteer in 6 × 6 matrix form [37]. The participant was asked to "spell" the nineteen (including spaces) letters in "THE QUICK FOX JUMPS" by focusing on the character inside the 6 × 6 matrix which they wanted to select. Two sequences were used to select a character. In a sequence, each row/column is intensified randomly. For each sequence, there are up to 12 intensifications (6 rows and 6 columns), and therefore a total of up to 24 intensifications are used to evoke a response to a character. The following measures were used to assess a P300 oddball response to intensified letters:

$$\begin{aligned}\mathrm{APR} &= \mathrm{Average}\left(P_{\mathrm{Target}}\right),\\ \mathrm{RPR} &= \frac{\left(\mathrm{Average}\left(P_{\mathrm{Target}}\right) - \mathrm{Average}\left(P_{\mathrm{Non\text{-}target}}\right)\right)}{\mathrm{Average}\left(P_{\mathrm{Target}}\right)}.\end{aligned} \tag{2}$$

APR stands for "absolute P300 response" which considers only the P300 signal power in μV^2, whereas RPR stands for "relative P300 response" which considers the difference between the responses to target letters and nontarget letters.

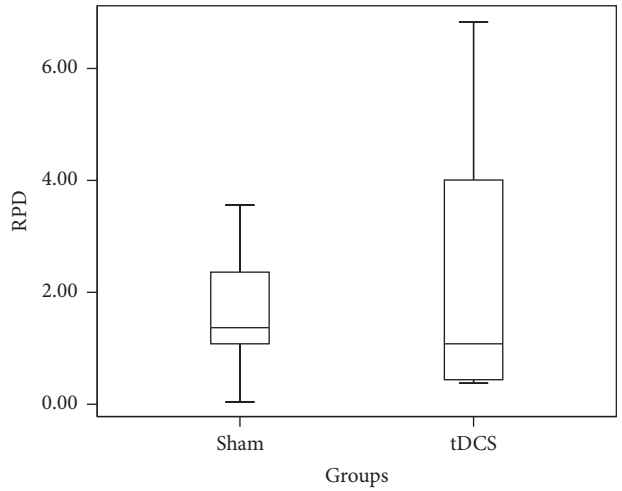

Figure 2: Box and whisker plot of the step in relative ERD power in μV^2 for C3 before and after motor imagery cue for the 10 participants.

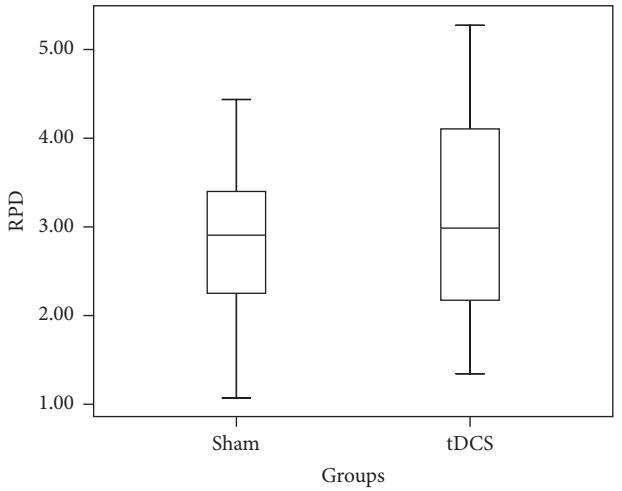

Figure 3: Box and whisker plot of the step in relative ERS power in μV^2 for C3 before and after motor imagery cue for the 10 participants.

EEG signal was measured for 19 target letters per subject per experiment totaling 380 EEG target samples. A larger number of "nontarget" samples were also measured (due to oddball experiment inherently generating more nontarget than target letters). These were used for RPR calculation.

P_{Target} is the average signal power in μV^2 between 250 ms and 450 ms of 19 intensified target letters. $P_{\text{Non-target}}$ is the average signal power in μV^2 between 250 ms and 450 ms of all intensified nontarget letters.

3. Results and Discussion

3.1. Effect on ERD/ERS. Relative Power Difference (RPD) in ERD is measured for individual subjects across C3 for both real A-tDCS and sham A-tDCS conditions. A one-way ANOVA resulted in a p value of 0.46. The box plot in Figure 2 summarizes the data in the two groups. The overlap of two groups is clearly visible, and this supports the above p value. The same analysis was carried out for the RPD of ERS across C3. The box plot in Figure 3 summarizes the data in the two groups and clearly depicts overlap in the data from the two groups (real A-tDCS and sham A-tDCS). A one-way ANOVA test of mean difference yielded a p value of 0.49. The average power increment after application of the A-tDCS was 26.17%.

The Relative Power Difference in ERD across channel C4 for both real and sham groups was measured and summarized in the box plot of Figure 4. The box plot clearly depicts the nonsignificance of difference (one-way ANOVA, $p = 0.80$) between sham and real groups. The average power change after the application of A-tDCS was 59%. The same analysis was performed on the ERS data from channel C4 (Figure 5) which clearly shows the overlap of the two groups (one-way ANOVA, $p = 0.52$) which gives the statistically insignificant difference between the two groups. In this case, the average power decrement after A-tDCS was found to be 10.39%. The Mu rhythm was then split into lower Mu (8 Hz–10 Hz) and upper Mu (10 Hz–13 Hz) and the RPD values in these two frequency bands across two channels C3 and C4 were calculated. One-way ANOVA results (p values: 0.98, 0.15, 0.78, and 0.337) clearly show the statistical insignificance in both lower and upper Mu.

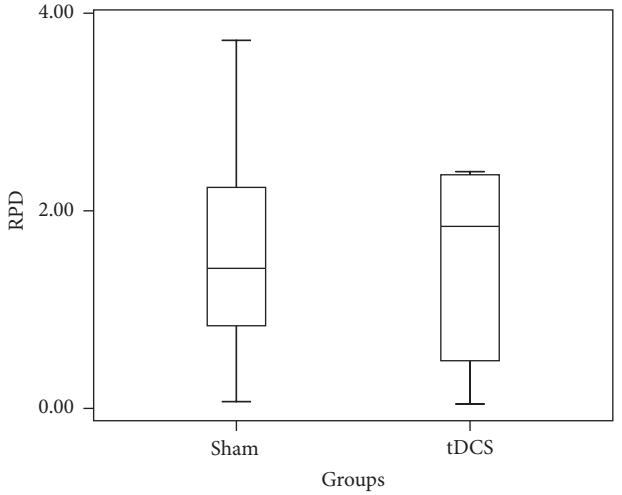

Figure 4: Box and whisker plot of the step in ERD power in μV^2 for C4 before and after motor imagery cue for the 10 participants.

3.2. Effect on P300. The average change in the RPR across channel Oz for all subjects was a 22% increase following A-tDCS when compared to sham (data for subjects 9 and 10 was corrupt and thus not included). The box plot in Figure 6 depicts RPR values of both groups. From Figure 6, there is no clear separation of sham and A-tDCS groups. The real group appears to have a smaller standard deviation than that of the sham group (sham: 0.13, A-tDCS: 0.07). The absolute value of P300 however across Oz is not significantly different between groups (Figure 8) with a p value of 0.42. The same analysis was carried out on the data from channel Pz resulting in a p value

Table 2: Summary of experimental results.

Power measure		Sham				tDCS				ANOVA	
		Oz		Pz		Oz		Pz			
		Average	Standard deviation	Average	Standard deviation	Average	Standard deviation	Average	Standard deviation	Oz	Pz
P300	Relative	0.573	0.13	0.526	0.176	0.666	0.07	0.553	0.076	**0.103**	0.578
	Absolute	35.81	10.54	19.56	7.41	32.08	19.31	12.61	3.45	0.422	**0.0002**
		C3		C4		C3		C4		C3	C4
Motor imagery	ERD	1.59	1.003	1.64	1.25	2.16	2.19	1.82	1.73	0.46	0.80
	ERS	2.98	1.288	3.84	1.36	3.49	1.93	3.44	1.36	0.49	0.52

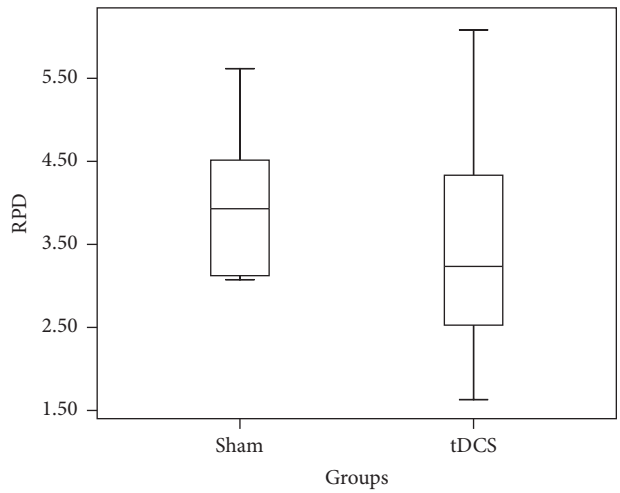

Figure 5: Box and whisker plot of the step in ERS power in μV^2 for C4 before and after motor imagery cue for the 10 participants.

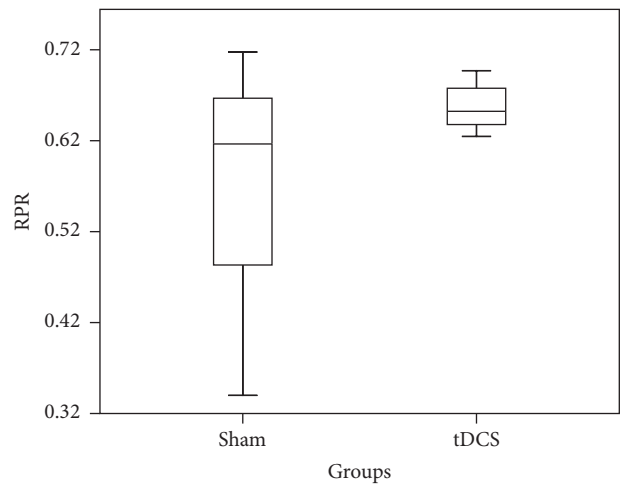

Figure 6: Box plot showing relative P300 response distribution of sham and tDCS across channel Oz for time window 250 ms–450 ms.

of 0.578, which suggests a statistically insignificant difference between the t-DCS and the sham groups. The RPR data across Pz is summarized in a box plot in Figure 7. We note that the real group has a lower standard deviation (0.076) when compared to the sham group (0.176), though this difference may not be significant. The power at every time instant across all the subjects was averaged for both the sham and the real groups.

The absolute P300 response for channel Oz is summarized in Figure 10. Although there appears to be a high APR for the real group when compared to the sham group between 314 ms and 380 ms, a one-way ANOVA performed on the APR data from each group indicates a statistically insignificant difference between the groups ($p = 0.42$). A similar analysis was performed across the APR data for channel Pz (depicted in Figure 11) and gives a clear difference in the APR between 270 ms and 400 ms where major differences around 300 ms can be observed (one-way ANOVA with a p value 0.0002, Figure 9). All the averages and standard deviations across C3, C4, Pz, and Oz for sham and tDCS are summarized in Table 2. Although ANOVA is robust under an equal variance assumption, we have nevertheless confirmed the findings with the nonparametric Kruskal-Wallis test which yielded nearly similar p values.

4. Conclusions

Our results show that A-tDCS has had a significant effect on the absolute P300 response. This may help the development of neurorehabilitation methods targeting the parietal lobe. Heightening of the P300 response using A-tDCS may also help improve the accuracy of P300 based oddball paradigm spellers for neurologically impaired subjects. These spellers, although they have been shown to work in principle, have had limited practical applications partly because potential users often have reduced neural activity in one or multiple areas of the brain due to illness or damage. A rehabilitation regime of A-tDCS stimulation, used in conjunction with oddball paradigm spellers, could improve their usability, hence benefiting their users by allowing them to communicate. These users primarily include locked-in syndrome sufferers from conditions such as motor neuron disease (MND), stroke, and traumatic brain injury.

On the other hand, our study also demonstrated that the A-tDCS had no effect on ERD/ERS responses during motor tasks. This presents a complex picture of the effect of tDCS in general, as it may be specific to brain areas and functions. This appears to be consistent with a number of studies that

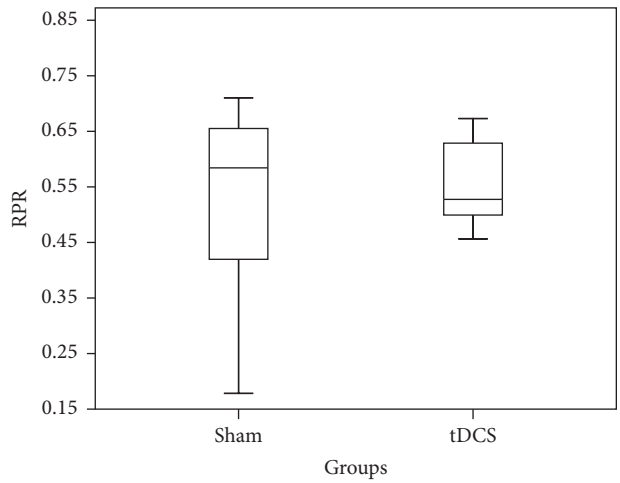

Figure 7: Box plot showing relative P300 response distribution of sham and tDCS across channel Pz for time window 250 ms–450 ms.

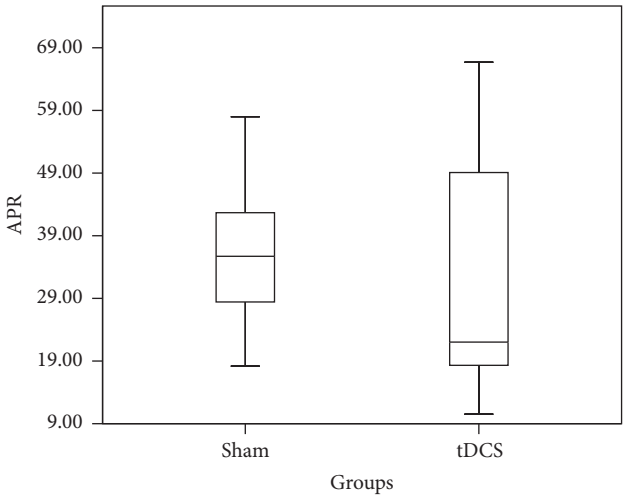

Figure 8: Box plot showing absolute P300 response in μV^2 distribution of sham and tDCS across channel Oz for time window 250 ms–450 ms.

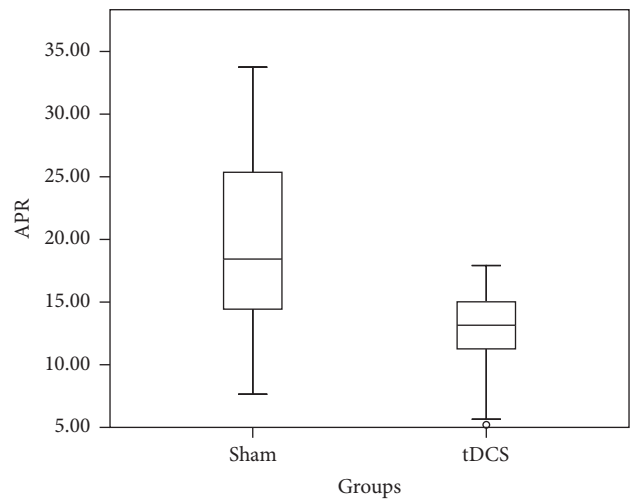

Figure 9: Box plot showing absolute P300 response in μV^2 distribution of sham and tDCS across Pz channel for time window 250 ms–450 ms.

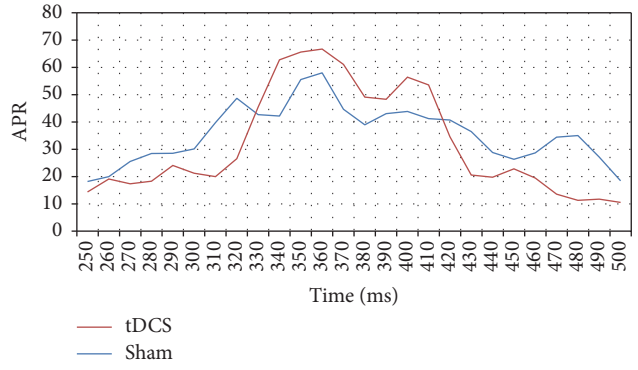

Figure 10: Graph of absolute P300 response in μV^2 of 8 subjects across channel Oz for tDCS and sham conditions for time window 250 ms–450 ms.

when taken together exhibit varied findings on the effects of A-tDCS on EEG measurable cortical activity [38–40].

It may be the case that the lack of double-blinding in a number of earlier positive studies may have played a role in their results (Table 1) since failing to double-blind a study may allow for the invigilator to influence the subject as to the dosage given. There is also the possibility of a progressive training element over time as familiarity increases with the sequencing. One possible factor affecting A-tDCS effect on ERD-ERS might be that competing mechanisms of inhibitory and executory mechanisms may be at play when A-tDCS is operational, thus not allowing for a consistent outcome. The outcomes in our study may also be because the execution or imagination of the arm and hand movement occurs within the great functional and anatomical complexity of the Supplementary Motor Area (SMA) and its somatotopic organization in the form of a pure motor area and a mixed sensorimotor area [41]. The orientation and pathways may have a bearing on the outcome as has been reported in another study that found unexpected results from tDCS [34]. The authors of [34] took the standpoint that so far it has not been shown whether the excitability changes resulting from tDCS of the frontal cortex or even subcortical stimulation are similar to those induced by motor cortical tDCS. Participant genotype may also be a factor, as a study failed to demonstrate MEP facilitation after A-tDCS in one group carrying a specific genotype with only a hint of early facilitation which was not statistically significant [42].

The positive P300 effect observed might also indicate that the A-tDCS effect is not localized, which is in line with findings of widespread activation in several brain regions [33]. And, hence, A-tDCS might have more effects on nonlocalized EEG patterns such as P300 and fewer effects on localized EEG pattern such as motor related ERD/ERS. This hypothesis would need further research to be tested using combined fMRI and tDCS studies, for instance, where the effect of

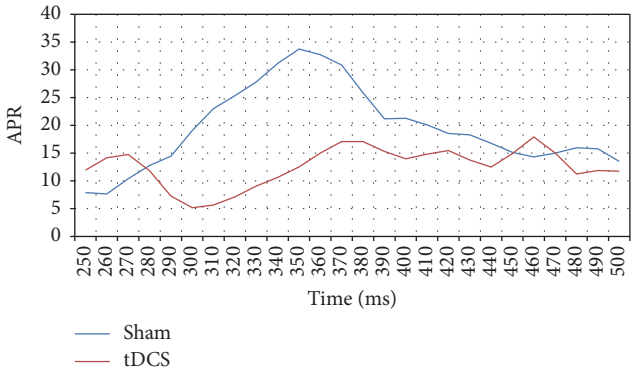

Figure 11: Graph of absolute P300 response in μV^2 of 8 subjects across Pz channel for tDCS and sham conditions for time window 250 ms–450 ms.

stimulation on the activation of particular cortical regions can be studied. What is evident is that A-tDCS can have an effect on some brain potentials and not others and that this complex picture can only be understood with robust and well-controlled studies.

Future work will also focus on the effect of secondary factors such as age, gender, and psychometric profiles as well as using computer simulation of current flows combined with subject imaging data to work out optimal electrode placement for desired applications. An interesting question would be whether replicating the same montage in two morphologically different individuals reproduces the same stimulation patterns. This can be answered with detailed subject specific and anatomically accurate computer simulation of current flows in the cortical areas of the brain. This then could lead to individualized imaging driven montages which may be a better way of conducting controlled studies in all targets of tDCS.

Finally, because the efficacy of A-tDCS is still a debated topic in the literature, it is unlikely that one paper will provide a definitive answer for all aspects of A-tDCS impact on EEG. As in many scientific controversies, systematic studies need to be done looking at the literature for a consensus to be built. It is therefore important that robustly controlled studies are carried out and that positive, as well as negative, studies are duly reported.

Competing Interests

The authors declare that they have no competing interests.

Acknowledgments

The authors would like to thank HPC Wales for the Research and Innovation Grant and University of South Wales for Centenary Postgraduate Fellowship.

References

[1] C. A. Dockery, R. Hueckel-Weng, N. Birbaumer, and C. Plewnia, "Enhancement of planning ability by transcranial direct current stimulation," *The Journal of Neuroscience*, vol. 29, no. 22, pp. 7271–7277, 2009.

[2] R. Sparing, M. Dafotakis, I. G. Meister, N. Thirugnanasambandam, and G. R. Fink, "Enhancing language performance with non-invasive brain stimulation-a transcranial direct current stimulation study in healthy humans," *Neuropsychologia*, vol. 46, no. 1, pp. 261–268, 2008.

[3] M. A. Nitsche, A. Schauenburg, N. Lang et al., "Facilitation of implicit motor learning by weak transcranial direct current stimulation of the primary motor cortex in the human," *Journal of Cognitive Neuroscience*, vol. 15, no. 4, pp. 619–626, 2003.

[4] F. Fregni, P. S. Boggio, M. Nitsche et al., "Anodal transcranial direct current stimulation of prefrontal cortex enhances working memory," *Experimental Brain Research*, vol. 166, no. 1, pp. 23–30, 2005.

[5] A. Flöel, "TDCS-enhanced motor and cognitive function in neurological diseases," *NeuroImage*, vol. 85, pp. 934–947, 2014.

[6] P. Wei, W. He, Y. Zhou, and L. Wang, "Performance of motor imagery brain-computer interface based on anodal transcranial direct current stimulation modulation," *IEEE Transactions on Neural Systems and Rehabilitation Engineering*, vol. 21, no. 3, pp. 404–415, 2013.

[7] J. Matsumoto, T. Fujiwara, O. Takahashi, M. Liu, A. Kimura, and J. Ushiba, "Modulation of mu rhythm desynchronization during motor imagery by transcranial direct current stimulation," *Journal of NeuroEngineering and Rehabilitation*, vol. 7, no. 1, article 27, 2010.

[8] R. Ferrucci, F. Mameli, I. Guidi et al., "Transcranial direct current stimulation improves recognition memory in Alzheimer disease," *Neurology*, vol. 71, no. 7, pp. 493–498, 2008.

[9] P. S. Boggio, R. Ferrucci, S. P. Rigonatti et al., "Effects of transcranial direct current stimulation on working memory in patients with Parkinson's disease," *Journal of the Neurological Sciences*, vol. 249, no. 1, pp. 31–38, 2006.

[10] S. J. Young, M. Bertucco, R. Sheehan-Stross, and T. D. Sanger, "Cathodal transcranial direct current stimulation in children with dystonia: a pilot open-label trial," *Journal of Child Neurology*, vol. 28, no. 10, pp. 1238–1244, 2013.

[11] P. S. Boggio, R. Ferrucci, F. Mameli et al., "Prolonged visual memory enhancement after direct current stimulation in Alzheimer's disease," *Brain Stimulation*, vol. 5, no. 3, pp. 223–230, 2012.

[12] S.-W. Yook, S. Park, J. Seo, S. Kim, and M. Ko, "Suppression of seizure by cathodal transcranial direct current stimulation in an epileptic patient—a case report," *Annals of Rehabilitation Medicine*, vol. 35, no. 4, pp. 579–582, 2011.

[13] D. S. You, D.-Y. Kim, M. H. Chun, S. E. Jung, and S. J. Park, "Cathodal transcranial direct current stimulation of the right Wernicke's area improves comprehension in subacute stroke patients," *Brain and Language*, vol. 119, no. 1, pp. 1–5, 2011.

[14] P. C. Gandiga, F. C. Hummel, and L. G. Cohen, "Transcranial DC stimulation (tDCS): a tool for double-blind sham-controlled clinical studies in brain stimulation," *Clinical Neurophysiology*, vol. 117, no. 4, pp. 845–850, 2006.

[15] M. B. Iyer, U. Mattu, J. Grafman, M. Lomarev, S. Sato, and E. M. Wassermann, "Safety and cognitive effect of frontal DC brain polarization in healthy individuals," *Neurology*, vol. 64, no. 5, pp. 872–875, 2005.

[16] F. Notturno, L. Marzetti, V. Pizzella, A. Uncini, and F. Zappasodi, "Local and remote effects of transcranial direct current stimulation on the electrical activity of the motor cortical

network," *Human Brain Mapping*, vol. 35, no. 5, pp. 2220–2232, 2014.

[17] A. Roy, B. Baxter, and B. He, "High-definition transcranial direct current stimulation induces both acute and persistent changes in broadband cortical synchronization: A Simultaneous tDCS-EEG Study," *IEEE Transactions on Biomedical Engineering*, vol. 61, no. 7, pp. 1967–1978, 2014.

[18] D. J. Krusienski, E. W. Sellers, D. J. McFarland, T. M. Vaughan, and J. R. Wolpaw, "Toward enhanced P300 speller performance," *Journal of Neuroscience Methods*, vol. 167, no. 1, pp. 15–21, 2008.

[19] M. Salvaris and F. Sepulveda, *Visual Modifications on the P300 Speller BCI Paradigm*, IOP, 2009.

[20] M. A. Roula, J. Kulon, and Y. Mamatjan, "Brain-computer interface speller using hybrid P300 and motor imagery signals," in *Proceedings of the 4th IEEE RAS & EMBS International Conference on Biomedical Robotics and Biomechatronics (BioRob '12)*, IEEE, Rome, Italy, June 2012.

[21] M. Fabiani, G. Gratton, D. Karis, and E. Donchin, "Definition, identification and reliability of measurement of P300 component of event-related brain potetial," *Advances in Psychophisiology*, vol. 2, article 78, 1987.

[22] S. Ramaraju, A. Izzidien, M. A. Roula, and P. McCarthy, "Effect of tDCS application on P300 potentials: a randomized, double blind placebo controlled study," in *Proceedings of the IEEE Symposium on Computational Intelligence, Cognitive Algorithms, Mind, and Brain (CCMB '14)*, pp. 111–114, Orlando, Fla, USA, December 2014.

[23] A. Antal, T. Z. Kincses, M. A. Nitsche, O. Bartfai, and W. Paulus, "Excitability changes induced in the human primary visual cortex by transcranial direct current stimulation: direct electrophysiological evidence," *Investigative Ophthalmology and Visual Science*, vol. 45, no. 2, pp. 702–707, 2004.

[24] J.-W. Lee, S.-W. Yoon, W.-S. Park, M. Heo, D.-G. Lee, and S.-K. Jeong, "Effects of the electrode type on N100 and P300 in tDCS applications," *Journal of Physical Therapy Science*, vol. 26, no. 9, pp. 1441–1443, 2014.

[25] D.-Y. Kim, J.-Y. Lim, E. K. Kang et al., "Effect of transcranial direct current stimulation on motor recovery in patients with subacute stroke," *American Journal of Physical Medicine and Rehabilitation*, vol. 89, no. 11, pp. 879–886, 2010.

[26] F. Pichiorri, F. Cincotti, F. De Vico et al., "Towards a brain computer Interface-based rehabilitation: from bench to bedside," in *Proceedings of the 5th International Brain-Computer Interface Conference (BCI '11)*, pp. 268–271, 2011.

[27] S. Fok, R. Schwartz, M. Wronkiewicz et al., "An EEG-based brain computer interface for rehabilitation and restoration of hand control following stroke using ipsilateral cortical physiology," in *Proceedings of the Annual International Conference of the IEEE Engineering in Medicine and Biology Society (EMBC '11)*, IEEE, 2011.

[28] S. Shahid, R. K. Sinha, and G. Prasad, "Mu and beta rhythm modulations in motor imagery related post-stroke EEG: a study under BCI framework for post-stroke rehabilitation," *BMC Neuroscience*, vol. 11, supplement 1, p. P127, 2010.

[29] G. F. Spitoni, R. L. Cimmino, C. Bozzacchi, L. Pizzamiglio, and F. Di Russo, "Modulation of spontaneous alpha brain rhythms using low-intensity transcranial direct-current stimulation," *Frontiers in Human Neuroscience*, vol. 7, article 529, 2013.

[30] R. Chavarriaga, A. Biasiucci, A. Molina et al., "tDCS Modulates Motor Imagery-Related BCI Features," in *Converging Clinical and Engineering Research on Neurorehabilitation*, vol. 1 of *Biosystems & Biorobotics*, pp. 647–651, Springer, Berlin, Germany, 2013.

[31] Y. Kasashima, T. Fujiwara, Y. Matsushika et al., "Modulation of event-related desynchronization during motor imagery with transcranial direct current stimulation (tDCS) in patients with chronic hemiparetic stroke," *Experimental Brain Research*, vol. 221, no. 3, pp. 263–268, 2012.

[32] A. F. DaSilva, M. S. Volz, M. Bikson, and F. Fregni, "Electrode positioning and montage in transcranial direct current stimulation," *Journal of Visualized Experiments: JoVE*, vol. 51, p. 2744, 2011.

[33] H. R. Siebner, N. Lang, V. Rizzo et al., "Preconditioning of low-frequency repetitive transcranial magnetic stimulation with transcranial direct current stimulation: evidence for homeostatic plasticity in the human motor cortex," *The Journal of Neuroscience*, vol. 24, no. 13, pp. 3379–3385, 2004.

[34] M. A. Nitsche, D. Liebetanz, A. Antal, N. Lang, F. Tergau, and W. Paulus, "Modulation of cortical excitability by weak direct current stimulation-technical," *Supplements to Clinical Neurophysiology*, vol. 56, no. 3, pp. 255–276, 2003.

[35] M. A. Nitsche and W. Paulus, "Sustained excitability elevations induced by transcranial DC motor cortex stimulation in humans," *Neurology*, vol. 57, no. 10, pp. 1899–1901, 2001.

[36] A. Delorme and S. Makeig, "EEGLAB: an open source toolbox for analysis of single-trial EEG dynamics including independent component analysis," *Journal of Neuroscience Methods*, vol. 134, no. 1, pp. 9–21, 2004.

[37] L. A. Farwell and E. Donchin, "Talking off the top of your head: toward a mental prosthesis utilizing event-related brain potentials," *Electroencephalography and Clinical Neurophysiology*, vol. 70, no. 6, pp. 510–523, 1988.

[38] A. L. Mangia, M. Pirini, and A. Cappello, "Transcranial direct current stimulation and power spectral parameters: a tDCS/EEG co-registration study," *Frontiers in Human Neuroscience*, vol. 8, article 601, 2014.

[39] T. L. Costa, M. Gualtieri, M. T. S. Barboni, R. K. Katayama, P. S. Boggio, and D. F. Ventura, "Contrasting effects of transcranial direct current stimulation on central and peripheral visual fields," *Experimental Brain Research*, vol. 233, no. 5, pp. 1391–1397, 2015.

[40] J. Miller, B. Berger, and P. Sauseng, "Anodal transcranial direct current stimulation (tDCS) increases frontal-midline theta activity in the human EEG: a preliminary investigation of non-invasive stimulation," *Neuroscience Letters*, vol. 588, pp. 114–119, 2015.

[41] S. H. Lim, D. S. Dinner, P. K. Pillay et al., "Functional anatomy of the human supplementary sensorimotor area: results of extraoperative electrical stimulation," *Electroencephalography and Clinical Neurophysiology*, vol. 91, no. 3, pp. 179–193, 1994.

[42] A. Antal, D. Terney, S. Kühnl, and W. Paulus, "Anodal transcranial direct current stimulation of the motor cortex ameliorates chronic pain and reduces short intracortical inhibition," *Journal of Pain and Symptom Management*, vol. 39, no. 5, pp. 890–903, 2010.

Hindawi Publishing Corporation
BioMed Research International
Volume 2016, Article ID 5469587, 5 pages
http://dx.doi.org/10.1155/2016/5469587

Research Article

Analysis of the Influence of Complexity and Entropy of Odorant on Fractal Dynamics and Entropy of EEG Signal

Hamidreza Namazi,[1] Amin Akrami,[2] Sina Nazeri,[3] and Vladimir V. Kulish[1]

[1]*School of Mechanical and Aerospace Engineering, Nanyang Technological University, Singapore*
[2]*School of Metallurgy and Material Engineering, University of Tehran, Tehran, Iran*
[3]*Faculty of Cognitive Sciences and Human Development, Universiti Malaysia Sarawak, 94300 Kota Samarahan, Malaysia*

Correspondence should be addressed to Hamidreza Namazi; hnamazi@ntu.edu.sg

Received 22 June 2016; Accepted 22 August 2016

Academic Editor: Jongsang Son

An important challenge in brain research is to make out the relation between the features of olfactory stimuli and the electroencephalogram (EEG) signal. Yet, no one has discovered any relation between the structures of olfactory stimuli and the EEG signal. This study investigates the relation between the structures of EEG signal and the olfactory stimulus (odorant). We show that the complexity of the EEG signal is coupled with the molecular complexity of the odorant, where more structurally complex odorant causes less fractal EEG signal. Also, odorant having higher entropy causes the EEG signal to have lower approximate entropy. The method discussed here can be applied and investigated in case of patients with brain diseases as the rehabilitation purpose.

1. Introduction

EEG as one of the famous methods for monitoring brain activity specially has been used by scientists in order to study the brain reaction to external stimuli. Scientists have used different approaches to study EEG signals [1–5]. One useful method to study the EEG signal is the fractal method. Fractal time series shows the long-range correlations, meaning that each fluctuation in the time series is correlated with last fluctuations (memory concept), where the correlations change based on power law [6]. Fractal theory has been used widely in biology and medicine in different cases such as DNA [7, 8], human memory [9], bone structure [10], and human stride time series [11].

Olfactory stimulation is one of important types of external stimulation which has aroused the attention of many scientists. Beside the numerous works done on analysis of EEG signal due to olfactory stimulation [12–16], very limited works reported in the literature focus on fractal analysis of the EEG signal in response to olfactory stimuli. In an interesting research Kurihara et al. [17] designed a fractal dimensional map of brain for subjects who received olfactory stimuli. Using this map they studied the activity of different regions of the brain due to stimulation. The result of their analysis showed that cacao or chocolate (as an odor stimulant) had a clearer effect on the fractal dimension of EEG signal compared to the usual fragrant oils. In another research, Murali and Vladimir [18] analyzed the fractal spectra of human EEG signal induced by odors. The result of their analysis showed that fractal approach predicts the EEG signal due to stimulation using different odorants.

On the other hand, some scientists have analyzed the entropy of EEG signal due to olfactory stimulation. Employing entropy as a measure to analyze the EEG signal due to olfactory stimulation also was very limited. Min et al. [19] computed Shannon entropy of EEG signal as the measure of information content in case of odor stimulation of subjects classified by occupation. Analysis of the averaged entropy from the EEGs of subjects showed that, among the professional perfume researchers, changes of average entropy were more apparent in the frontal region of the brain, while for the general workers and perfume salespersons such changes were more conspicuous in the overall posterior temporal, parietal, and frontal regions. In another work Kroupi et al. [20] used permutation entropy for pleasantness recognition of olfactory stimulus. They showed that the permutation

Table 1: Characteristics of odorants.

Name	Compound	Molecular complexity	Entropy (cal/mol·K)
Benzyl alcohol	C_7H_8O	55.4	85.55
Dimethyl succinate	$C_6H_{10}O_4$	114	118.24
Diethyl malonate	$C_7H_{12}O_4$	125	132.42
Diethyl succinate	$C_8H_{14}O_4$	135	136.29
Diethyl malate	$C_8H_{14}O_5$	177	145.50

entropy of the EEG conveys olfactory-based information which is able to distinguish between pleasant and unpleasant odors. They also showed that an increase or decrease in the permutation entropy of unpleasant odors with respect to pleasant ones depends on the brain regions. Manzanedo et al. [21] applied three olfactory stimuli on subjects and by analysis of their EEG signal using Shannon entropy. They found out the significant effect of olfactory stimulation on the EEG signal.

Besides all efforts done on analysis of EEG signal due to olfactory stimulation, no study has been reported that relates the complexity and entropy of olfactory stimuli to the fractal dynamics and entropy of EEG signal. In this research we test the complexity and entropy of EEG signal versus the complexity and entropy of odorants, respectively, and show their coupling.

2. Method

In order to investigate the effect of odorant's complexity on fractality of EEG signal, the odorant's complexity should be quantified. For this purpose we considered the molecular complexity of odorants. In general, bigger and/or less symmetric molecules have higher molecular complexity. The molecular complexity (C) of an odorant is defined using Bertz formula [22]:

$$C = C_n + C_e. \quad (1)$$

In this equation, C_n and C_e are functions of bond connectivity (n) and element diversity or kinds of atoms, respectively.

As another parameter to investigate, we study the influence of odorant's entropy at 25°C on the entropy of EEG signal. As it is known, at 0°K odorants have zero entropy and as the temperature increases their entropy increases.

In order to investigate the influence of odorant's complexity and entropy on fractality and entropy of EEG signal, we selected five pleasant odorants (look at Table 1) from Fenaroli's Handbook of Flavor Ingredients [23].

As it is shown in Table 1, the odorants have molecular complexities in the range of 55.4 (benzyl alcohol) and 177 (diethyl malate). The work by Hendrickson et al. [22] has been used in order to compute the molecular complexities. It was mentioned that, in general, bigger and/or less symmetric molecules have higher molecular complexity.

Also, as it is shown in Table 1, the odorants have entropy in the range of 85.55 (benzyl alcohol) to 145.50 (diethyl malate). The values of odorants' entropies in 25°C were collected from http://realtime.molinstincts.com/.

2.1. Data Collection. The experiments were conducted on forty healthy students (20 male and 20 female; 20–22 years old). A physician examined subjects before the experiment to ensure that subjects are healthy. Subjects did not drink beverages which contain alcohol/caffeine within 48 hours before the experiments.

Internal Review Board of the university approved all procedures, and the written informed consent was obtained from subjects, after we explained the study to them.

In order to insulate the subjects, we have done the experiments in an electrically shielded, acoustically isolated, and dimly illuminated room. We instructed the subjects to focus on their breathing while sitting comfortably, without talking and without doing any movement. Also, they were asked to not think about anything.

We diluted odorants in mineral oil in order to equalize their concentrations. We presented each odorant using 10 mL vials. We measured the concentrations of odorants using an olfactometer which was connected to a gas analyzer, to ensure that the resulting vapor concentrations did not differ. The presentation of each odorant to gas analyzer was done 5 times with interstimulus interval of 2 minutes.

The EEG data (with sampling frequency of 256 Hz) were collected using Mindset 24 device. The electrode impedance was kept lower than 5 KΩ. At first, the data collection was done free of any stimulus. Then, we presented different odorants in separate experiments to the subject's nose, and the subject sniffed the odorants, and we recorded the EEG signal. It is noteworthy that we considered interstimulus time of 5 minutes between different odorants' presentations. With the purpose of off-line artifacts rejection, a bipolar EOG was recorded.

To test the reproducibility of the results, we repeated the data collection where in total two trials were collected from each subject for each stimulus. A physician controlled all experiments.

2.2. Data Analysis. Since the recorded EEG data were noisy, first these data were filtered using Wavelet toolbox in MATLAB. After filtering the data, other MATLAB programs computed the fractal dimension and entropy of EEG signals using Box counting [24] and approximate entropy techniques [25].

2.3. Statistical Analysis. Mean values of fractal exponent and approximate entropy for the EEG signal were compared between different conditions using one-way repeated measures ANOVA. Mauchly's test ($\alpha = 0.05$) was conducted to test the sphericity. Trend analysis was conducted based on the odorants' properties. Omega squared (ω^2) was used for a repeated measures design. Effect size, r, was employed for pairwise comparisons.

3. Results

Here we report the result of analysis. It is noteworthy that all subjects and all trials were included in the analysis. Mauchly's test indicated that the assumption of sphericity had not

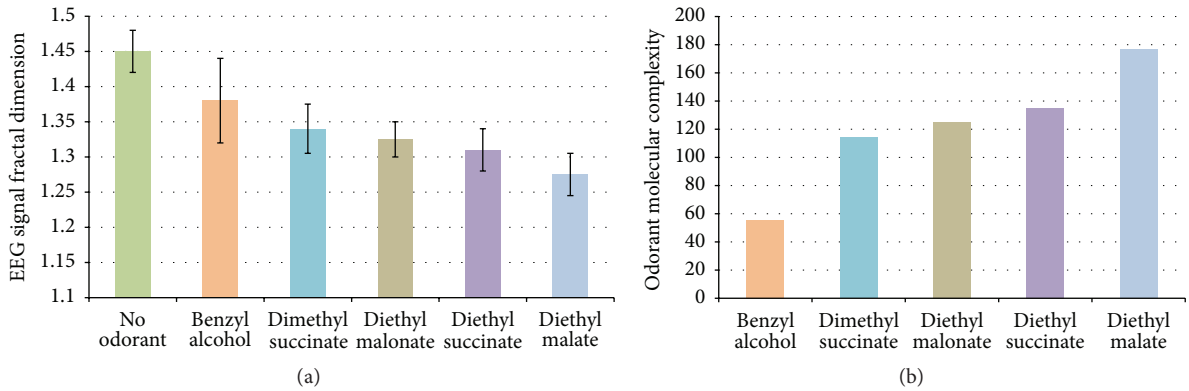

Figure 1: Fractal dimension for EEG signal (a) due to different odorants and the odorants' molecular complexities (b). Error bars indicate standard deviations.

been violated in case of outcomes (fractal exponent and approximate entropy of EEG signal).

The variations of fractal dimension for EEG signal due to different odorants and the odorants' molecular complexities are shown in Figure 1. The results stand for the mean values.

Since $F_{\text{crit}}(5, 234) = 2.25$ at $\alpha = 0.05$, the result of statistical analysis [$F(5, 234) = 150$, $p = 0.001$] stands for the significant influence of odorants on the fractal dimension of EEG signal, with the effect size $\omega^2 = 0.69$. Generally, odorants reduced the fractality of EEG signal. This result agrees with the result of work reported in [26], which states that the application of stimulus reduces the fractality of EEG signal. Olfactory stimuli conditions had a significant linear trend ($p = 0.001$), indicating that diethyl malate caused a bigger variation in the fractality of EEG signal compared to diethyl succinate, followed by diethyl malonate, dimethyl succinate, and benzyl alcohol, respectively, reflecting the trend of molecular complexity of odorants, that is, diethyl malate bigger than diethyl succinate and bigger than diethyl malonate, dimethyl succinate, and benzyl alcohol, respectively. The effect sizes in Table 2 show that diethyl malate caused the greatest change in the fractality of EEG signal.

The variations of approximate entropy for EEG signal due to different odorants and the odorants' entropy are shown in Figure 2. The results stand for the mean values.

Since $F_{\text{crit}}(5, 234) = 2.25$ at $\alpha = 0.05$, the result of statistical analysis [$F(5, 234) = 69.5$, $p = 0.001$] stands for the significant influence of odorants on the entropy of EEG signal, with the effect size $\omega^2 = 0.60$. Generally, odorants reduced the approximate entropy of EEG signal. This result agrees with the result of work reported in [27], which states that the application of stimulus reduces the approximate entropy of EEG signal. Olfactory stimuli conditions had a significant linear trend ($p = 0.002$), indicating that diethyl malate caused a bigger variation in the approximate entropy of EEG signal compared to diethyl succinate, followed by diethyl malonate, dimethyl succinate, and benzyl alcohol, respectively, reflecting the trend of entropy of the odorants, that is, diethyl malate bigger than diethyl succinate and bigger than diethyl malonate, dimethyl succinate, and benzyl alcohol. The effect sizes in Table 2 show that diethyl malate caused the biggest change in approximate entropy of EEG signal.

Table 2: Effect sizes of pairwise comparisons.

Condition	Fractal dimension effect size (r)	Approximate entropy effect size (r)
No odorant versus benzyl alcohol	0.59	0.46
No odorant versus dimethyl succinate	0.86	0.78
No odorant versus diethyl malonate	0.91	0.88
No odorant versus diethyl succinate	0.92	0.89
No odorant versus diethyl malate	0.94	0.90
Benzyl alcohol versus dimethyl succinate	0.37	0.33
Benzyl alcohol versus diethyl malonate	0.51	0.52
Benzyl alcohol versus diethyl succinate	0.59	0.59
Benzyl alcohol versus diethyl malate	0.74	0.65
Dimethyl succinate versus diethyl malonate	0.23	0.35
Dimethyl succinate versus diethyl succinate	0.41	0.49
Dimethyl succinate versus diethyl malate	0.70	0.60
Diethyl malonate versus diethyl succinate	0.26	0.26
Diethyl malonate versus diethyl malate	0.67	0.46
Diethyl succinate versus diethyl malate	0.50	0.27

Overall, the coupling between characteristics of odorant and EEG signal was observed, where the odorant having

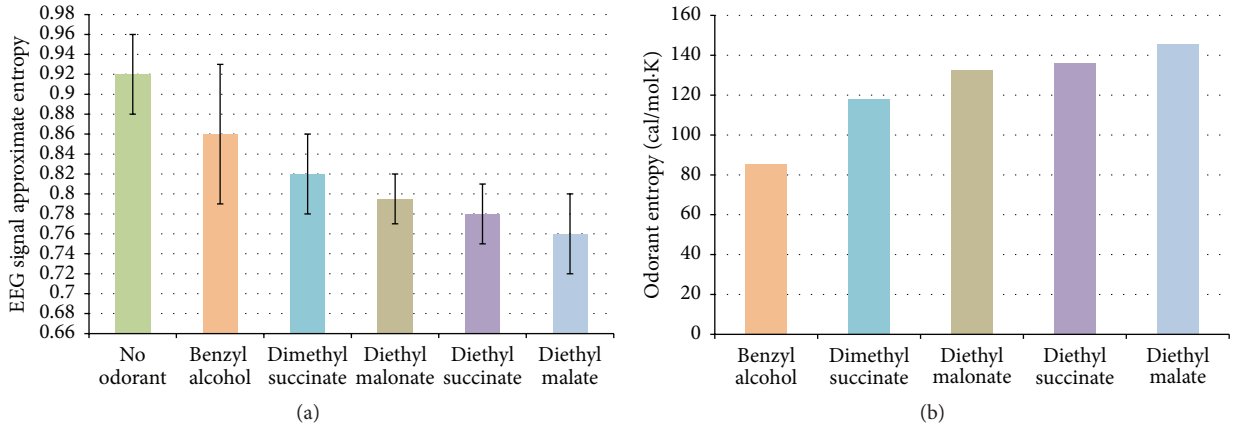

Figure 2: Approximate entropy for EEG signal (a) due to different odorants and the odorants' entropies (b). Error bars indicate standard deviations.

higher complexity and entropy causes the bigger change in fractality and entropy of EEG signal.

4. Discussion

In this research we studied the effect of odorant's complexity and entropy on fractality and approximate entropy of EEG signal. Our results demonstrated plasticity of the olfactory-motor phenomenon while smelling different odorants, as the trend of the complexity of odorants is reflected in the trend of the reduction of fractality of EEG signal. For instance, diethyl malate with highest value of molecular complexity caused the biggest variation in EEG signal's fractality, compared to other odorants. This behavior was seen in comparison with other odorants as well. On the other hand, the result of our analysis showed similar trend of variations in case of odorant's entropy and EEG signal's approximate entropy. Overall, the coupling between characteristics of odorant and EEG signal was observed, where the odorant having higher complexity and entropy causes bigger change in fractality and entropy of EEG signal.

The behavior seen in this research can be explained through olfactory perception system. When human smells an odorant, the neurons in the nasal passage send the message to the brain about the odorant which yield to perception [28]. Thus, based on our result, when odorant with higher molecular complexity is sensed by olfactory receptor neurons, these neurons are aroused more and accordingly a stronger message is sent to the brain. Then, this stronger signal has stronger effect on the brain which accordingly is mapped on the EEG signal having lower fractality.

In order to elaborate the behavior seen in variation of approximate entropy we should refer to its definition. Approximate entropy is indicator of randomness of time series where lower value of approximate entropy stands for less randomness. In [6] it was shown that when human receives an external stimulus the EEG signal's Hurst exponent increases from $H = 0.5$ (random state). This increment stands for a less random signal. Thus, here, decreasing the value of the approximate entropy is logical, as by applying the stimulus to subjects, the Hurst exponent increases and accordingly approximate entropy decreases.

In fact the study done in this research is important due to the method of analysis and the usefulness of its result. Since EEG signal is a chaotic time series that is nonstationary, many of signal analysis methods cannot be used to describe its nonstationary behavior. So, to address the nonstationary behavior of EEG time series, nonlinear processing techniques with their implicit dependence on nonlinear dynamics, chaos, and fractals should be used [29]. As was mentioned before, fractal theory has showed its strength for this purpose as a useful technique.

Entropy also has shown its strength in investigating the dynamics (stochastic rules) of the process generating the trajectory by monitoring the time evolution of the corresponding process. In fact, different types of entropy capture many of the quantitative features of the EEG signal.

On the other hand, rehabilitation has been an important approach in analysis and modeling of neurological signal. Many works investigated the effect of olfactory stimuli on the brains of patients with some neurological disorders [30–33]. In this way, our method of analysis can be investigated for this case to analyze how the odorant's characteristics can affect their brain activity in order to improve its response. Also, our analyses can help the current efforts for the modeling of brain reaction to external stimulation. For instance, the result of our investigation in this research can be linked with our Fractional Diffusion Model brain reaction to external stimulation in [6], in order to write the observed coupling in the mathematical form.

In general, understanding the relation between external stimuli and brain reaction helps the development of the therapy of different brain diseases.

Competing Interests

The authors declare that they have no competing financial interests.

References

[1] M. Adib and E. Cretu, "Wavelet-based artifact identification and separation technique for EEG signals during galvanic vestibular stimulation," *Computational and Mathematical Methods in Medicine*, vol. 2013, Article ID 167069, 13 pages, 2013.

[2] M. Musselman and D. Djurdjanovic, "Time-frequency distributions in the classification of epilepsy from EEG signals," *Expert Systems with Applications*, vol. 39, no. 13, pp. 11413–11422, 2012.

[3] E. D. Übeyli, "Analysis of EEG signals by combining eigenvector methods and multiclass support vector machines," *Computers in Biology and Medicine*, vol. 38, no. 1, pp. 14–22, 2008.

[4] V. Lawhern, S. Kerick, and K. A. Robbins, "Detecting alpha spindle events in EEG time series using adaptive autoregressive models," *BMC Neuroscience*, vol. 14, article 101, 2013.

[5] A. S. Al-Fahoum and A. A. Al-Fraihat, "Methods of EEG signal features extraction using linear analysis in frequency and time-frequency domains," *ISRN Neuroscience*, vol. 2014, Article ID 730218, 7 pages, 2014.

[6] H. Namazi and V. V. Kulish, "Fractional diffusion based modelling and prediction of human brain response to external stimuli," *Computational and Mathematical Methods in Medicine*, vol. 2015, Article ID 148534, 11 pages, 2015.

[7] H. Namazi, V. V. Kulish, and A. Wong, "Mathematical modelling and prediction of the effect of chemotherapy on cancer cells," *Scientific Reports*, vol. 5, Article ID 13583, 2015.

[8] H. Namazi, V. V. Kulish, F. Delaviz, and A. Delaviz, "Diagnosis of skin cancer by correlation and complexity analyses of damaged DNA," *Oncotarget*, vol. 6, no. 40, pp. 42623–42631, 2015.

[9] H. Namazi, R. Khosrowabadi, J. Hussaini, S. Habibi, A. A. Farid, and V. V. Kulish, "Analysis of the influence of memory content of auditory stimuli on the memory content of EEG signal," *Oncotarget*, vol. 7, no. 35, pp. 56120–56128, 2016.

[10] K.-H. Huh, J.-S. Baik, W.-J. Yi et al., "Fractal analysis of mandibular trabecular bone: optimal tile sizes for the tile counting method," *Imaging Science in Dentistry*, vol. 41, no. 2, pp. 71–78, 2011.

[11] H. Namazi and V. V. Kulish, "Mathematical based modeling and prediction of the effect of external stimuli on human gait," *International Journal for Numerical Methods in Biomedical Engineering*, 2016.

[12] C. Martin and N. Ravel, "Beta and gamma oscillatory activities associated with olfactory memory tasks: different rhythms for different functional networks?" *Frontiers in Behavioral Neuroscience*, vol. 8, article 218, 2014.

[13] C. Huart, V. Legrain, T. Hummel, P. Rombaux, and A. Mouraux, "Time-frequency analysis of chemosensory event-related potentials to characterize the cortical representation of odors in humans," *PLoS ONE*, vol. 7, no. 3, Article ID e33221, 2012.

[14] G. Placidi, D. Avola, A. Petracca, F. Sgallari, and M. Spezialetti, "Basis for the implementation of an EEG-based single-trial binary brain computer interface through the disgust produced by remembering unpleasant odors," *Neurocomputing*, vol. 160, pp. 308–318, 2015.

[15] H. Harada, Y. Eura, K. Shiraishi, T. Kato, and T. Soda, "Coherence analysis of EEG changes during olfactory stimulation," *Clinical EEG Electroencephalography*, vol. 29, no. 2, pp. 96–100, 1998.

[16] A. Saha, A. Konar, A. Chatterjee, A. Ralescu, and A. K. Nagar, "EEG analysis for olfactory perceptual-ability measurement using a recurrent neural classifier," *IEEE Transactions on Human-Machine Systems*, vol. 44, no. 6, pp. 717–730, 2014.

[17] K. Kurihara, N. Suzuki, and H. Ogawa, *Olfaction and Taste XI*, Springer, 1994.

[18] S. Murali and K. V. Vladimir, "Analysis of fractal and fast Fourier transform spectra of human electroencephalograms induced by odors," *International Journal of Neuroscience*, vol. 117, no. 10, pp. 1383–1401, 2007.

[19] B.-C. Min, S.-H. Jin, I.-H. Kang et al., "Analysis of mutual information content for EEG responses to odor stimulation for subjects classified by occupation," *Chemical Senses*, vol. 28, no. 9, pp. 741–749, 2003.

[20] E. Kroupi, D. Sopic, and T. Ebrahimi, "Non-linear EEG features for odor pleasantness recognition," in *Proceedings of the 6th International Workshop on Quality of Multimedia Experience (QoMEX '14)*, pp. 147–152, Singapore, September 2014.

[21] E. Manzanedo, A. B. Solana, E. Molina et al., "EEG metrics evaluation in simultaneous EEG-fMRI olfactory experiment," in *XIII Mediterranean Conference on Medical and Biological Engineering and Computing 2013: MEDICON 2013, 25–28 September 2013, Seville, Spain*, vol. 41 of *IFMBE Proceedings*, pp. 815–818, Springer, Berlin, Germany, 2014.

[22] J. B. Hendrickson, P. Huang, and A. G. Toczko, "Molecular complexity: a simplified formula adapted to individual atoms," *Journal of Chemical Information and Computer Sciences*, vol. 27, no. 2, pp. 63–67, 1987.

[23] G. A. Burdock, *Fenaroli's Handbook of Flavor Ingredients*, CRC Press, 6th edition, 2009.

[24] H. Namazi, V. V. Kulish, J. Hussaini et al., "A signal processing based analysis and prediction of seizure onset in patients with epilepsy," *Oncotarget*, vol. 7, no. 1, pp. 342–350, 2015.

[25] S. M. Pincus, I. M. Gladstone, and R. A. Ehrenkranz, "A regularity statistic for medical data analysis," *Journal of Clinical Monitoring*, vol. 7, no. 4, pp. 335–345, 1991.

[26] H. Namazi, V. V. Kulish, and A. Akrami, "The analysis of the influence of fractal structure of stimuli on fractal dynamics in fixational eye movements and EEG signal," *Scientific Reports*, vol. 6, Article ID 26639, 2016.

[27] S. A. Hosseini and M. B. Naghibi-Sistani, "Emotion recognition method using entropy analysis of EEG signals," *International Journal of Image, Graphics and Signal Processing*, vol. 5, pp. 30–36, 2011.

[28] C. S. Sell, *Chemistry and the Sense of Smell*, John Wiley & Sons, New York, NY, USA, 2014.

[29] M. Ignaccolo, M. Latka, W. Jernajczyk, P. Grigolini, and B. J. West, "The dynamics of EEG entropy," *Journal of Biological Physics*, vol. 36, no. 2, pp. 185–196, 2010.

[30] Y. Masaoka, H. Satoh, M. Kawamura, and I. Homma, "Respiratory responses to olfactory stimuli in Parkinson's disease," *Respiratory Physiology and Neurobiology*, vol. 161, no. 2, pp. 136–141, 2008.

[31] E. Wattendorf, A. Welge-Lüssen, K. Fiedler et al., "Olfactory impairment predicts brain atrophy in Parkinson's disease," *The Journal of Neuroscience*, vol. 29, no. 49, pp. 15410–15413, 2009.

[32] P. E. Gilbert, P. J. Barr, and C. Murphy, "Differences in olfactory and visual memory in patients with pathologically confirmed Alzheimer's disease and the Lewy body variant of Alzheimer's disease," *Journal of the International Neuropsychological Society*, vol. 10, no. 6, pp. 835–842, 2004.

[33] P. E. Gilbert and C. Murphy, "The effect of the ApoE $\varepsilon 4$ allele on recognition memory for olfactory and visual stimuli in patients with pathologically confirmed Alzheimer's disease, probable Alzheimer's disease, and healthy elderly controls," *Journal of Clinical and Experimental Neuropsychology*, vol. 26, no. 6, pp. 779–794, 2004.

Hindawi Publishing Corporation
BioMed Research International
Volume 2016, Article ID 3939815, 7 pages
http://dx.doi.org/10.1155/2016/3939815

Research Article

Data-Driven User Feedback: An Improved Neurofeedback Strategy considering the Interindividual Variability of EEG Features

Chang-Hee Han, Jeong-Hwan Lim, Jun-Hak Lee, Kangsan Kim, and Chang-Hwan Im

Department of Biomedical Engineering, Hanyang University, Seoul 133-731, Republic of Korea

Correspondence should be addressed to Chang-Hwan Im; ich@hanyang.ac.kr

Received 27 April 2016; Accepted 25 July 2016

Academic Editor: Asode A. Shetty

It has frequently been reported that some users of conventional neurofeedback systems can experience only a small portion of the total feedback range due to the large interindividual variability of EEG features. In this study, we proposed a data-driven neurofeedback strategy considering the individual variability of electroencephalography (EEG) features to permit users of the neurofeedback system to experience a wider range of auditory or visual feedback without a customization process. The main idea of the proposed strategy is to adjust the ranges of each feedback level using the density in the offline EEG database acquired from a group of individuals. Twenty-two healthy subjects participated in offline experiments to construct an EEG database, and five subjects participated in online experiments to validate the performance of the proposed data-driven user feedback strategy. Using the optimized bin sizes, the number of feedback levels that each individual experienced was significantly increased to 139% and 144% of the original results with uniform bin sizes in the offline and online experiments, respectively. Our results demonstrated that the use of our data-driven neurofeedback strategy could effectively increase the overall range of feedback levels that each individual experienced during neurofeedback training.

1. Introduction

Neurofeedback is a type of biofeedback technology that has generally been used to train the ability of self-regulation based on the real-time analysis of neural signals such as electroencephalography (EEG), magnetoencephalography (MEG), and real-time functional magnetic resonance imaging (fMRI) [1]. Over the past decades, several experimental studies have demonstrated that neurofeedback training can be used effectively for the treatment of patients with various psychiatric diseases or neurological disorders such as attention deficit hyperactivity disorder (ADHD), autism, depression, Tourette syndrome, insomnia, and epilepsy [2–7]. Furthermore, recent studies have reported that neurofeedback training can temporally enhance the cognitive performances of healthy individuals [8–10]. Thanks to these positive effects, neurofeedback has been gaining increased attention [11].

Among the various neural signal acquisition modalities including EEG, MEG, and fMRI [12–14], EEG has been the most widely used for implementing neurofeedback systems due to its several advantages over other neuroimaging modalities, such as high temporal resolution, portability, and reasonable cost [15]. Since the 1960s, when the concept of EEG-based neurofeedback was first introduced [16], most of the EEG-based neurofeedback studies used a spectral power of a specific frequency band [17]. For example, "alpha" neurofeedback training is known to improve cognitive performance in human subjects [8], and "beta" neurofeedback training is known to affect attentional processing [18]. Recent studies have adopted a variety of EEG features, such as the ratio of two or more spectral powers, to improve the overall performance of neurofeedback [19].

Despite the recent development of EEG-based neurofeedback strategies, however, the EEG-based neurofeedback systems still suffer from some limitations. One of the most

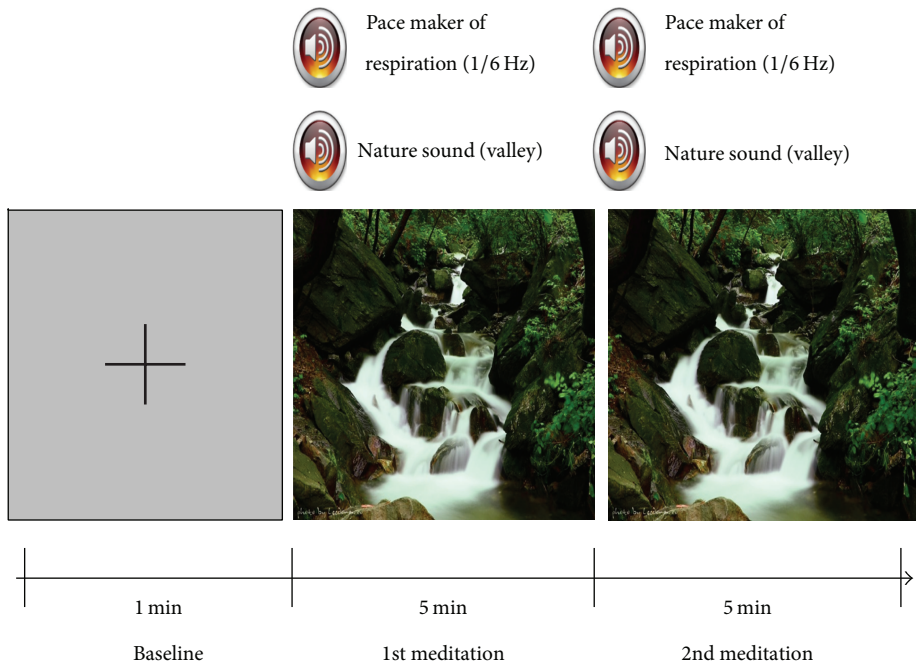

Figure 1: A schematic diagram describing our experimental paradigm. A babbling brook sound, a picture of a beautiful valley, and a quiet pure-tone beep sound (respiration pacemaker) with a period of three seconds were simultaneously provided to each study participant.

representative limitations is the large interindividual variability of the EEG features that have been used for neurofeedback [20–22]. Due to the large variability of individual EEG signals, it is generally difficult to develop "universal" neurofeedback systems that can be applied to all users without any time-consuming customization or individualization processes [23–25]. Therefore, some users of the current neurofeedback systems may experience only a small portion of the entire feedback range (e.g., see Figure 3 in advance). Although the use of a customization or individualization session before using a neurofeedback system would enhance the performance of the neurofeedback systems, such time-consuming and cumbersome sessions might decrease the satisfaction of the users. Therefore, it is still necessary to make an effort to develop EEG features with small interindividual variations or to increase the feedback ranges that each individual experiences.

In the present study, we attempted to make the users of the neurofeedback systems experience a wider range of auditory or visual feedback. To this aim, we proposed a new neurofeedback strategy, named as the data-driven user feedback strategy, which uses nonuniform bin sizes to divide the entire range of an EEG feature into many bins, each of which is assigned to a corresponding feedback level, based on the offline EEG database acquired from a group of individuals.

2. Methods

2.1. Subjects. Two groups of healthy subjects were enrolled in our experiments. The first group, consisting of 22 healthy subjects (17 males and 5 females; mean age 23.73 ± 3.12 years), participated in offline experiments to construct an EEG database, and, the second group, consisting of five healthy subjects (four males and one female; mean age 25.20± 1.17 years), participated in online experiments to validate the performance of the proposed neurofeedback strategy. Subjects who participated in the offline experiment were not enrolled in the online experiment again because we wanted to test whether the new subjects could show good performance using the proposed neurofeedback strategy based on the other participants' database. All participants had normal or corrected-to-normal vision and none had a previous history of neurological, psychiatric, or other severe diseases that might otherwise affect the experimental results. Before each experiment, comprehensive information on the experiments was given to each participant, and written informed consent was obtained from each subject. This study was reviewed and approved by the Institutional Review Board Committee of Hanyang University.

2.2. Experimental Procedure. To verify the feasibility of the proposed neurofeedback strategy, we conducted offline and online experiments. In the offline experiment, each participant in the first group performed a "meditation" paradigm, which helped the study participants to relax. The meditation paradigm consisted of resting, first meditation, and second meditation periods (Figure 1). During the resting period, a black fixation cross appeared at the center of an LCD monitor for 1 min, while each subject was asked to gaze at the fixation cross without moving his or her body. Then, a babbling brook sound, a picture of a beautiful valley, and a quiet pure-tone beep sound with a period of three seconds were simultaneously provided to each subject. The

study participants were asked to take a slow breath to the beat of the beep sound, while they consistently watched the picture on the monitor and listened to the brook sound. This five-minute session was repeated twice with a short break time. In the online experiments, each participant in the second group performed the same meditation task as in the offline experiment, except that real-time visual feedback was provided reflecting the participant's current meditation state. The size of a circle and the length of a bar displayed on a monitor varied according to the level of the participant's meditation state.

2.3. EEG Recording and Preprocessing. EEG signals were recorded using a multichannel EEG acquisition system (ActiveTwo, BioSemi, Amsterdam, Netherlands). Two EEG electrodes (Fp1 and Fp2) were mounted on the prefrontal area of the subject's scalp according to the international 10–20 system, assuming a headband-type portable EEG neurofeedback system. The ground electrode was replaced with two electrodes, a common mode sense (CMS) active electrode and a driven right leg (DRL) passive electrode, both of which were located in the posterior region. The EEG data were sampled at 2,048 Hz, and then the spectral power of the alpha band (8–12 Hz) was calculated using a fast Fourier transform.

2.4. Data-Driven Neurofeedback Strategy. As aforementioned, neurofeedback can be used to enhance cognitive performance of an individual or treat patients with neuropsychiatric diseases and neurological disorders. Although there is no formal procedure for the conventional neurofeedback training, the entire dynamic range of an EEG feature is usually evenly divided into multiple segments, each of which is then assigned to a corresponding level of auditory or visual feedbacks. In this case, some users who have narrow dynamic ranges of the EEG feature might accordingly experience relatively narrow ranges of feedback compared with other users who have broad dynamic ranges. The dynamic range of the EEG feature of an individual can be recorded before the neurofeedback training and set differently for each individual, which is referred to as the customization session; however, this customization session generally needs to be conducted every time a user wants to try the neurofeedback system because of the high intertrial variability of EEG data [26, 27]. In the present study, to enable most users to experience a wider dynamic range of feedback during neurofeedback training without a customization process, we used nonuniform bin sizes to divide up the entire EEG feature range. The size of each bin was determined based on the grand distribution of the EEG feature (in this study, alpha band power averaged over Fp1 and Fp2 was used to evaluate meditation states). The fundamental concept of the proposed method was introduced in our preliminary study [28]. This paper is the extended version of the preliminary study, and we additionally confirmed its online performance using other EEG dataset in this study. The proposed method will be explained in detail in the next paragraph.

In the first step, a database of an EEG feature was constructed, while a group of participants was performing a specific mental task (a meditation task in this study). Using the database, a grand histogram was obtained. The grand histogram could show overall distribution of the EEG feature values. In this study, we used frontal alpha band (8–12 Hz) power as the EEG feature [29–31]. Alpha band powers were evaluated for 60 EEG epochs with a length of 2 seconds. Each epoch was randomly sampled from artifact-free periods of resting EEG (20 epochs) as well as EEG recorded during the first- and second-meditation tasks (20 epochs each). The initial bin size of the histogram was set arbitrarily; we first divided the entire dynamic range into seven bins (please see step 1 of Figure 2), where each bin represents evenly divided frequency bands. In the second step, a scale factor was introduced, which determined the number of subdivisions of each initial bin. Basically, when the number of EEG epochs included in an initial bin range is large, the bin is divided into relatively more subdivisions. For example, if the scale factor of an initial bin is 0.1, the size of the subdivisions of the bin becomes 0.1 times the original bin size; that is, the bin is divided into 10 subdivisions. The scale factor was modeled with a third-order polynomial, $f(x) = ax^3 + bx^2 + cx + d$, where x is the number of EEG epochs included in an initial bin range and coefficients a, b, c, and d are unknowns that need to be determined. The order of the polynomial was selected empirically after confirming that the third-order polynomial could model the overall shape of the scale factor fairly well. We also limited the maximum of the scale factor to 50 to avoid an excessive increment of the number of subdivisions. The coefficients of the polynomial were determined using an optimization procedure with an objective function defined as the average increment in the number of feedback levels that each individual experiences. More specifically, the following equation was used as the objective function of the optimization:

$$\text{Increasing Rate}\,(\%) = \left(N_{\text{prop}} - N_{\text{conv}}\right) \times \left(\frac{1}{N_{\text{conv}}}\right) \times 100, \quad (1)$$

where N_{conv} and N_{prop} represent the average numbers of feedback levels that each individual experiences when conventional and proposed neurofeedback strategies are used, respectively. In calculating the objective function, the total number of feedback levels of the conventional neurofeedback strategy, N_{conv}, was set to be always identical to that of the proposed neurofeedback strategy, N_{prop}. Contrary to the proposed strategy, the entire range of the EEG feature was evenly divided in the case of the conventional neurofeedback strategy. A Nelder-Mead simplex direct search algorithm implemented in a MATLAB optimization toolbox (MathWorks, Natick, MA, USA) was used for the optimization. The algorithm was designed to solve classical unconstrained optimization problems of minimizing a given nonlinear function without a need for the calculation of derivatives [32]. We selected this algorithm because it is simple to use and could quickly yield reliable results. In the final step, each initial bin was divided into smaller subdivisions based on the optimized scale factor, and, accordingly, the total number of feedback levels was also adjusted.

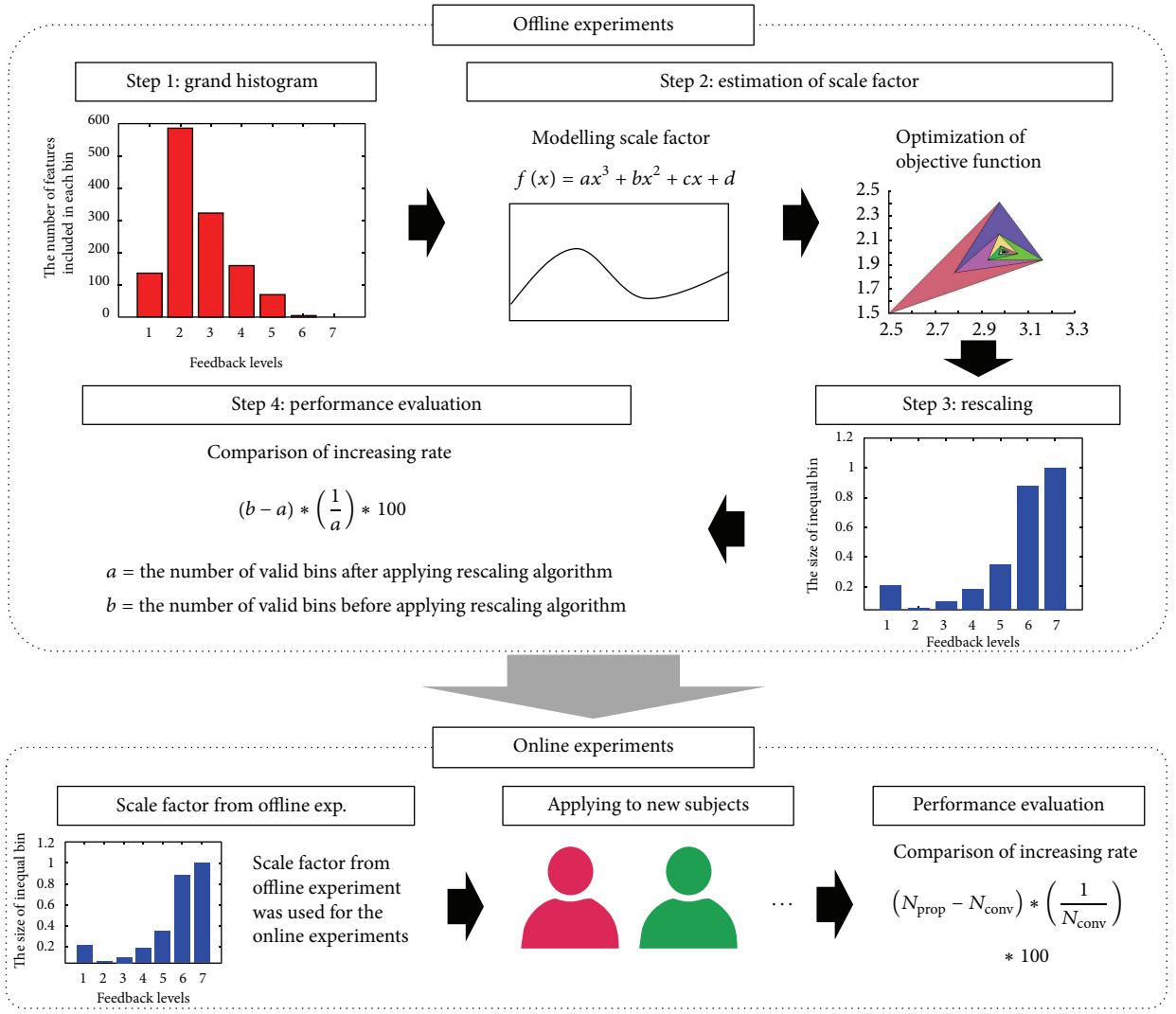

Figure 2: A schematic illustration of the overall procedure of the proposed neurofeedback strategy.

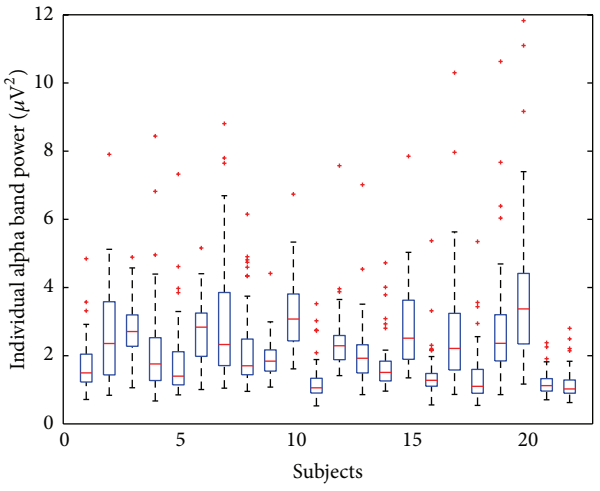

Figure 3: Changes in the EEG meditation feature of each individual participant acquired during resting and meditation periods.

3. Results

To evaluate whether study participants performed the given meditation task well, a statistical analysis was performed. A paired t-test was applied to confirm a statistically significant difference in the alpha band powers in the resting and meditative states. The result of the statistical analysis showed that the alpha power was significantly increased during meditation periods (2.19 ± 0.69) compared to resting periods (1.88 ± 0.76) (units: μV^2; p value: 0.03). This result is in line with the findings in many previous studies that consistently reported increased frontal alpha band activity during meditation tasks [29–31].

Figure 3 shows the distributions of the frontal alpha powers of each participant, which were recorded during both resting and meditation conditions. As seen in the figure, large interindividual variability was observed. Specifically, some participants (subject numbers 11, 16, 21, and 22) showed relatively small dynamic ranges of the alpha powers, while

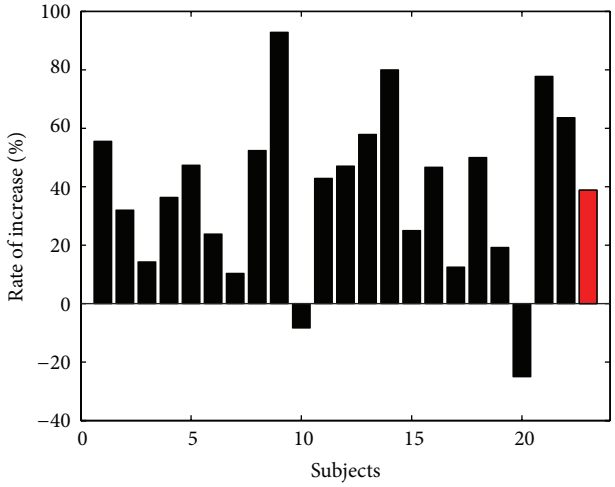

Figure 4: Results of offline experiments. The number of feedback levels that each subject experienced was increased in most participants. A red bar shows the average rate of increase.

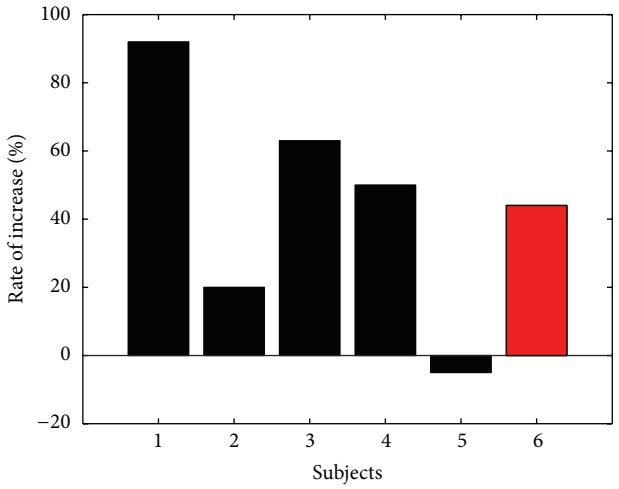

Figure 5: Results of online experiments. The average number of feedback levels that each participant experienced increased to 144% of the original results with uniform bin size. A red bar shows the average rate of increase.

other participants (subject numbers 2, 7, 10, 15, 17, and 20) showed relatively large dynamic ranges.

Figure 4 shows the increasing rate of each individual participant's feedback levels after the optimized scale factor was applied. The average number of feedback levels that each individual experienced increased to 139% of the original results with uniform bin sizes when the proposed neurofeedback strategy was applied. Twenty participants experienced increased numbers of feedback levels, while only two participants experienced reduced numbers of feedback levels, and the rate of decrement for those subjects was only about 20%.

Figure 5 shows the results of the online experiments for validation. In the online experiments with real-time feedback, the scale factor optimized using the offline datasets was directly applied without modification. When the proposed neurofeedback strategy was used, the average number of feedback levels that each participant experienced increased to 144% of the original results with uniform bin sizes. Four out of five participants experienced increased numbers of feedback levels, while one participant experienced a reduced number of feedback levels, with a decrement of less than 5%.

To demonstrate further the practicality of the proposed neurofeedback strategy, we asked participants to stare continuously at the real-time feedback (a varying circle and a varying vertical bar) as well as the picture of a valley during the online experiment. The size of the circle and the length of the bar varied with respect to the changes in the EEG meditation feature, but the feedback levels were set differently according to the conditions (conventional or proposed neurofeedback strategy). The supplementary movie file demonstrates that the user of the neurofeedback system could experience wider ranges of feedback without any training sessions or predata acquisition sessions (see supplementary movie file in Supplementary Material available online at http://dx.doi.org/10.1155/2016/3939815).

4. Discussion

It has been frequently reported in the literature and also shown in this study that some neurofeedback users can experience only a small portion of the total feedback range due to the large interindividual variability of EEG features. Most previous EEG-based neurofeedback studies focused on developing an individual customization strategy with the aim of addressing the large interindividual variability issue [23–25]. However, the customization strategy still has several difficulties, because it necessarily requires time-consuming and cumbersome calibration sessions before the neurofeedback training. Even after an individual customization session, the dynamic range of the EEG features of an individual can vary day by day, and, thus, repetitive training sessions are often required. In our present study, to enable most users to experience a wider range of feedback levels without any customization processes, an improved neurofeedback strategy was proposed. In contrast to the general neurofeedback strategy that uses a uniform bin size, the proposed neurofeedback strategy used nonuniform bin sizes to divide the entire range of EEG features based on the EEG database recorded from a group of individuals. The number of subdivisions in each bin was determined through an optimization process using a simplex search algorithm with an objective function to maximize the average number of feedback levels that each individual experienced. In this study, the EEG feature database was constructed using EEG data recorded from 22 healthy participants, while they were performing a meditation task paradigm. Then, the performance of the proposed neurofeedback strategy was confirmed through online experiments with five additional participants. The results of the proposed neurofeedback strategy exhibited increments in the numbers of feedback levels as high as 139% and 144% of the original results with a uniform bin size for the offline and online experiments, respectively.

Although the proposed neurofeedback strategy might not be the ultimate solution to circumvent the general limitations

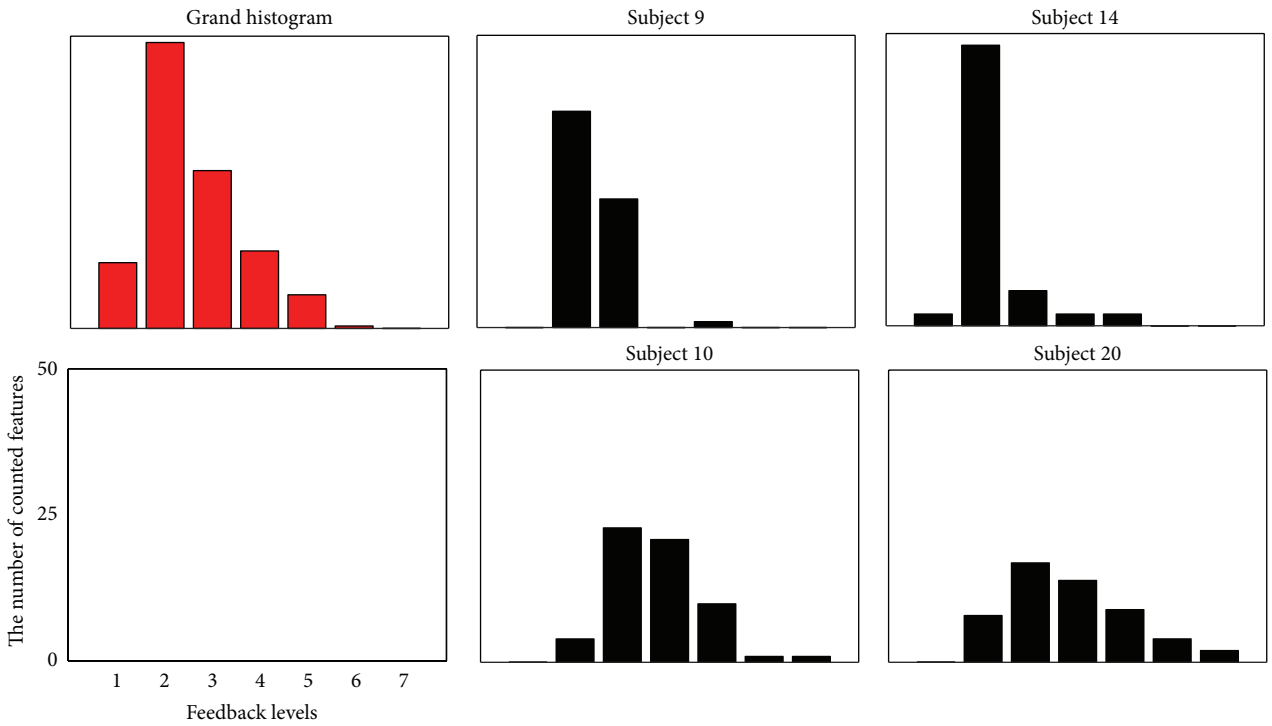

Figure 6: Grand and individual histograms of EEG meditation features. The red graph (upper left) shows the grand histogram, and the black graphs (the other four histograms) indicate the histograms of four individual participants.

of the current neurofeedback approaches, that is, the large interindividual variability issue, this strategy can enhance the performance of the neurofeedback systems without the need for customization or individualization sessions. If the optimized scale factor to adjust the sizes of nonuniform bins is predetermined using a large EEG database, most new users can use the neurofeedback training programs directly and experience increased feedback ranges. In this study, we only used a meditation task paradigm that can be used to train users to stay in a relaxed state; however, our neurofeedback strategy can also be generally used for other neurofeedback applications such as the treatment of patients with ADHD or depression. In other words, the proposed strategy can be used with various EEG features such as frontal alpha asymmetry and coherence between different channels if prerecorded databases are available. Notably, our strategy showed fairly good performance despite the fact that only a small number of EEG datasets were used to construct the feature database. In our present study, the database was constructed using EEG data recorded from only 22 subjects, but it showed an increment of feedback levels of around 50% in the online experiments. We expect that the performance of the proposed neurofeedback strategy would be further enhanced if a larger database could be used.

In both the offline and online experiments, few study participants (subjects 10 and 20 in the offline experiments; subject 5 in the online experiments) experienced reduced numbers of feedback levels after applying the proposed neurofeedback strategy (see Figures 4 and 5). We found that the participants who did not show good performance had histogram distributions significantly different from that of the grand histogram. In Figure 6, two participants, subjects 9 and 14, showed distributions similar to that of the grand histogram and thus showed the best and second-best increments in the numbers of feedback levels. In contrast, the other two participants included in Figure 6 (subjects 10 and 20, who showed the worst performances) showed distributions considerably different from that of the grand histogram. Nevertheless, about 90% of all study participants showed enhanced performance, and, thus, the proposed neurofeedback strategy is expected to be effective for most users. We expect that these exceptional cases can be potentially reduced if a larger EEG database is used and a better modeling of the scale factor is possible, which is a topic we would like to pursuit in future studies. In addition, further experiments need to be conducted in future studies in order to investigate the test-retest reliability of our method, considering the high intertrial variability of EEG features.

Competing Interests

The authors declare that there are no competing interests regarding the publication of this paper.

Acknowledgments

This work was supported by the National Research Foundation of Korea (NRF) grants funded by the Korea Government (MSIP) (nos. 2015R1A2A1A15054662 and NRF-2015M3C7A1065052).

References

[1] D. C. Hammond, "What is neurofeedback?" *Journal of Neurotherapy*, vol. 10, no. 4, pp. 25–36, 2006.

[2] T. Fuchs, N. Birbaumer, W. Lutzenberger, J. H. Gruzelier, and J. Kaiser, "Neurofeedback treatment for attention-deficit/hyperactivity disorder in children: a comparison with methylphenidate," *Applied Psychophysiology and Biofeedback*, vol. 28, no. 1, pp. 1–12, 2003.

[3] R. Coben, M. Linden, and T. E. Myers, "Neurofeedback for autistic spectrum disorder: a review of the literature," *Applied Psychophysiology Biofeedback*, vol. 35, no. 1, pp. 83–105, 2010.

[4] D. E. J. Linden, I. Habes, S. J. Johnston et al., "Real-time self-regulation of emotion networks in patients with depression," *PLoS ONE*, vol. 7, no. 6, Article ID e38115, 2012.

[5] C. Zhuo and L. Li, "The application and efficacy of combined neurofeedback therapy and imagery training in adolescents with tourette syndrome," *Journal of Child Neurology*, vol. 29, no. 7, pp. 965–968, 2014.

[6] A. Cortoos, E. De Valck, M. Arns, M. H. M. Breteler, and R. Cluydts, "An exploratory study on the effects of tele-neurofeedback and tele-biofeedback on objective and subjective sleep in patients with primary insomnia," *Applied Psychophysiology Biofeedback*, vol. 35, no. 2, pp. 125–134, 2010.

[7] M. B. Sterman and T. Egner, "Foundation and practice of neurofeedback for the treatment of epilepsy," *Applied Psychophysiology and Biofeedback*, vol. 31, no. 1, pp. 21–35, 2006.

[8] S. Hanslmayr, P. Sauseng, M. Doppelmayr, M. Schabus, and W. Klimesch, "Increasing individual upper alpha power by neurofeedback improves cognitive performance in human subjects," *Applied Psychophysiology and Biofeedback*, vol. 30, no. 1, pp. 1–10, 2005.

[9] E. Angelakis, S. Stathopoulou, J. L. Frymiare, D. L. Green, J. F. Lubar, and J. Kounios, "EEG neurofeedback: a brief overview and an example of peak alpha frequency training for cognitive enhancement in the elderly," *Clinical Neuropsychologist*, vol. 21, no. 1, pp. 110–129, 2007.

[10] W. Nan, J. P. Rodrigues, J. Ma et al., "Individual alpha neurofeedback training effect on short term memory," *International Journal of Psychophysiology*, vol. 86, no. 1, pp. 83–87, 2012.

[11] G. J. M. van Boxtel and J. H. Gruzelier, "Neurofeedback: introduction to the special issue," *Biological Psychology*, vol. 95, no. 1, pp. 1–3, 2014.

[12] J. Gruzelier and T. Egner, "Critical validation studies of neurofeedback," *Child and Adolescent Psychiatric Clinics of North America*, vol. 14, no. 1, pp. 83–104, 2005.

[13] N. Weiskopf, "Real-time fMRI and its application to neurofeedback," *NeuroImage*, vol. 62, no. 2, pp. 682–692, 2012.

[14] V. Zotev, R. Phillips, H. Yuan, M. Misaki, and J. Bodurka, "Self-regulation of human brain activity using simultaneous real-time fMRI and EEG neurofeedback," *NeuroImage*, vol. 85, pp. 985–995, 2014.

[15] S. Durston, "Imaging genetics in ADHD," *NeuroImage*, vol. 53, no. 3, pp. 832–838, 2010.

[16] J. Kamiya, "Conscious control of brain waves," *Psychology Today*, vol. 1, pp. 56–60, 1968.

[17] J. H. Gruzelier, "EEG-neurofeedback for optimising performance. I: a review of cognitive and affective outcome in healthy participants," *Neuroscience & Biobehavioral Reviews*, vol. 44, pp. 124–141, 2014.

[18] T. Egner and J. H. Gruzelier, "EEG Biofeedback of low beta band components: frequency-specific effects on variables of attention and event-related brain potentials," *Clinical Neurophysiology*, vol. 115, no. 1, pp. 131–139, 2004.

[19] P. Hashemian and S. A. Sadjadi, "Evaluation of neurofeedback therapy in adolescents with major depressive disorder who take fluoxetine," *Journal of Psychiatry*, vol. 18, no. 1, article 180, 2 pages, 2015.

[20] C. Yucha and D. Montgomery, *Evidence-Based Practice in Biofeedback and Neurofeedback*, AAPB, Wheat Ridge, Colo, USA, 2008.

[21] I. N. Konareva, "Correlations between the psychological peculiarities of an individual and the efficacy of a single neurofeedback session (by the EEG characteristics)," *Neurophysiology*, vol. 38, no. 3, pp. 201–208, 2006.

[22] S. Enriquez-Geppert, R. J. Huster, R. Scharfenort, Z. N. Mokom, J. Zimmermann, and C. S. Herrmann, "Modulation of frontal-midline theta by neurofeedback," *Biological Psychology*, vol. 95, no. 1, pp. 59–69, 2014.

[23] M. E. J. Kouijzer, H. T. van Schie, J. M. H. de Moor, B. J. L. Gerrits, and J. K. Buitelaar, "Neurofeedback treatment in autism. Preliminary findings in behavioral, cognitive, and neurophysiological functioning," *Research in Autism Spectrum Disorders*, vol. 4, no. 3, pp. 386–399, 2010.

[24] M. M. Lansbergen, M. van Dongen-Boomsma, J. K. Buitelaar, and D. Slaats-Willemse, "ADHD and EEG-neurofeedback: a double-blind randomized placebo-controlled feasibility study," *Journal of Neural Transmission*, vol. 118, no. 2, pp. 275–284, 2011.

[25] B. U. Hammer, A. P. Colbert, K. A. Brown, and E. C. Ilioi, "Neurofeedback for insomnia: a pilot study of Z-score SMR and individualized protocols," *Applied Psychophysiology and Biofeedback*, vol. 36, no. 4, pp. 251–264, 2011.

[26] M. C. Salinsky, B. S. Oken, and L. Morehead, "Test-retest reliability in EEG frequency analysis," *Electroencephalography and Clinical Neurophysiology*, vol. 79, no. 5, pp. 382–392, 1991.

[27] M. Näpflin, M. Wildi, and J. Sarnthein, "Test-retest reliability of resting EEG spectra validates a statistical signature of persons," *Clinical Neurophysiology*, vol. 118, no. 11, pp. 2519–2524, 2007.

[28] C.-H. Han and C.-H. Im, "Data-driven user feedback: an improved neurofeedback strategy considering individual variability of EEG features," in *Proceedings of the 18th IEEE International Symposium on Consumer Electronics (ISCE '14)*, pp. 1–2, IEEE, JeJu Island, South Korea, June 2014.

[29] T. Takahashi, T. Murata, T. Hamada et al., "Changes in EEG and autonomic nervous activity during meditation and their association with personality traits," *International Journal of Psychophysiology*, vol. 55, no. 2, pp. 199–207, 2005.

[30] L. I. Aftanas and S. A. Golocheikine, "Non-linear dynamic complexity of the human EEG during meditation," *Neuroscience Letters*, vol. 330, no. 2, pp. 143–146, 2002.

[31] F. Travis, D. A. F. Haaga, J. Hagelin et al., "A self-referential default brain state: patterns of coherence, power, and eLORETA sources during eyes-closed rest and transcendental meditation practice," *Cognitive Processing*, vol. 11, no. 1, pp. 21–30, 2010.

[32] J. A. Nelder and R. Mead, "A simplex method for function minimization," *The Computer Journal*, vol. 7, no. 4, pp. 308–313, 1965.